

## **General Disclaimer**

### **One or more of the Following Statements may affect this Document**

- This document has been reproduced from the best copy furnished by the organizational source. It is being released in the interest of making available as much information as possible.
- This document may contain data, which exceeds the sheet parameters. It was furnished in this condition by the organizational source and is the best copy available.
- This document may contain tone-on-tone or color graphs, charts and/or pictures, which have been reproduced in black and white.
- This document is paginated as submitted by the original source.
- Portions of this document are not fully legible due to the historical nature of some of the material. However, it is the best reproduction available from the original submission.

NATIONAL AERONAUTICS AND SPACE ADMINISTRATION  
NASA Lewis Research Center  
Structural Research Section  
21000 Brookpark Road  
Cleveland, OH 44135

Grant NAG 3-208

Report VPI-E-83.10

GEOMETRICALLY NONLINEAR ANALYSIS OF  
LAYERED COMPOSITE PLATES AND SHELLS

by

Wei-Chang Chao and J. N. Reddy  
Department of Engineering Science and Mechanics  
Virginia Polytechnic Institute and State University  
Blacksburg, VA 24061

February 1983



ORIGINAL PAGE IS  
OF POOR QUALITY

## GEOMETRICALLY NONLINEAR ANALYSIS OF LAYERED COMPOSITE PLATES AND SHELLS

### ABSTRACT

A degenerated three-dimensional finite element based on the total Lagrangian, incremental, formulation of a three-dimensional layered anisotropic medium is developed, and its use in the geometrically nonlinear, static as well as dynamic, analysis of layered composite plates and shells is demonstrated via several example problems. For comparison purposes a two-dimensional finite element based on the Sanders shell theory with the von Karman (nonlinear) strains is also presented. The elements have the following features:

- Geometrically linear and nonlinear analysis
- Static and transient analyses
- Natural vibration (linear) analyses
- Plates and shell elements
- Arbitrary loading and boundary conditions
- Arbitrary lamination scheme and lamina properties

The element can be used, with minor changes, in any existing general purpose programs.

The 3-D dimensional degenerated element has computational simplicity over a fully three-dimensional element, and the element accounts for full geometric nonlinearities in contrast to the 2-dimensional elements based on the Sanders shell theory. As demonstrated

via numerical examples, the deflections obtained by the 2-D shell element deviate from those obtained by the 3-D element for deep shells. Further, the 3-D element can be used to model general shells that are not necessarily doubly-curved. For example, the twisted plates cannot be modeled using the 2-D shell element. Of course, the 3-D degenerated element is computationally more demanding than the 2-D shell theory element for a given problem. In summary, the present 3-D element is an efficient element for the analysis of layered composite plates and shells undergoing large displacements and transient motion.

## TABLE OF CONTENTS

	<u>Page</u>
A BSTRACT .....	i
LIST OF FIGURES.....	vi
LIST OF TABLES.....	vii
 <u>Chapter</u>	
1. INTRODUCTION.....	1
1.1 Motivation.....	1
1.2 A Review of the Literature.....	3
1.3 The Present Theory.....	7
2. A SHEAR DEFORMABLE SHELL ELEMENT.....	8
2.1 Governing Equations.....	8
2.2 Finite Element Model.....	13
3. A DEGENERATED THREE-DIMENSIONAL FINITE ELEMENT.....	16
3.1 Introduction.....	16
3.2 Formulation of the Incremental Equations of Motion.....	16
3.3 Finite-Element Formulation.....	19
3.3.1 Geometry of the Element.....	19
3.3.2 Displacement Field in the Element.....	22
3.3.3 Element Stiffness Matrix.....	23
3.3.4 Time Integration and Mass Matrix.....	25
4. NUMERICAL VALIDATION OF THE ELEMENTS.....	29
4.1 Introduction.....	29
4.2 Static Analysis.....	29
4.2.1 Cylindrical Panel Under the Influence of Gravity...	29
4.2.2 Cylindrical Shell Subjected to Radial Pressure.....	31
4.2.3 Cylindrical Shell Subjected to Center Point Load...	36
4.2.4 Spherical Shell Subjected to Point Load at the Center.....	36
4.3 Natural Vibration of Cantilevered Twisted Plates.....	41
4.4 Transient Analysis.....	41
4.4.1 Cantilevered Beam Under Uniformly Distributed Load.....	41
4.4.2 Spherical Cap Under Axisymmetric Pressure Loading.....	48

<u>Chapter</u>	<u>Page</u>
5. NUMERICAL RESULTS FOR COMPOSITE PLATES AND SHELLS.....	52
5.1 Introduction.....	52
5.2 Static Analysis.....	52
5.2.1 Orthotropic Cylinder Subjected to Internal Pressure.....	52
5.2.2 Nine-Layer Cross-Ply ( $0^\circ/90^\circ/0^\circ/\dots$ ) Spherical Shell Subjected to Uniform Loading.....	55
5.2.3 Two-Layer Cross-Ply and Angle-Ply ( $45^\circ/-45^\circ$ ) Cylindrical Shells Under Uniform Loading.....	55
5.2.4 Two-Layer Cross-Ply and Angle-Ply ( $45^\circ/-45^\circ$ ) Spherical Shells Under Uniform Loading.....	55
5.3 Transient Analysis.....	59
5.3.1 Two-Layer Cross-Ply Plate Under Uniform Load.....	59
5.3.2 Two-Layer Cross-Ply Shell Under Uniform Load.....	59
5.3.3 Four-Layer Angle-Ply ( $45^\circ/-45^\circ/45^\circ/-45^\circ$ ) Cylindrical Shell Under Uniform Load.....	62
5.3.4 Two-Layer Angle-Ply ( $45^\circ/-45^\circ$ ) Spherical Shell Under Uniform Load.....	62
6. SUMMARY AND CONCLUSIONS.....	66
6.1 Summary of the Present Study.....	66
6.2 Conclusions.....	66
6.3 Recommendations for Additional Study.....	66
7. REFERENCES.....	68
APPENDIX I: Element Stiffness and Mass Matrices for Shear Deformable Shell Theory Element.....	73
APPENDIX II: Nomenclature.....	75

# LIST OF FIGURES

<u>Figure</u>		<u>Page</u>
2.1	Laminated shell geometry and lamina details.....	9
3.1	Motion of a continuous body in Cartesian coordinates.....	17
3.2	Geometry of the degenerated three-dimensional element.....	20
4.1	Geometry of the cylindrical shell used in Problem 1 of Section 4.1.....	30
4.2	Vertical deflection along the midsection OC.....	32
4.3	Displacement $v$ along the supported edge AB.....	33
4.4	Geometry of the cylindrical shell problem discussed in in Section 4.2.2.....	34
4.5	Load deflection curve for the clamped cylindrical shell problem discussed in Section 4.2.2.....	35
4.6	Geometry of the cylindrical shell problem discussed in Section 4.2.3.....	38
4.7	Load-deflection curve for the cylindrical shell problem discussed in Section 4.2.3.....	39
4.8	Geometry of the spherical shell discussed in Section 4.2.4.....	40
4.9	Load-deflection curve for the spherical shell problem discussed in Section 4.2.4.....	42
4.11	Load-deflection curve for the static bending of the cantilevered beam shown in Figure 4.10.....	47
4.12	Nonlinear deflection at the tip of the cantilevered beam (transverse deflection vs. time).....	49
4.13	Center transverse displacement versus time for a spherical cap under axisymmetric dynamic loading (load = 100 psi)...	51
5.1	Geometry of the cylindrical shell problem discussed in Section 5.2.1.....	53
5.2	Center transverse deflection versus internal pressure.....	54
5.3	Deflection versus load parameter for nine-layer cross-ply ( $0^\circ/90^\circ/0^\circ/\dots$ ) spherical shell discussed in Section 5.2.2.....	56

5.4	Deflection versus the load parameter for two-layer composite cylindrical shell (see Figure 4.1).....	57
5.5	Nondimensionalized deflection versus the load for laminated shells discussed in Section 5.2.4.....	58
5.6	Deflection versus time for two-layer plate $[0^\circ/90^\circ]$ under uniformly distributed step load.....	60
5.7	Center deflection versus time for two-layer cross-ply cylindrical shell subjected to uniform step load.....	61
5.8	Comparison of the center deflection obtained by two different time steps for the problem discussed in Section 5.3.2.....	63
5.9	Center deflection versus time for four-layer angle-ply $[45^\circ/-45^\circ/45^\circ/-45^\circ]$ cylindrical shell subjected to uniformly distributed load.....	64
5.10	Center deflection versus time for two-layer angle-ply $[45^\circ/-45^\circ]$ spherical shell under uniformly distributed step loading.....	65

## LIST OF TABLES

<u>Table</u>		<u>Page</u>
4.1	Comparison of Linear Center Deflections Obtained by the 2-D and 3-D Elements for Problem 4.2.2.....	37
4.2	Natural Frequencies of Twisted Plates Vibration ( $a/b = 1$ , $a/h = 20$ ).....	43
4.3	Natural Frequencies of Twisted Plate Vibration ( $b/a =$ $3$ , $a/h = 20$ ).....	44
4.4	Natural frequencies of Twisted Plate Vibration ( $a/b = 1$ , $a/h = 5$ ).....	45
4.5	Natural Frequencies of Twisted Plate Vibration ( $a/b = 1/3$ , $a/h = 5$ ).....	46

1.1 Motivation

Composite materials and reinforced plastics are increasingly used in aircraft, space vehicles, automobiles, and pressure vessels. With the increased use of fiber-reinforced composites as structural elements, studies involving the thermomechanical behavior of shell components made of composites are receiving considerable attention. Functional requirements and economic considerations of design have forced designers to use accurate but economical methods of determining stresses, natural frequencies, buckling loads, etc.

An accurate prediction of the behavior of shell structures requires a realistic modeling of the actual geometry, material behavior, and kinematic description of the components. The partial differential equations describing the large-deflection behavior of anisotropic composite shells of arbitrary geometry are not amenable to classical analytical methods. Consequently, numerical and approximate methods must be used to predict desired design quantities (such as stresses, frequencies, and buckling loads). In the last two and a half decades the finite element method has emerged as the most powerful analysis method of structural analysis.

The majority of the research papers in the open literature on shells is concerned with bending, vibration, and buckling of isotropic shells. As composite materials are making their way into many engineering structures, analyses of shells made of such materials become important. Further, with the increased application of advanced fiber composites in jet engine fan or compressor blades and high performance



aircraft, studies involving transient response of composite shell structures are needed to assess the capability of these materials under dynamic loads. At the time the project was undertaken, a finite-element analysis of the nonlinear transient response of laminated anisotropic shells was not available.

Finite-element analyses of shell structures in the past have used one of the three types of elements: 1. A 2-dimensional (2-D) element based on a two-dimensional shell theory; 2. A 3-D element based on three-dimensional elasticity theory; and 3. A 3-D degenerated element derived from the 3-D elasticity theory. The 2-D shell theory is derived from the three dimensional continuum field equations via, for example, an analytical integration through the thickness is employed to reduce the theory to a two-dimensional theory. In doing so the static and kinematic resultants are defined and used to derive the equations. In contrast to the 2-D shell theory, in the 3-D degenerated element, the shell geometry and displacement fields are discretized from the outset in the sense of finite elements, and the element contains full geometric nonlinearity. The unavailability of a convenient, general nonlinear shell theory makes the 2-D shell element restrictive in its use. The nonlinearity included in the 2-D shell element is that due to the von Karman strains, in which the products of the derivatives of the transverse deflection are neglected.

In contrast to the 2-D shell theory, no specific shell theory is employed in the 3-D degenerated element; instead, the geometry and the displacement fields are directly discretized and interpolated as in the analysis of continuum problems. The 2-D elements based on shell theory are the most economical, followed by the 3-D degenerated element. While the 3-D element is most accurate,

at least in theory, the computational cost prohibits its use in the nonlinear transient analysis of shells.

The present study is motivated by the lack of a finite-element analysis of geometrically nonlinear transient response of laminated anisotropic shells. The present study involved the development of a 3-D degenerated shell element for the analysis of a layered anisotropic medium, accounting for full geometric nonlinearity and transverse normal and shear stresses. The following literature survey provides a background for the present work.

## 1.2 A Review of the Literature

There exist a number of theories for layered anisotropic shells. Many of these theories were developed originally for thin shells, and are based on the Kirchhoff-Love kinematic hypothesis that plane sections normal to the undeformed midsurface remain plane and normal after deformation. Excellent surveys of various shell theories can be found in the works of Naghdi [1] and Bert [2]. Here we review the literature on composite shells.

The first analysis that incorporated the bending-stretching coupling (due to unsymmetric lamination in composites) is due to Ambartsumyan [3,4]. In his analyses Ambartsumyan assumed that the individual orthotropic layers were oriented such that the principal axes of material symmetry coincided with the principal coordinates of the shell reference surface. Thus, Ambartsumyan's work dealt with what is now known as laminated orthotropic shells rather than laminated anisotropic shells; in laminated anisotropic shells the individual layers are, in general, anisotropic and the principal axes of material

symmetry of the individual layers do not necessarily coincide with the principal coordinates of the shell.

In 1962 Dong, Pister and Taylor [5] formulated a theory of thin shells laminated of anisotropic material. The theory is an extension of the theory developed by Stavsky [6] for laminated anisotropic plates to Donnell's shallow shell theory. Cheng and Ho [7] presented an analysis of laminated anisotropic cylindrical shells using Flügge's shell theory. A first approximation theory for the unsymmetric deformation of nonhomogeneous, anisotropic, elastic cylindrical shells was derived by Widera and Chung [8] by means of the asymptotic integration of the elasticity equations. For a homogeneous, isotropic material, the theory reduces to the Donnell's equations.

All of the theories discussed above are based on the Kirchhoff-Love hypotheses in which the transverse shear deformation is neglected. The Love's first approximation theories are expected to yield sufficiently accurate results when (i) the lateral dimension to thickness ratio is large; (ii) the dynamic excitations are within the low-frequency range; (iii) the material anisotropy is not severe. However, application of such theories to layered anisotropic composite shells could lead to as much as 30% or more errors in deflections, stresses, or frequencies. For example, the thick-walled composite cylinders used for aircraft landing gears require a laminated thick-shell theory for their analysis.

The effect of transverse shear deformation and transverse isotropy, as well as thermal expansion through the shell thickness were considered by Gulati and Essenberg [9] and Zukas and Vinson [10]. Gulati and Essenberg [9] showed that the circumferential displacement components and the twist couple would arise due to the anisotropy and transverse

shear deformation. Whitney and Sun [11] developed a shear deformable theory for laminated cylindrical shells that includes both transverse shear deformation and transverse normal strain as well as expansional strains. Recently, Widera and Logan [12,13] presented refined theories for nonhomogeneous anisotropic cylindrical shells.

As far as the finite-element analysis of shells is concerned, layered composite shells have not received nearly as much attention as ordinary shells. The works of Dong [14] on statically-loaded orthotropic shell of revolution, Dong and Selna [15] on free vibration of the same, Wilson and Parsons [16] on static axisymmetric loading of arbitrarily thick orthotropic shells of revolution, and Schmit and Monforton [17] on laminated anisotropic cylindrical shells are the only ones that considered the finite element method before the 1970's (note that the latter reference is the only one that considered laminated anisotropic shells). In the 1970's there was an increased interest in the finite-element analysis of bending and vibration of laminated anisotropic shells. Apparently the first finite-element application in laminated anisotropic shells of arbitrary geometry is due to Thompson and Bert [18], who treated free (i.e., natural) vibration of general laminated anisotropic thin shells. Other finite-element analyses of layered anisotropic composite shells include the works of Panda and Natarajan [19], Shivakumar and Krishna Murty [20], Rao [21], Seide and Chang [22], and Venkatesh and Rao [23]. Recently, Hsu, et al. [24] and Reddy [25] presented finite-element analyses of laminated thick cylindrical shells and laminated thick doubly curved shells, respectively.

All of the literature cited above is limited to the small displacement theory of shells. In the analysis of thin flexible composite shells one should take large deflections into account. Because of the high modulus and high strength properties that composites have, structural components could undergo large deflections before they become inelastic. Therefore, an accurate prediction of displacements and stresses is possible only when one accounts for the geometric nonlinearity.

Finite-element analyses of the large-displacement theory are based on the principle of virtual work or the associated principle of stationary potential energy. Horrigmoe and Bergan [26] presented classical variational principles for nonlinear problems by considering incremental deformations of a continuum. A survey of various principles in incremental form in different reference configurations, such as the total Lagrangian and the updated Lagrangian formulation, is presented by Wunderlich[27]. In the total Lagrangian description, all static and kinematic variables are referred to the initial configuration. In the updated Lagrangian description all variables are referred to the current configuration. Stricklin et al. [28] presented a survey of various formulations and solution procedures for nonlinear static and dynamic structural analysis. The formulations included are the pseudo-force method, total Lagrangian method, the updated Lagrangian method, and the convected coordinate method. The solution methods included are the solution by direct minimization of total potential, Newton-Raphson and modified Newton-Raphson, and the first- and second-order self correcting methods.

The only large-deflection analyses of laminated composite shells that can be found in the literature are the static analysis of Noor and Hartley [29] and Chang and Sawamiphakdi [30]. Noor and Hartley employed the shallow shell theory with transverse shear strains and geometric nonlinearities to develop triangular and quadrilateral finite elements. Chang and Sawamiphakdi presented a formulation of the 3-D degenerated element for geometrically nonlinear analysis of laminated composite shells. The formulation is based on the updated Lagrangian description and it does not include any numerical results for laminated shells.

From the review of the literature it is clear that the 3-D degenerated element has not been exploited fully for geometrically nonlinear analysis of laminated anisotropic shells. Further, the transient analysis has not been reported in the literature. Guided by these observations the present work was undertaken in the fall of 1981.

### 1.3 The Present Study

The present study was undertaken to develop a finite-element analysis capability for the static and dynamic analysis of geometrically nonlinear theory of layered anisotropic shells. The 3-D degenerated element with total Lagrangian description is used to analyze various shell problems.

Following this introduction, a description of the 2-D shell element is presented in Chapter 2. In Chapter 3 a detailed discussion of the 3-D degenerated element is given. Application and comparison of the two elements are illustrated via a number of shell problems.

## Chapter II

## A SHEAR DEFORMABLE SHELL ELEMENT

2.1 Governing Equations

The basic equations of three-dimensional elasticity theory can be simplified for thin flexible bodies. A set of simplifying assumptions that provide a reasonable description of the behavior of thin elastic shells are as follows:

1. the thickness of the shell is small compared to the other dimensions;
2. the transverse normal stress is negligible;
3. normals to the reference surface of the shell before deformation remain straight but not necessarily normal after deformation;
4. the thickness-to-radius of the shell is assumed to be small compared to unity; and
5. in the second order terms, the derivatives of membrane displacements are small compared to the derivatives of the transverse displacement.

The shell under consideration is composed of a finite number of orthotropic layers of uniform thickness, as shown in Fig. 2.1. An orthogonal curvilinear coordinate system  $(\xi_1, \xi_2, \zeta)$  is chosen such that the  $\xi_1$ - and  $\xi_2$ -curves are lines of principal curvature on the midsurface  $\zeta = 0$ , and  $\zeta$ -curves are straight lines perpendicular to the surface  $\zeta = 0$ . A line element of the shell is given by (see [31])

$$(ds)^2 = [(1 + \zeta/R_1)\alpha_1 d\xi_1]^2 + [(1 + \zeta/R_2)\alpha_2 d\xi_2]^2 + (d\zeta)^2 \quad (2.1)$$

where  $\alpha_i$  and  $R_i$  ( $i = 1, 2$ ) are the surface metrics and radii of

ORIGINAL PAGE IS  
OF POOR QUALITY

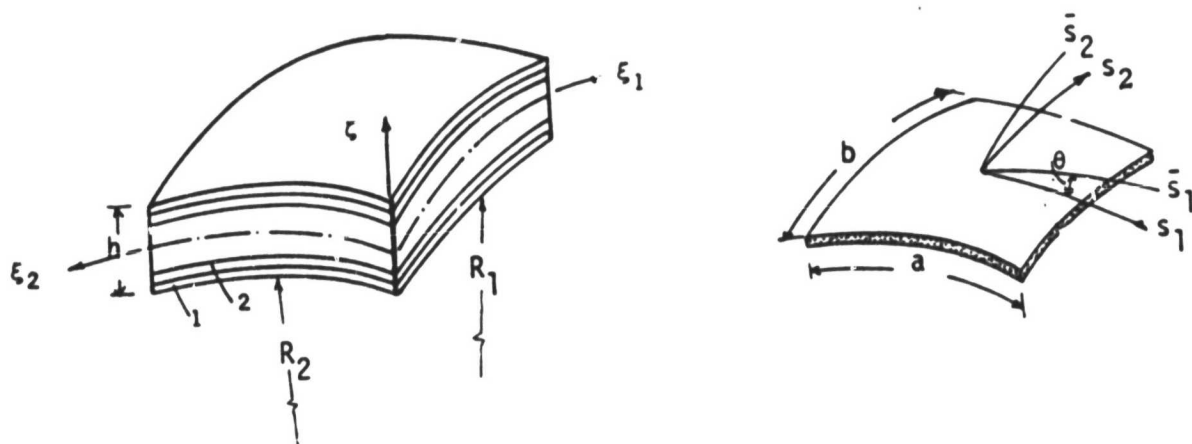


Figure 2.1 Laminated shell geometry and lamina details



curvature, respectively. In general,  $\alpha_i$  and  $R_i$  are functions of  $\xi_i$  only.

For constant values of  $\alpha_1, \alpha_2, R_1$ , and  $R_2$ , the equations of motion are given by (with  $c_0 = \frac{1}{2} (1/R_1 - 1/R_2)$  and  $dx_i = \alpha_i d\xi_i$ ; see [25])

$$\begin{aligned}
 \frac{\partial N_1}{\partial x_1} + \frac{\partial}{\partial x_2} (N_6 + c_0 M_6) + \frac{Q_1}{R_1} &= P_1 \frac{\partial^2 u_1}{\partial t^2} + [P_2 + P_3 \left(\frac{1}{R_1} + \frac{1}{R_2}\right)] \frac{\partial^2 \phi_1}{\partial t^2} \\
 \frac{\partial}{\partial x_1} (N_6 - c_0 M_6) + \frac{\partial N_2}{\partial x_2} + \frac{Q_2}{R_2} &= P_1 \frac{\partial^2 u_2}{\partial t^2} + [P_2 + P_3 \left(\frac{1}{R_1} + \frac{1}{R_2}\right)] \frac{\partial^2 \phi_2}{\partial t^2} \\
 \frac{\partial Q_1}{\partial x_1} + \frac{\partial Q_2}{\partial x_2} - \left(\frac{N_1}{R_1} + \frac{N_2}{R_2} - q\right) &= [P_1 + P_2 \left(\frac{1}{R_1} + \frac{1}{R_2}\right)] \frac{\partial^2 u_3}{\partial t^2} \\
 \frac{\partial M_1}{\partial x_1} + \frac{\partial M_6}{\partial x_2} - Q_1 &= P_3 \frac{\partial^2 \phi_1}{\partial t^2} + [P_2 + P_3 \left(\frac{1}{R_1} + \frac{1}{R_2}\right)] \frac{\partial^2 u_1}{\partial t^2} \\
 \frac{\partial M_6}{\partial x_1} + \frac{\partial M_2}{\partial x_2} - Q_2 &= P_3 \frac{\partial^2 \phi_2}{\partial t^2} + [P_2 + P_3 \left(\frac{1}{R_1} + \frac{1}{R_2}\right)] \frac{\partial^2 u_2}{\partial t^2} \quad (2.2)
 \end{aligned}$$

where  $u_i$  are the displacements of the reference surface along the  $\xi_i$  and  $\zeta$  axes,  $\phi_i$  are the rotations of the reference surface with respect to the  $\xi_i$ -axis,  $q$  is the distributed load,  $N_i$  and  $M_i$  are the stress and moment resultants, and  $Q_i$  is the shear force resultant:

$$\begin{aligned}
 (N_i, M_i) &= \sum_{k=1}^L \int_{\zeta_{k-1}}^{\zeta_k} \sigma_i(l, \zeta) d\zeta, \quad i = 1, 2, 6 \\
 Q_i &= \sum_{k=1}^L K_i^2 \int_{\zeta_{k-1}}^{\zeta_k} \sigma_i d\zeta, \quad i = 4, 5, \quad (2.3)
 \end{aligned}$$

Here  $P_i$  are the inertias

ORIGINAL PAGE IS  
OF POOR QUALITY

$$(p_1, p_2, p_3) = \sum_{k=1}^L \int_{\zeta_{k-1}}^{\zeta_k} \rho^{(k)}(1, \zeta, \zeta^2) d\zeta \quad (2.4)$$

and  $K_i$  ( $i = 4, 5$ ) are shear correction factors.

The strain-displacement relations for a large rotation (small strains) theory of shells are given by (see [32])

$$\begin{aligned} \epsilon_1 &= \epsilon_1^0 + \zeta \kappa_1 \\ \epsilon_2 &= \epsilon_2^0 + \zeta \kappa_2 \\ \epsilon_4 &= \epsilon_4^0 \\ \epsilon_5 &= \epsilon_5^0 \\ \epsilon_6 &= \epsilon_6^0 + \zeta \kappa_6 \end{aligned} \quad (2.5)$$

where

$$\begin{aligned} \epsilon_1^0 &= \frac{\partial u_1}{\partial x_1} + \frac{u_3}{R_1} + \frac{1}{2} \left[ \left( \frac{\partial u_3}{\partial x_1} + \frac{u_1}{R_1} \right)^2 + \left( \frac{\partial u_1}{\partial x_1} + \frac{u_3}{R_1} \right)^2 + \left( \frac{\partial u_2}{\partial x_1} \right)^2 \right] \\ \epsilon_2^0 &= \frac{\partial u_2}{\partial x_2} + \frac{u_3}{R_2} + \frac{1}{2} \left[ \left( \frac{\partial u_3}{\partial x_2} + \frac{u_2}{R_2} \right)^2 + \left( \frac{\partial u_2}{\partial x_2} + \frac{u_3}{R_2} \right)^2 + \left( \frac{\partial u_1}{\partial x_2} \right)^2 \right] \\ \epsilon_6^0 &= \frac{\partial u_1}{\partial x_2} + \frac{\partial u_2}{\partial x_1} + \left( \frac{\partial u_3}{\partial x_1} + \frac{u_1}{R_1} \right) \left( \frac{\partial u_3}{\partial x_2} + \frac{u_2}{R_2} \right) + \left( \frac{\partial u_1}{\partial x_2} + \frac{u_3}{R_1} \right) \frac{\partial u_1}{\partial x_2} + \left( \frac{\partial u_2}{\partial x_1} + \frac{u_3}{R_2} \right) \frac{\partial u_2}{\partial x_1} \\ \epsilon_4^0 &= \phi_2 + \frac{\partial u_3}{\partial x_2} - \frac{u_2}{R_2} \\ \epsilon_5^0 &= \phi_1 + \frac{\partial u_3}{\partial x_1} - \frac{u_1}{R_1} \\ \kappa_1 &= \frac{\partial \phi_1}{\partial x_1} + \frac{1}{R_1} \left( \frac{\partial u_1}{\partial x_1} + \frac{u_3}{R_1} \right) \end{aligned}$$

$$\begin{aligned}\kappa_2 &= \frac{\partial \phi_2}{\partial x_2} + \frac{1}{R_2} \left( \frac{\partial u_2}{\partial x_2} + \frac{u_3}{R_2} \right) \\ \kappa_6 &= \frac{\partial \phi_1}{\partial x_1} + \frac{\partial \phi_2}{\partial x_2} - c_0 \left( \frac{\partial u_2}{\partial x_1} - \frac{\partial u_1}{\partial x_2} \right)\end{aligned}\quad (2.6)$$

Invoking the fourth assumption, the contribution from the underlined terms in Eq. (2.6) can be neglected. The transverse normal strain and normal stresses are neglected in the present theory.

The shell constitutive equations are given by

$$\begin{aligned}N_i &= A_{ij} \epsilon_j^0 + B_{ij} \kappa_j \\ M_i &= B_{ij} \epsilon_j^0 + D_{ij} \kappa_j \\ Q_2 &= A_{44} \epsilon_4^0 + A_{45} \epsilon_5^0 \\ Q_1 &= A_{45} \epsilon_4^0 + A_{55} \epsilon_5^0\end{aligned}\quad (i, j = 1, 2, 6) \quad (2.7)$$

Here  $A_{ij}$ ,  $B_{ij}$  and  $D_{ij}$  ( $i, j = 1, 2, 6$ ) denote the extensional,\* flexural-extensional coupling, and flexural stiffnesses:

$$(A_{ij}, B_{ij}, D_{ij}) = \sum_{k=1}^L \int_{\zeta_{k-1}}^{\zeta_k} Q_{ij}^{(k)}(1, \zeta, \zeta^2) d\zeta. \quad (2.8)$$

where  $L$  denotes the total number of layers, and  $Q_{ij}^{(k)}$  are the plane-stress reduced stiffnesses of the  $k$ -th lamina, referred to the shell axes.

Equations (2.1)-(2.8) completely describe the dynamic equilibrium of a layered, anisotropic shell. These equations can be solved in closed form for the small displacement theory of simple-supported,

\*Quantities  $A_{44}$ ,  $A_{45}$ ,  $A_{55}$  and  $A_{66}$  are actually shear stiffnesses, not extensional ones.

cross-ply plates under sinusoidal distribution of the transverse load (see [33,34]). In order to solve practically important problems that involve other loadings, boundary conditions, geometry, and lamination schemes, one must consider approximate method of analysis. In the following section, an isoparametric finite-element analysis of the shell equations (2.1)-(2.8) is presented.

## 2.2 Finite-Element Model

A typical finite element is a doubly-curved shell element whose projections on the  $\xi_1$ - $\xi_2$ -plane is an isoparametric quadrilateral element. Over the typical shell element  $\Omega^{(e)}$ , the displacements  $(u_1, u_2, u_3, \phi_1, \phi_2)$  are interpolated by expressions of the form,

$$\begin{aligned} u_i &= \sum_{j=1}^N u_i^j \phi_j(\xi_1, \xi_2) \quad , \quad i = 1, 2, 3 \\ \phi_i &= \sum_{j=1}^N \phi_i^j \phi_j(\xi_1, \xi_2) \quad , \quad i = 1, 2 \end{aligned} \quad (2.9)$$

where  $\phi_j$  are the interpolation functions, and  $u_i^j$  and  $\phi_i^j$  are the nodal values of  $u_i$  and  $\phi_i$ , respectively. For a linear isoparametric element with nine nodes ( $N=9$ ), this interpolation results in a stiffness matrix of order 45 by 45.

Substitution of Eq. (2.9) into the variational formulation of Eq. (2.2) yields an element equation of the form (see Reddy [34])

$$[K]\{\Delta\} + [M]\{\ddot{\Delta}\} = \{F\} \quad (2.10)$$

where  $\{\Delta\} = \{\{u_1\}, \{u_2\}, \{u_3\}, \{\phi_1\}, \{\phi_2\}\}^T$ ,  $[K]$  and  $[M]$  are element stiffness and mass matrices, respectively, and  $\{F\}$  is the force vector. In the interest of brevity, the coefficients of mass and stiffness matrices are included in Appendix I.

To complete the approximation, we should approximate the time derivatives in Eq. (2.10). Here we use the Newmark direct integration scheme (the constant-average-acceleration method). Use of the Newmark method to Eq. (2.10) yields (see Reddy [34])

$$[\hat{K}]\{\Delta\}_{n+1} = \{\hat{F}\}_{n,n+1} \quad (2.11)$$

where

$$[\hat{K}] = [K] + a_0[M], \quad \{\hat{F}\} = \{F\}_{n+1} + [M](a_0\{\Delta\}_n + a_1\{\dot{\Delta}\}_n + a_2\{\ddot{\Delta}\}_n),$$

$$a_0 = 1/(\beta\Delta t^2), \quad a_1 = a_0\Delta t, \quad a_2 = \frac{1}{2\beta} - 1. \quad (2.12)$$

Once the solution  $\{\Delta\}$  is known at  $t_{n+1} = (n+1)\Delta t$ , the first and second derivatives (velocity and accelerations) of  $\{\Delta\}$  at  $t_{n+1}$  can be computed from

$$\begin{aligned} \{\ddot{\Delta}\}_{n+1} &= a_0(\{\Delta\}_{n+1} - \{\Delta\}_n) - a_1\{\dot{\Delta}\}_n - a_2\{\ddot{\Delta}\}_n \\ \{\dot{\Delta}\}_{n+1} &= \{\dot{\Delta}\}_n + a_3\{\ddot{\Delta}\}_n + a_4\{\ddot{\Delta}\}_{n+1} \end{aligned} \quad (2.13)$$

where  $a_3 = (1 - \alpha)\Delta t$ , and  $a_4 = \alpha\Delta t$ .

The element equations (2.11) can be assembled, boundary conditions can be imposed, and the resulting equations can be solved at each time step using the information known from the preceding time step solution. At time  $t = 0$ , the initial values of  $\{\Delta\}$ ,  $\{\dot{\Delta}\}$ , and  $\{\ddot{\Delta}\}$  (obtained by solving Eq. (2.10) at  $t = 0$ ) are used to initiate the time marching scheme.

In the present study the nine-node rectangular isoparametric element was employed. Analogous to the shear deformable theory of layered composite plates [34], the present theory can be recognized as a shear deformable theory derived from the classical shell theory by treating the slope-deflection relations ( $\epsilon_4, \epsilon_5 = 0$ ) as constraints, and

including the constraints into the variational formulation of the shell equations by the penalty function method (see Reddy [25]). The elements derived using such theory are very stiff (so-called locking is observed) for thin shells, but yield good results for moderately thick shells. To overcome the locking phenomenon, the reduced integration technique (see Zienkiewicz, Taylor and Too [35]) must be employed in the evaluation of the stiffness coefficients associated with the shear energy terms (i.e., penalty terms). More specifically, the 2x2 Gauss rule must be used for shear terms (i.e., those involving  $A_{44}$ ,  $A_{45}$ , and  $A_{55}$ ) and the standard 3x3 Gauss rule must be used for the bending terms when the nine node quadratic isoparametric element.

## Chapter III

DEGENERATED THREE DIMENSIONAL FINITE ELEMENT3.1 Introduction

The primary objective of this chapter is to review the formulation of equations governing geometrically nonlinear motion of a continuous medium. Due to the nature of the present manuscript, only necessary equations are presented. For additional details the reader is referred to [36-40].

We describe the motion of a continuous body in a Cartesian coordinate system. The simultaneous position of all material points (i.e., the configuration) of the body at time  $t$  is denoted by  $C_t$ , and  $C_0$  and  $C_{t+\Delta t}$  denote the configurations at reference time  $t = t_0$  and time  $t + \Delta t$ , respectively (see Fig. 3.1). In the updated Lagrangian description all kinetic and kinematic variables are referred to the current configuration at each time and load step. In the total Lagrangian description all dependent variables are referred to the reference configuration. The updated Lagrangian is more suitable for motions that involve very large distortions of the body (e.g., high-velocity impact). The total Lagrangian is more convenient for motions that involve only moderately large deformations. In the present study the total Lagrangian formulation is adopted.

3.2 Formulation of the Incremental Equations of Motion

Here we present a derivation of the equilibrium equations at different time steps using the total Lagrangian approach. The coordinates of a typical point in  $C_t$  is denoted by  ${}^t\mathbf{x} = ({}^t x_1, {}^t x_2, {}^t x_3)$ . The displacement of a particle at time  $t$  is given by

ORIGINAL PAGE IS  
OF POOR QUALITY

~~ORIGINAL PAGE IS  
OF POOR QUALITY~~

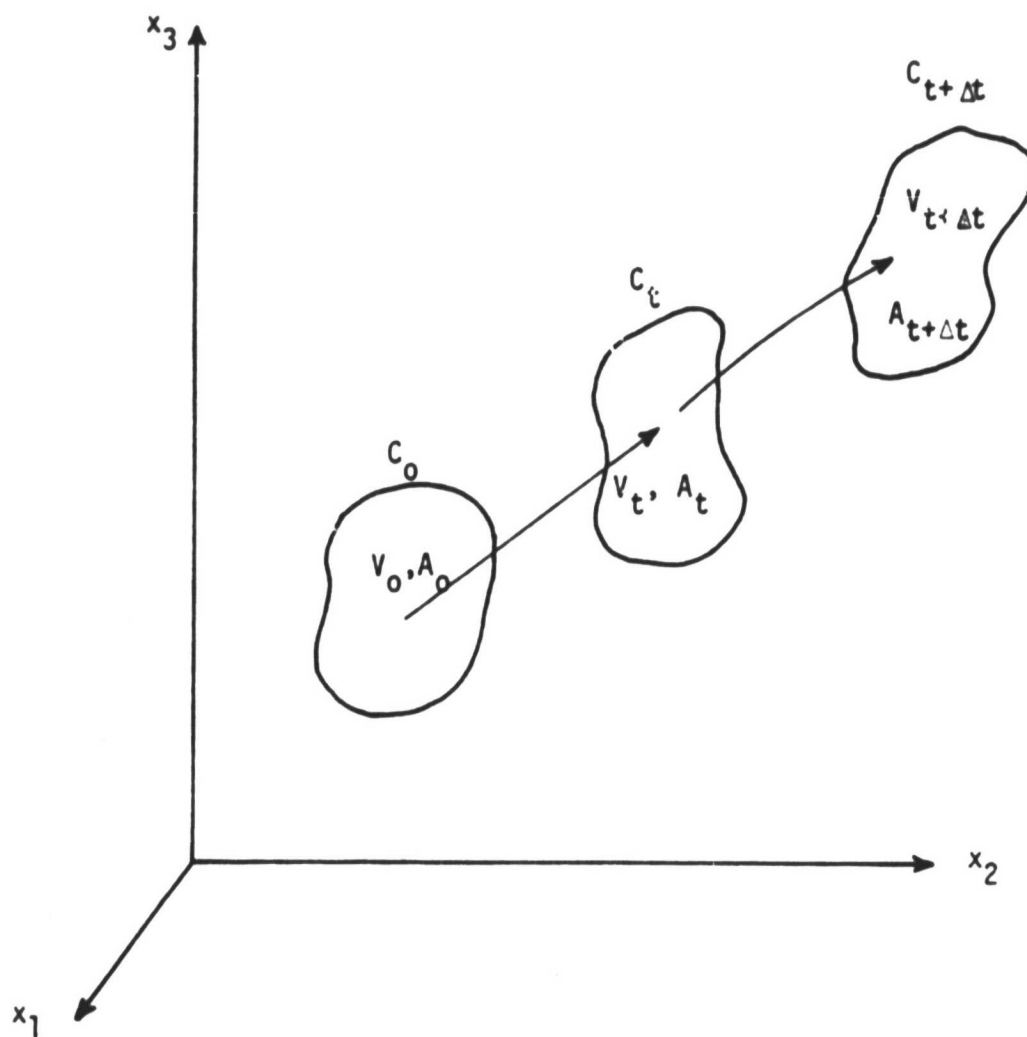


Figure 3.1 Motion of a continuous body in Cartesian coordinates



$$\underline{t}_u = \underline{t}_x - \underline{0}_x \text{ or } t_{u_i} = t_{x_i} - 0_{x_i} \quad (3.1)$$

The increment of displacement during time  $t$  to  $t + \Delta t$  is defined by

$$u_i = {}^{t+\Delta t}u_i - t_{u_i} \quad (3.2)$$

The principle of virtual displacements can be employed to write the equilibrium equations at any fixed time  $t$ . The principle, applied to the large-displacements case, can be expressed mathematically as follows:

$$\begin{aligned} \int_{V_0} \rho_0 {}^{t+\Delta t} \ddot{u}_i \delta u_i dV_0 + \int_{V_0} {}^{t+\Delta t} S_{ij} \delta ({}^{t+\Delta t} \epsilon_{ij}) dV_0 \\ = \int_{A_0} {}^{t+\Delta t} T_i \delta u_i dA_0 + \int_{V_0} {}^{t+\Delta t} F_i \delta u_i dV_0 \end{aligned} \quad (3.3)$$

where summation on repeated indices is implied;  $V_0$ ,  $A_0$ , and  $\rho_0$  denote, respectively, a volume element, area element, and density in the initial configuration,  $S_{ij}$  are the components of the second Piola-Kirchhoff stress tensor,  $\epsilon_{ij}$  the components of the Green-Lagrangian strain tensor,  $T_i$  the components of boundary stresses, and  $F_i$  are the components of the body force vector. The superposed dots on  $u_i$  denote differentiation with respect to time, and  $\delta$  denotes the variational symbol. In writing Eq. (3.3) it is assumed that  $\epsilon_{ij}$  is related to the displacement components by the kinematic relations

$${}^{t+\Delta t} \epsilon_{ij} = \frac{1}{2} ({}^{t+\Delta t} u_{i,j} + {}^{t+\Delta t} u_{j,i} + {}^{t+\Delta t} u_{m,i} {}^{t+\Delta t} u_{m,j}) \quad (3.4)$$

where  $u_{i,j} = \partial u_i / \partial x_j$ . The strain components  ${}^{t+\Delta t} \epsilon_{ij}$  can be expressed in terms of current strain and incremental strain components:

$$\begin{aligned}
{}^{t+\Delta t}\epsilon_{ij} &= \frac{1}{2} ({}^t u_{i,j} + {}^t u_{j,i} + {}^t u_{m,i} {}^t u_{m,j}) \\
&+ \frac{1}{2} (u_{i,j} + u_{j,i} + {}^t u_{m,i} u_{m,j} + u_{m,i} {}^t u_{m,j}) + \frac{1}{2} u_{m,i} u_{m,j} \\
&\equiv {}^t \epsilon_{ij} + (e_{ij} + \eta_{ij})
\end{aligned} \tag{3.5}$$

where  $e_{ij}$  and  $\eta_{ij}$  denote the linear and nonlinear incremental strains.

The stress components  ${}^{t+\Delta t}S_{ij}$  can be decomposed into two parts:

$${}^{t+\Delta t}S_{ij} = {}^t S_{ij} + S_{ij} \tag{3.6}$$

where  $S_{ij}$  is the incremental stress tensor. The incremental stress components  $S_{ij}$  are related to the incremental Green-Lagrange strain components,  $\epsilon_{ij} = e_{ij} + \eta_{ij}$ , by the generalized Hooke's law:

$$S_{ij} = C_{ijkl} \epsilon_{kl} \tag{3.7}$$

where  $C_{ijkl}$  are the components of the elasticity tensor. Using Eq. (3.4)-(3.7), one can express Eq. (3.3) in the alternate form

$$\begin{aligned}
&\int_{V_0} \rho_0 {}^{t+\Delta t} \ddot{u}_i \delta u_i dV_0 + \int_{V_0} C_{ijkl} (e_{kl} \delta \eta_{ij} + \eta_{kl} \delta e_{ij}) dV_0 \\
&+ \int_{V_0} {}^t S_{ij} \delta e_{ij} dV_0 = \delta W - \int_{V_0} {}^t S_{ij} \delta \eta_{ij} dV_0
\end{aligned} \tag{3.8}$$

where  $\delta W$  is the virtual work due to external loads.

### 3.3 Finite-Element Formulation

#### 3.3.1 Geometry of the Element

Consider a solid three-dimensional element shown in Fig. 3.2. The coordinates of a typical point in the element can be written as

$$x_i = \sum_{j=1}^n \psi_j(\xi_1, \xi_2) \frac{1+\zeta}{2} (x_i^j)_{\text{top}} + \sum_{j=1}^n \psi_j(\xi_1, \xi_2) \frac{1-\zeta}{2} (x_i^j)_{\text{bottom}} \tag{3.9}$$

ORIGINAL PAGE IS  
OF POOR QUALITY

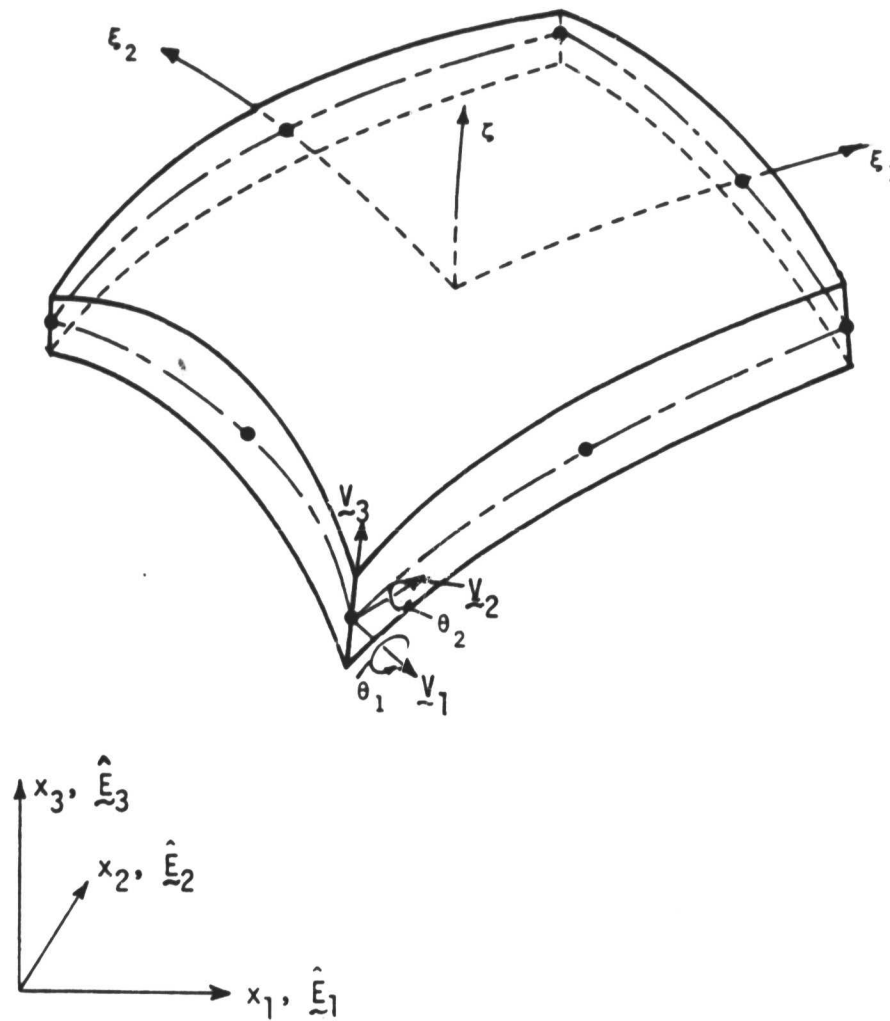


Figure 3.2 Geometry of the degenerated three-dimensional element

where  $n$  is the number of nodes,  $\psi_i(\xi_1, \xi_2)$  are the finite-element interpolation (or shape) functions, which, in the element take the value of unity at node  $i$  and zero at all other nodes,  $\xi_1$  and  $\xi_2$  are the normalized curvilinear coordinates in the middle plane of the shell, and  $\zeta$  is a linear coordinate in the thickness direction and  $x_1^i$ ,  $x_2^i$ , and  $x_3^i$  are the global coordinates at node  $i$ . Here  $\xi_1, \xi_2$ , and  $\zeta$  are assumed to vary between  $-1$  and  $+1$ . Now let (see Fig. 3.2)

$$v_{3k}^i = (x_k^i)_{\text{top}} - (x_k^i)_{\text{bottom}} \quad (3.10)$$

$$\hat{e}_3^i \equiv v_3^i / |v_3^i|$$

where  $v_{3k}^i$  is the  $k$ -th component of the vector  $v_3^i$ . Then Eq. (3.9) becomes

$$x_i = \sum_{j=1}^n [\psi_j(x_i^j)_{\text{mid}} + \psi_j \frac{\zeta}{2} h_j \hat{e}_{3i}^j] \quad (3.11)$$

where  $h_j$  is the thickness of the element at node  $j$ . For small deformation, the displacement of every point in the element can be written as

$$u_i = \sum_{j=1}^n \psi_j [u_i^j + \zeta \frac{h}{2} (\hat{e}_{1i}^j \theta_2^j - \hat{e}_{2i}^j \theta_1^j)] \quad (3.12)$$

where  $\theta_1^i$  and  $\theta_2^i$  are the rotations about (local) unit vectors  $\hat{e}_1^i$  and  $\hat{e}_2^i$ , respectively,  $u_1$ ,  $u_2$ , and  $u_3$  are the displacement components corresponding to the global coordinate  $x_1$ ,  $x_2$ ,  $x_3$  directions respectively, and  $u_1^i$ ,  $u_2^i$  and  $u_3^i$  are the values of the displacements

(referred to  $\underline{x}$ ) at node  $i$ . In writing Eq. (3.12), we assumed that a line that is straight and normal to the middle surface before deformation is still straight but not necessarily 'normal' to the middle surface after deformation. The strain energy corresponding to stress perpendicular to the middle surface is ignored to improve numerical conditioning when the three-dimensional element is employed. This constraint corresponds only to a part of the usual assumptions of a two-dimensional shell theory. The relaxation of the requirement that straight lines perpendicular to the middle surface remain normal to the deformed middle surface permits the shell to experience shear deformation - an important feature in thick shell situations.

### 3.3.2 Displacement Field in the Element

In the present study the current coordinates  $t_{x_i}$  are interpolated by the expression

$$t_{x_i} = \sum_{j=1}^n \psi_j (t_{x_i}^j + \frac{1}{2} \zeta h_j \hat{t}_{e_{3i}}^j) \quad (3.13)$$

and the displacement by

$$t_{u_i} = \sum_{j=1}^n \psi_j [t_{u_i}^j + \frac{1}{2} \zeta h_j (\hat{t}_{e_{3i}}^j - {}^0 e_{3i}^j)] \quad (3.14)$$

$$u_i = \sum_{j=1}^n \psi_j [u_i^j + \frac{1}{2} \zeta h_j (t^{+\Delta t} \hat{e}_{3i}^j - \hat{e}_{3i}^j)] \quad (3.15)$$

Here  $t_{u_i}^j$  and  $u_i^j$  denote, respectively, the displacement and incremental displacement components in the  $x_i$ -direction at the  $j$ -th node. The unit vectors  $\hat{e}_1^i$  and  $\hat{e}_2^i$  can be obtained from the relations

$$\hat{e}_1^i = (\hat{E}_2^x t_{e_3}^i) / |\hat{E}_2^x t_{e_3}^i|$$

$$\hat{e}_2^i = t_{e_3}^i x t_{e_1}^i \quad (3.16)$$

where  $\hat{E}_2$  is the unit vector along the (global)  $x_2$ -axis. If we assume that the angles  $\theta_1^i$  and  $\theta_2^i$  are very small, then we can write

$$\hat{e}_3^i = - t_{e_2}^i \theta_1^i + t_{e_1}^i \theta_2^i \quad (3.17)$$

Substituting Eq. (3.17) into Eq. (3.15), we obtain

$$u_i = \sum_{j=1}^n \psi_j [u_i^j + \frac{1}{2} \zeta h_j (- t_{e_2}^j \theta_1^j + t_{e_1}^j \theta_2^j)] \quad (3.18a)$$

or

$$\{u\} = [T]\{\Delta\} \quad (3.18b)$$

where  $\{u\}$  is the column of three displacements at a point,  $\{\Delta\}$  is the column of  $5n$  (five per node) displacements:  $u_i^j, \theta_1^j, \theta_2^j, j = 1, 2, \dots, n; i = 1, 2, 3$ , and  $[T]$  is the transformation matrix defined by Eq. (3.18a). Thus, for each time step one can find the normal vectors from Eq. (3.16) and (3.17) and the incremental displacements at each point from Eq. (3.18), once the five generalized displacements at each node are known. Next we discuss the procedure of determining the generalized displacements of an element.

### 3.3.3 Element Stiffness Matrix

The strain-displacement equations (3.4) can be expressed in the operator form

$$\{e\} = [A]\{u_o\} \quad (3.19)$$

where  $\{e\} = \{e_{11} \ e_{22} \ e_{33} \ 2e_{12} \ 2e_{13} \ 2e_{23}\}^T$ ,  $[A]$  is a function of  ${}^t u_{i,j}$ , and  $\{u_o\}$  is the vector of the components of the displacement gradient

$$\{u_o\} = \{u_{1,1} \ u_{1,2} \ u_{1,3} \ u_{2,1} \ u_{2,2} \ u_{2,3} \ u_{3,1} \ u_{3,2} \ u_{3,3}\}^T \quad (3.20)$$

The vector  $\{u_o\}$  is related to the displacement increments by

$$\{u_o\} = [N]\{u\} = [N][T]\{\Delta\} \quad (3.20)$$

and

$$\begin{aligned} \{e\} &= [A][N][T]\{\Delta\} \\ &\equiv [B]\{\Delta\} \end{aligned} \quad (3.21)$$

where  $[N]$  is the operator of differentials.

Substitution of Eq. (3.21) into Eq. (3.8) yields

$$\int_{V_o} \rho_o [T]^T \ddot{u} dv_o + ({}^t[K_L] + {}^t[K_{NL}])\{\Delta\} = {}^{t+\Delta t}\{R\} - {}^{t+\Delta t}\{F\} \quad (3.22)$$

where  ${}^t[K_L]$ ,  ${}^t[K_{NL}]$ ,  $\{R\}$ , and  $\{F\}$  are the linear and nonlinear stiffness matrices, force vector, and unbalanced force vectors:

$$\begin{aligned} {}^t[K_L] &= \int_{V_o} {}^t[B]^T [C] {}^t[B] dv_o, \quad {}^t[K_{NL}] = \int_{V_o} {}^t[B]^T [S] {}^t[B] dv_o \\ \{F\} &= \int_{V_o} {}^t[B]^T \{\hat{S}\} dv_o \end{aligned} \quad (3.23)$$

Here  $[S]$  and  $\{\hat{S}\}$  denote the matrix and vector, respectively, of the second Piola-Kirchhoff stress.

Since we are dealing with laminated composite structures, the important thing is how to perform the integration through the thickness. One way is to pick Gaussian points through the thickness and

then no explicit integration through the thickness is performed. The CPU time will be increased if the number of layers is increased, because the integration should be performed separately for each layer. The other way is to perform explicit integration through the thickness and reduce the integral to a two-dimensional problem. The Jacobian matrix, in general, is a function of  $\xi_1$ ,  $\xi_2$ , and  $\zeta$ . Zienkiewicz, et al. [35] suggested that terms in  $\zeta$  to the first power may be neglected, provided the thickness-to-curvature ratios are small. This approximation implies that the derivatives of  $x_i$  with respect to  $\xi_1$ ,  $\xi_2$ , and  $\zeta$  are substantially the same at either end of a mid-surface-normal line. Thus, the Jacobian  $[J]$  becomes independent of  $\zeta$  and explicit integration can be employed. If  $\zeta$  terms are retained in  $[J]$ , Gaussian points through the thickness should be added. In the present study, it is assumed that the Jacobian is independent of  $\zeta$ .

#### 3.3.4 Time Integration and Mass Matrix

Any attempt to solve Eq. (3.22), whether by direct integration or by modal analysis, should take advantage of the symmetry and bandedness of the stiffness matrix. The initial conditions for Eq. (3.22) are the displacements and velocities at time  $t = 0$ ; therefore, the direct integration requires the information at the previous time  $t$ , in order to predict the state of motion at the current time  $t+\delta t$ . The direct integration techniques can be divided into two types: explicit and implicit integrations (see [41-45]). In explicit integration, we solve  $\underline{u}$  at time  $t+\delta t$  based on the equilibrium conditions of the structure at time  $t$ . The central difference method is an example of explicit integration method. In the implicit method the solution at time  $t+\delta t$  is based on the equilibrium condition of the structure at



time  $t+\Delta t$ . The Houbolt, Wilson, and Newmark methods provide examples of the implicit method. In the present study the Newmark direct integration scheme is employed.

The Newmark integration scheme can be thought of as an extension of the linear acceleration method:

$${}^{t+\Delta t}\{\Delta\} = {}^t\{\Delta\} + \Delta t^2\{\ddot{\Delta}\} + \left[\left(\frac{1}{2} - \beta\right){}^t\{\ddot{\Delta}\} + \beta {}^{t+\Delta t}\{\ddot{\Delta}\}\right](\Delta t)^2 \quad (3.24)$$

$${}^{t+\Delta t}\{\dot{\Delta}\} = {}^t\{\dot{\Delta}\} + [(1 - \gamma){}^t\{\ddot{\Delta}\} + \gamma {}^{t+\Delta t}\{\ddot{\Delta}\}]\Delta t$$

where  $\{\Delta\}$  is the generalized displacement vector of any point and  $\beta$  and  $\gamma$  are the dimensionless parameters of generalized acceleration. Chan et al. [46] have discussed the special case  $\beta = \frac{1}{12}$  and  $\gamma = \frac{1}{2}$ , which coincides with a procedure developed by Fox and Goodwin [47]. For the constant average acceleration we have  $\beta = \frac{1}{3}$  and  $\gamma = \frac{1}{2}$ , and for the linear acceleration  $\beta = \frac{1}{6}$  and  $\gamma = \frac{1}{2}$ .

To apply the Newmark integration scheme to the equilibrium equations (3.22), we start from

$${}^{t+\Delta t}\{\Delta\}^{(k)} = {}^{t+\Delta t}\{\Delta\}^{(k-1)} + \{\Delta\}^{(k)} \quad (3.25)$$

where  $k$  is the iteration number. The velocity and acceleration of any point in the element can be written as

$$\dot{u}_i = \sum_{j=1}^n \psi_j \dot{u}_i^j + \sum_{j=1}^n \frac{1}{2} \psi_j \chi_j (\dot{e}_{3i}^j - \dot{e}_{3i}^j) \quad (3.26)$$

ORIGINAL PAGE IS  
OF POOR QUALITY

$$\ddot{u}_i = \sum_{j=1}^n \psi_j \ddot{u}_j + \sum_{i=1}^n \frac{1}{2} \psi_j \chi_j (\ddot{e}_{3i}^j - \ddot{e}_{3i}^j) \quad (3.27)$$

Since we are dealing with transient problems, the load vector  $\{R\}$  can be a function of time. From Eq. (3.27) we have for the  $i$ -th component

$$\begin{aligned} t+\Delta t \ddot{\Delta}_i &= a_0 (t+\Delta t \ddot{\Delta}_i - t \ddot{\Delta}_i) - a_2 \dot{\Delta}_i - a_3 \ddot{\Delta}_i \\ t+\Delta t \dot{\Delta}_i &= \dot{\Delta}_i + a_4 \ddot{\Delta}_i + a_5 t+\Delta t \ddot{\Delta}_i \end{aligned} \quad (3.28)$$

where

$$\begin{aligned} a_0 &= \frac{1}{\beta(\Delta t)^2} , \quad a_1 = \frac{\gamma}{\beta \Delta t} , \quad a_2 = \frac{1}{\beta \Delta t} \\ a_3 &= \frac{1}{2\beta} - 1 , \quad a_4 = \Delta t(1 - \gamma) , \quad a_5 = \gamma \Delta t \end{aligned} \quad (3.29)$$

Substituting Eq. (3.22) into Eq.(3.28), we obtain

$$\begin{aligned} t+\Delta t \ddot{e}_{3i}^j &= a_0 (\theta_1^j \hat{e}_{2i}^j - \theta_2^j \hat{e}_{1i}^j) - a_2 \dot{e}_{3i}^j - a_3 \ddot{e}_{3i}^j + \ddot{e}_{3i}^j \\ t+\Delta t \dot{e}_{3i}^j &= \dot{e}_{3i}^j + a_4 \ddot{e}_{3i}^j + a_5 t+\Delta t \ddot{e}_{3i}^j \end{aligned} \quad (3.30)$$

Finally the complete approximation of the equations of motion over an element becomes

$$(a_0 t[M] + t[K])\{\Delta^{(k)}\} = t+\Delta t \{R\} - t+\Delta t \{F^{(k-1)}\}$$

$$+ a_2 [\dot{t}\{P_1\} - \frac{1}{\Delta t} (\dot{t}\{P_2\} - \dot{t}\{P_3\})] + a_3 \{P_4\} \quad (3.31)$$

where

$$\begin{aligned} [M] &= \int_{V_0} \rho_0 \dot{t}[T]^T \dot{t}[T] dV_0 \\ \{P_1\} &= \int_{V_0} \rho_0 \dot{t}\{\dot{\Delta}\} [T] dV_0 \\ \{P_2\} &= \int_{V_0} \rho_0 \dot{t}^{t+\Delta t}\{\Delta\}^{(k-1)} [T] dV_0 \\ \{P_3\} &= \int_{V_0} \rho_0 \dot{t}\{\Delta\} [T] dV_0 \\ \{P_4\} &= \int_{V_0} \rho_0 \dot{t}\{\ddot{\Delta}\} [T] dV_0 \end{aligned} \quad (3.32)$$

Equation (3.31) can be expressed in the following final form:

$$[\hat{K}]\{\Delta\} = \dot{t}^{t+\Delta t}\{\hat{R}\} - \dot{t}^{t+\Delta t}\{F\}^{(k-1)} \quad (3.33)$$

where

$$[\hat{K}] = a_0 \dot{t}[M] + \dot{t}[K]$$

$$\dot{t}^{t+\Delta t}\{\hat{R}\} = \dot{t}^{t+\Delta t}\{R\} + a_2 [\dot{t}\{P_1\} - \frac{1}{\Delta t} (\dot{t}\{P_2\} - \dot{t}\{P_3\})] + a_3 \{P_4\} \quad (3.34)$$

This completes the finite-element formulation of the 3-D degenerated element.

## CHAPTER IV

### NUMERICAL VALIDATION OF THE ELEMENTS

#### 4.1 Introduction

The present chapter is devoted to the validation of the finite elements developed herein based on the two-dimensional shell theory and three-dimensional continuum theory. The elements are validated by comparing the present results with those available in the literature for static bending, natural vibration, and transient response of isotropic plates and shells. Numerical results are presented to bring out the limitations and restrictions of the present elements. All of the results presented here were obtained on an IBM 370/3081 computer with double precision arithmetic.

The results to be discussed are grouped into three major categories: (1) static bending, (2) natural vibration, and (3) transient response. All results, except for the vibrations, are presented in a graphical form.

#### 4.2 Static Analysis

Here we present a discussion of four example problems, all involving shell structures.

##### 4.2.1 Cylindrical Panel Under the Influence of Gravity (i.e., under its own weight)

Consider the circular cylindrical panel shown in Fig. 4.1. The geometric parameters and material properties are listed below:

$R = 25.0 \text{ ft}$	$E = 3 \times 10^6 \text{ psi}$
$a = 25.0 \text{ ft}$	$\nu = 0.0$
$h = 3.0 \text{ in.}$	$g = 90 \text{ psi}$
$\theta = 40^\circ$	

ORIGINAL PAGE IS  
OF POOR QUALITY

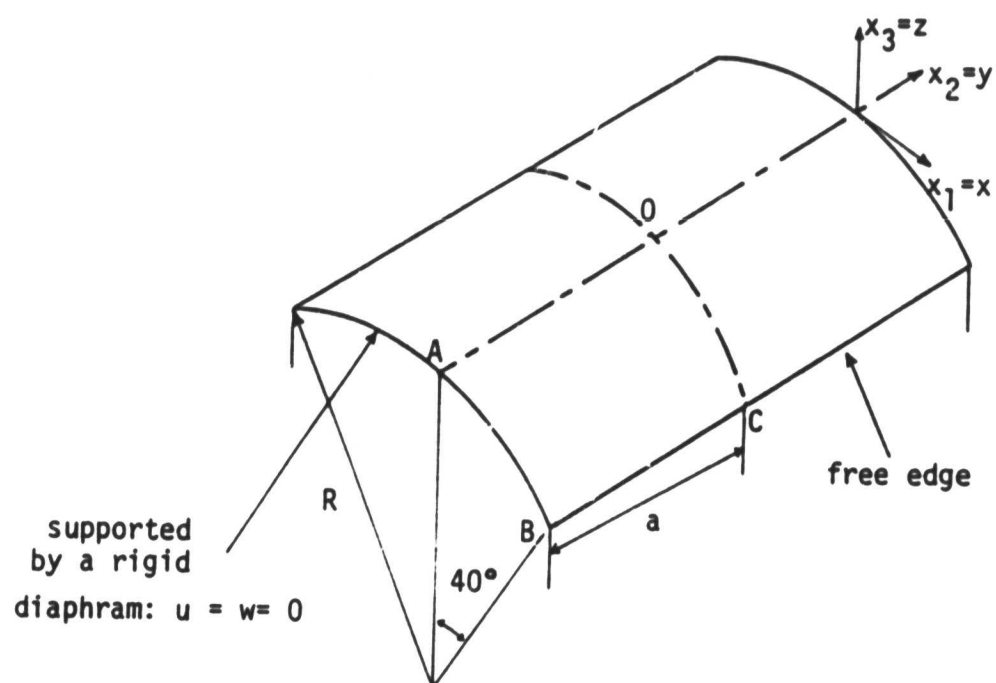


Figure 4.1 Geometry of the cylindrical shell used in Problem 1 of Section 4.1

The panel is supported on rigid diaphragms on the curved edges and free on the straight edges. We wish to find the deformation of the panel under its own weight. Many authors have employed this problem as a standard test problem for checking new elements or numerical schemes. The radial displacements along the central curved line are shown in Fig. 4.2 for both the 3-D element and the 2-D deformable shell element. The longitudinal displacements along the supported edges are shown in Fig. 4.3. A uniform mesh of  $2 \times 2$  eight-node elements was used in one quadrant for this analysis. The solutions agree very closely with those obtained in Reference [48].

#### 4.2.2 Cylindrical Shell Subjected to Radial Pressure

Consider the circular cylindrical panel shown in Fig. 4.4. The shell is clamped along four edges and subjected to uniform radial inward pressure. The loading is nonconservative, that is, the direction of the applied load is normal to the cylindrical surface at any time during the deformation. The geometric and material properties are

$$R = 2540 \text{ mm}, a = b = 254 \text{ mm}, h = 3.175 \text{ mm},$$

$$\theta = 0.1 \text{ rad}, E = 3.10275 \text{ kN/mm}^2, \nu = 0.3$$

Due to the symmetry of the geometry and deformation, only one quarter of the panel is analyzed. A load step of  $0.5 \text{ kN/m}^2$  was used in order to get a close representation of the deformation path. Fig. 4.5 shows the central deflection versus the pressure for the first of the three sets of panel dimensions:

(i)  $a = 254 \text{ mm}, b = 254 \text{ mm}$  ( deep shell)

(ii)  $a = 635 \text{ mm}, b = 635 \text{ mm}$

(iii)  $a = 1270 \text{ mm}, b = 1270 \text{ mm}$  ( shallow shell)

In cases (ii) and (iii) the analysis was limited to linear solutions.

ORIGINAL PAGE IS  
OF POOR QUALITY

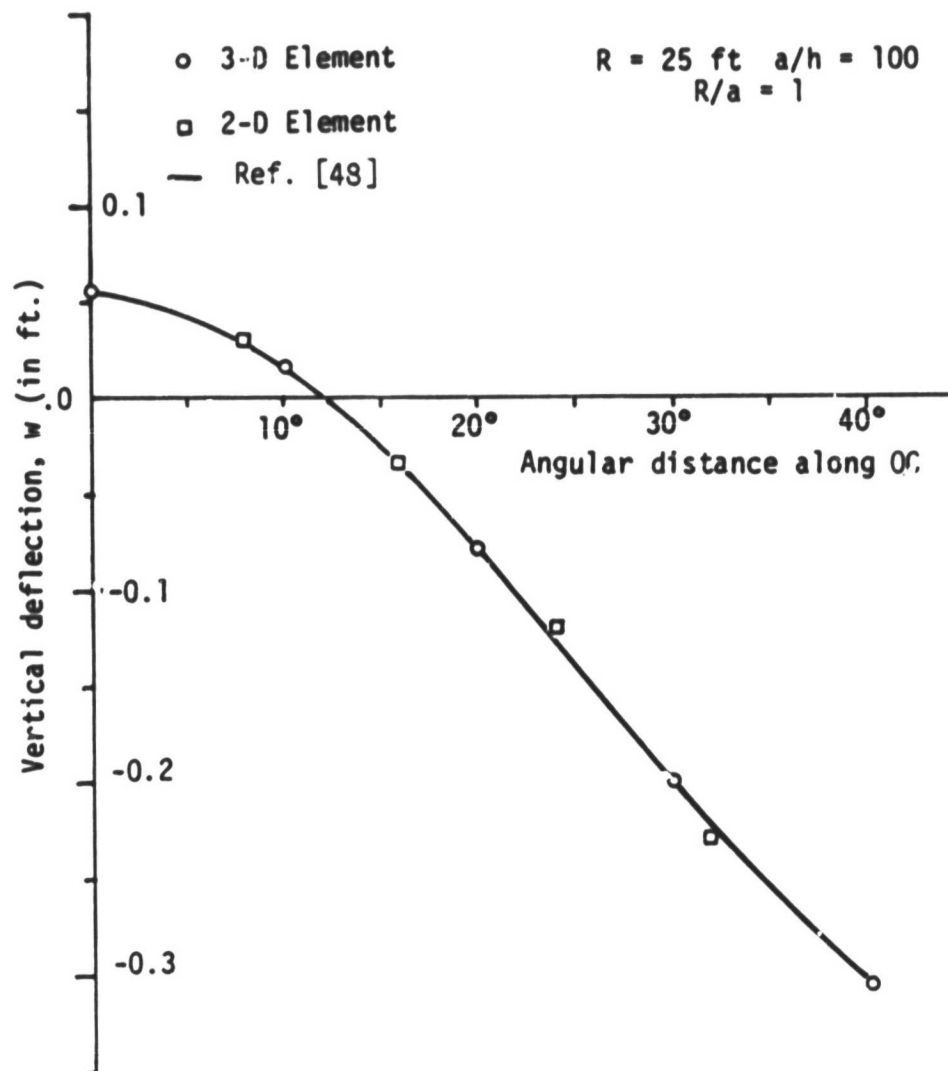


Figure 4.2 Vertical deflection along the midsection OC  
(see Fig. 4.1 for the geometry)

ORIGINAL PAGE IS  
OF POOR QUALITY

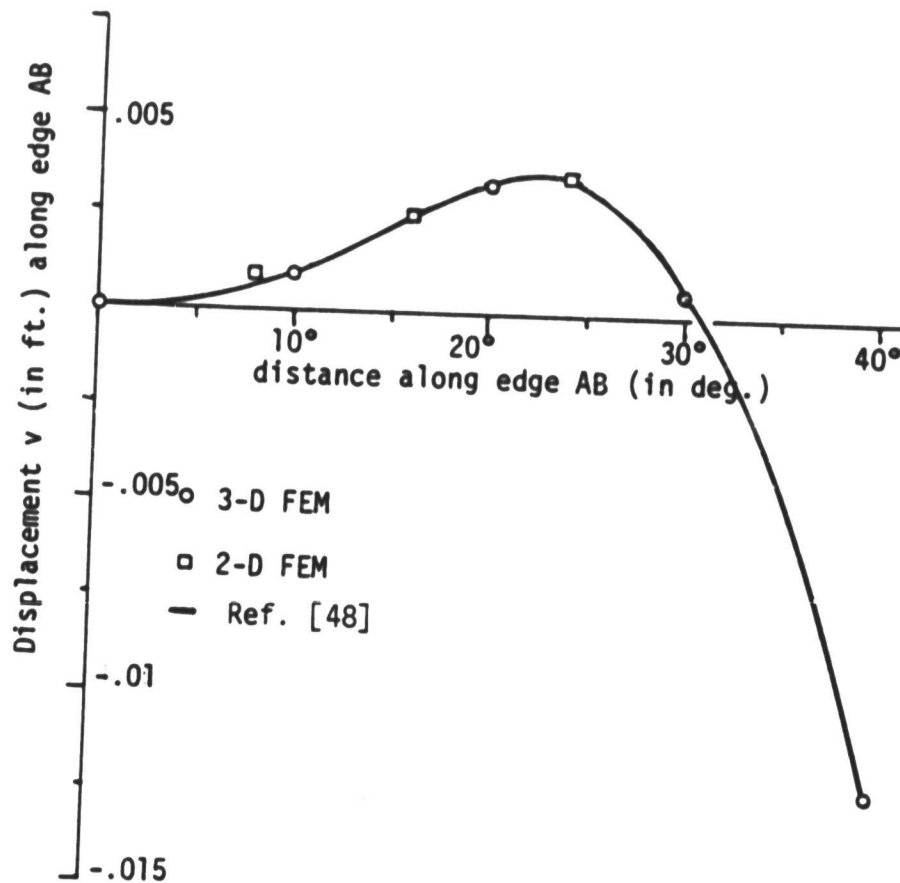


Figure 4.3 Displacement  $v$  along the supported edge AB



ORIGINAL PAGE IS  
OF POOR QUALITY

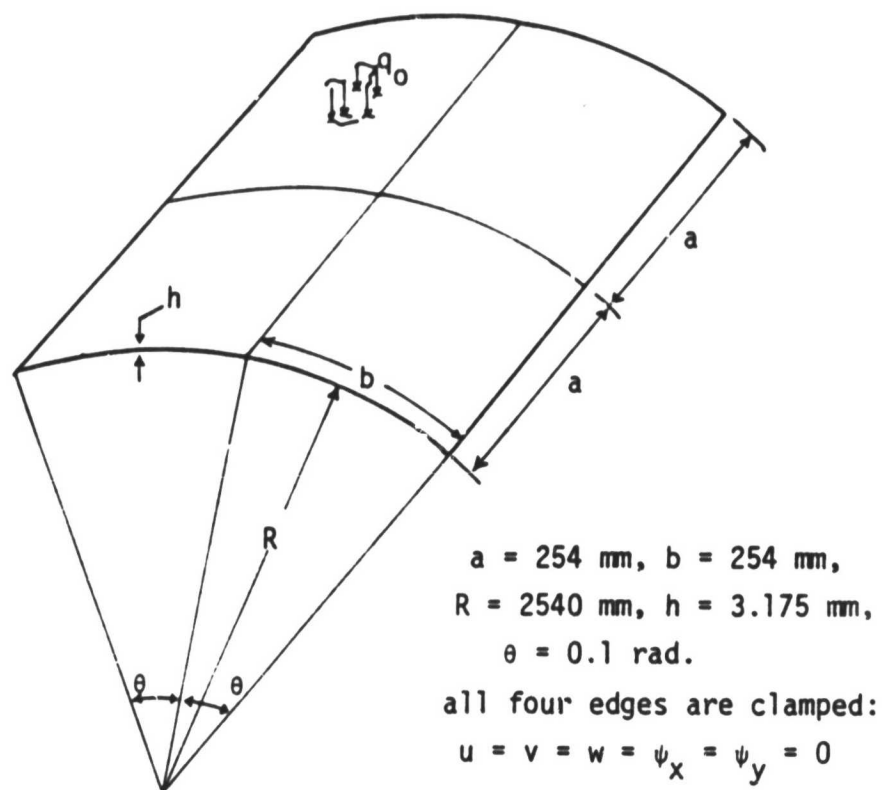


Figure 4.4 Geometry of the cylindrical shell problem discussed in Section 4.2.2.

ORIGINAL PAGE IS  
OF POOR QUALITY

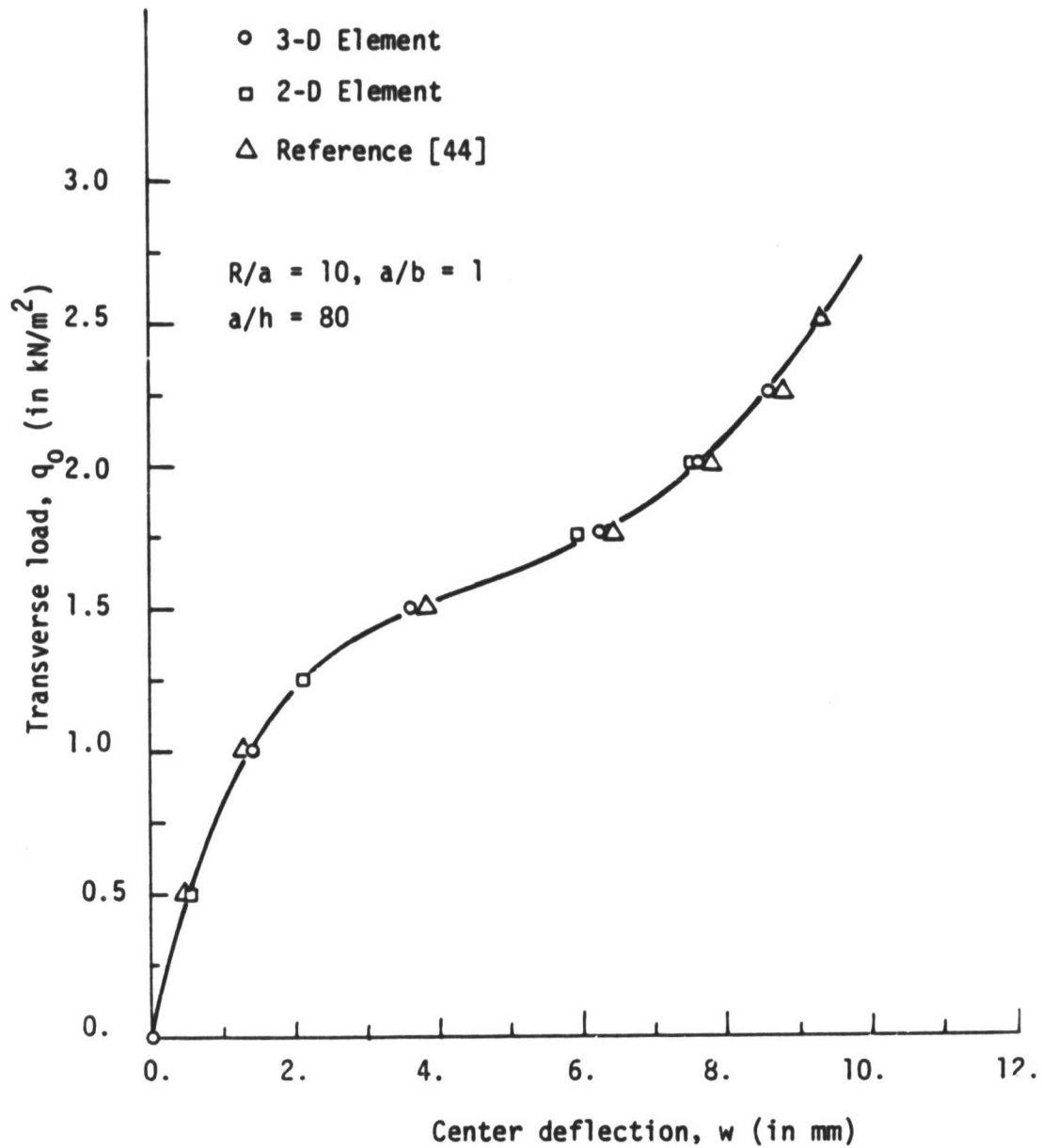


Figure 4.5 Load-deflection curve for the clamped cylindrical shell problem discussed in Section 4.2.2

Table 4.1 contains a comparison of the center deflections obtained by using the two elements for various meshes. From the results presented in the table it is clear that for shallow shells both elements give almost the same results. The difference in the deflections predicted by the two elements increases as the shell becomes shallow (case (iii)).

#### 4.2.3 Cylindrical Shell Subjected to Center Point Load

Figure 4.6 shows a circular cylindrical shell which has the same geometric (except,  $h = 12.7$  mm) and material properties as the one in Problem 2. The longitudinal boundaries are hinged and immovable, and the curved edges are free. A concentrated point load is applied at the center. One quarter of the panel was analyzed using a  $2 \times 2$  mesh of nine-node quadrilateral elements. The load step is 0.5 kN. Figure 4.7 contains the plot of the central deflection versus the load. The results agree very closely with those obtained by Dhatt [49].

#### 4.2.4 Spherical Shell Subjected to Point Load at the Center

The spherical shell shown in Fig. 4.8 is subjected to a concentrated load  $P$  at the crown. The boundaries are all hinged and immovable. The geometric parameters and material properties are given below:

$$R_1 = R_2 = 2540 \text{ mm}$$

$$a = b = 784.9 \text{ mm}$$

$$h = 99.45 \text{ mm}$$

$$E = 68.95 \text{ N/mm}$$

$$\nu = 0.3$$

One quarter of the shell was analyzed by a  $2 \times 2$  mesh of nine node quadrilateral elements. The load step is 10 kN. Figure 4.9 contains a

Table 4.1 Comparison of linear center deflections obtained by the 2-D and 3-D elements for Problem 2.

Case	Mesh	3-D	2-D
(i)	2x2	0.52579	0.52321
	3x3	0.52505	0.52265
(ii)	2x2	0.35888	0.39431
	3x3	0.3205	0.34228
(iii)	2x2	0.30636	0.37667
	3x3	0.28674	0.27021

ORIGINAL PAGE IS  
OF POOR QUALITY

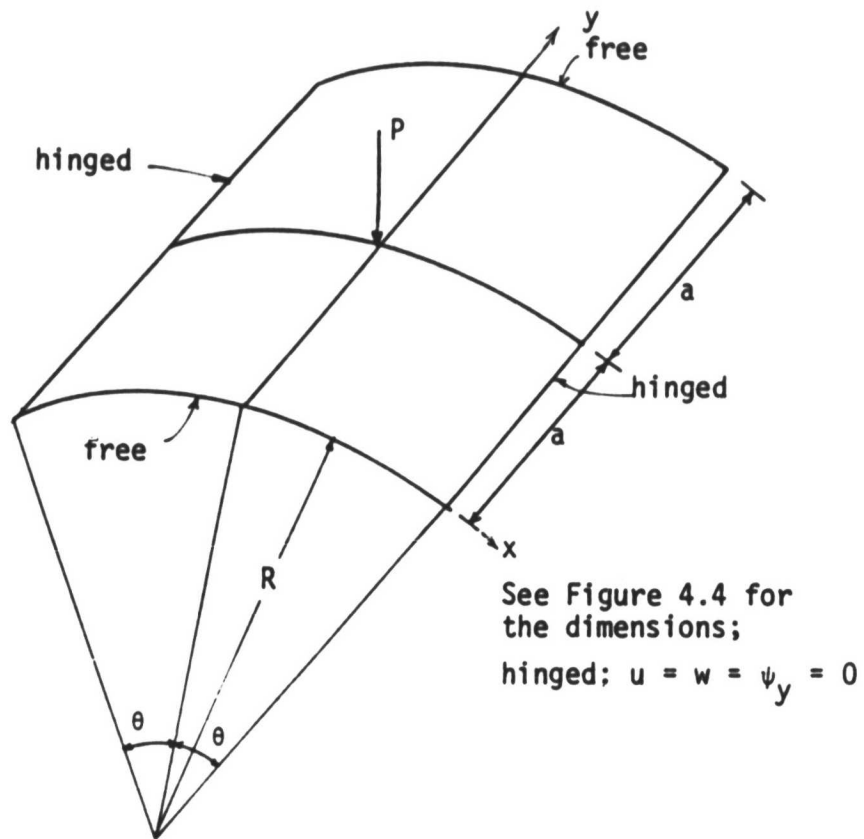


Figure 4.6 Geometry of the cylindrical shell problem discussed in Section 4.2.3

ORIGINAL PAGE IS  
OF POOR QUALITY

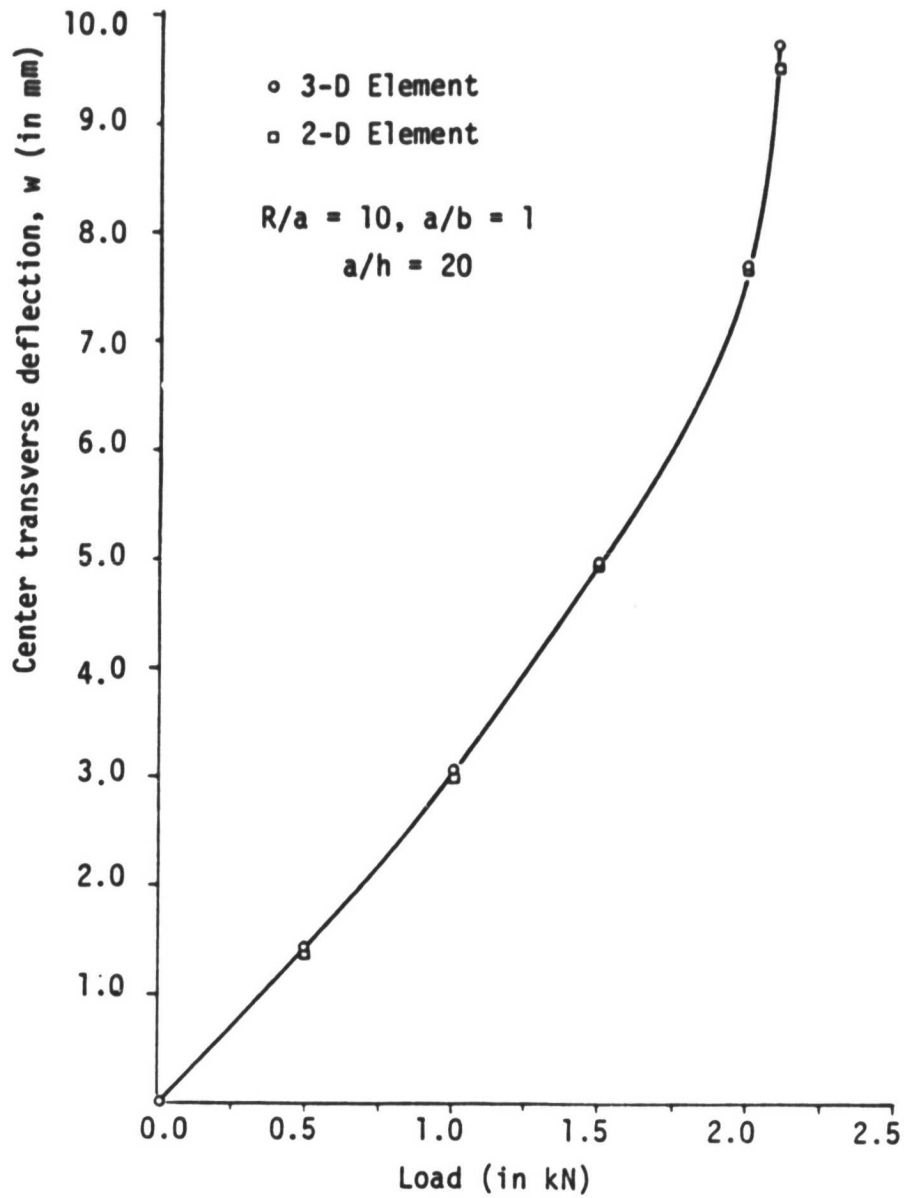


Figure 4.7 Load-deflection curve for the cylindrical shell problem discussed in Section 4.2.3

ORIGINAL PAGE IS  
OF POOR QUALITY

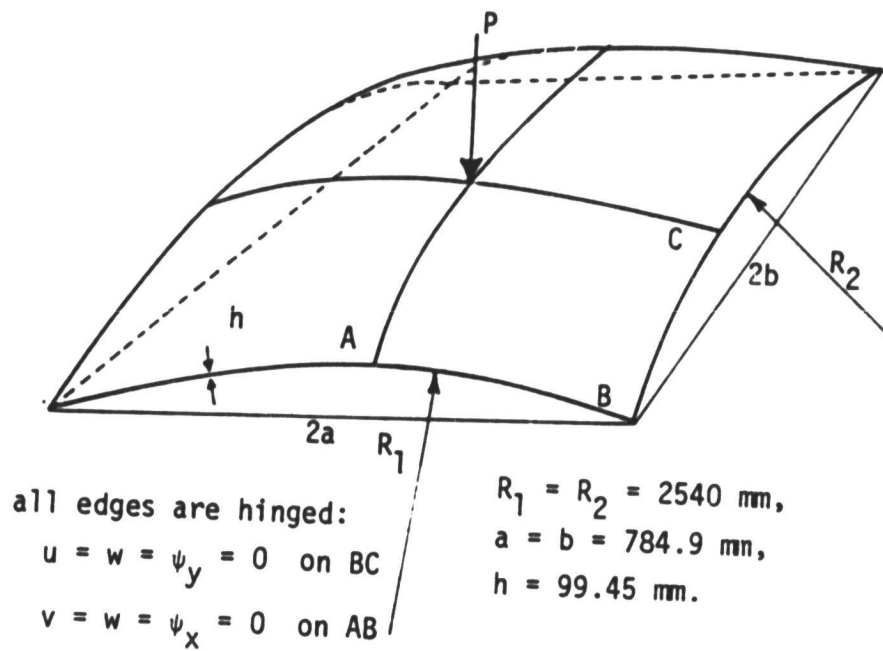


Figure 4.8 Geometry of the spherical shell discussed in Section 4.2.4.

comparison of the center deflections obtained using the 2-D and 3-D elements, which agree with that of Leicester [50], who used a shallow shell 2-D finite element.

#### 4.3 Natural Vibration of Cantilevered Twisted Plates

Here we discuss the results obtained for natural frequencies of cantilevered twisted plates. This analysis was motivated by their relevance to natural vibrations of turbine blades. Consider a cantilevered plate with a twist angle  $\theta$  at the free end. The plate is made of an isotropic material. Table 4.2 contains the natural frequencies of a square plate for various values of the twist angle  $\theta$ . A 2x2 mesh and 4x4 mesh of nine-node elements are employed to study the convergence trend. The results of the refined mesh are included in the parentheses. The results agree with many others published in a recent NASA report. Tables 4.2-4.5 contain natural frequencies of twisted plates for various aspect ratios and side-to-thickness ratios.

#### 4.4 Transient Analysis

Here we present results of the nonlinear transient analysis of a cantilevered beam and a spherical shell. Both problems have been solved by other investigators.

##### 4.4.1 Cantilevered Beam Under Uniformly Distributed Load

Consider a cantilever beam under a uniformly distributed transverse step load, as shown in Fig. 4.10. The geometric parameters and material properties are given below:

$$L = 10 \text{ in}$$

$$h = 1 \text{ in}$$

$$b = 1 \text{ in}$$

ORIGINAL PAGE IS  
OF POOR QUALITY



ORIGINAL PAGE IS  
OF POOR QUALITY

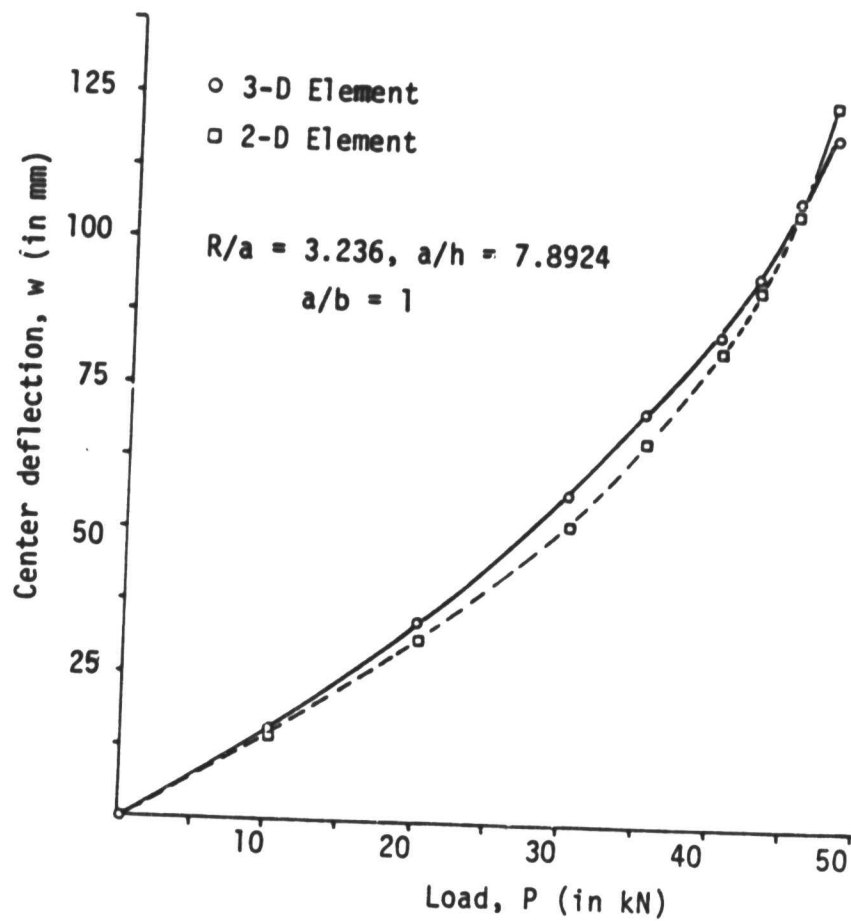


Figure 4.9 Load-deflection curve for the spherical shell problem discussed in Section 4.2.4

Table 4.2 Natural Frequencies of Twisted Plate Vibration ( $a/b = 1$ ,  $a/h = 20$ )

$$\bar{\omega} = \omega a^2 \sqrt{\rho h / D}, \quad D = \frac{E h^3}{12(1-\nu^2)}, \quad \nu = 0.3$$

Twist Angle	Mode					
	1	2	3	4	5	6
0°	* 3.4556 ** (3.4583)	8.4110 (8.3353)	22.0999 (21.0238)	28.2089 (26.7465)	31.9740 (30.1454)	55.1625 (52.0784)
15°	3.4359	10.2920	21.5199	27.2054	32.7430	44.5375
30°	3.3790 (3.3694)	13.7014 (14.2222)	19.9840 (18.9795)	25.0943 (26.8104)	34.3341 (34.4591)	45.8987 (45.7547)
45°	3.2908	18.1009	15.9097	23.5680	35.5332	45.7013
60°	6.1800	17.8319	15.5635	24.1842	36.1466	44.9152

\* 2 x 2, 9-node mesh

\*\* 4 x 4, 9-node mesh

Table 4.3 Natural Frequencies of Twisted Plate Vibration ( $b/a = 3$ ,  $a/h = 20$ ,  $3 \times 3$ , 9-node mesh)

$$\bar{\omega} = \omega b^2 \sqrt{\rho h / D} \quad , \quad D = \frac{E h^3}{12(1-\nu^2)} \quad , \quad \nu = 0.3$$

Twist Angle	1	2	3	Mode 4	5	6	7
0°	3.4150	20.8772	21.6190	65.9706	66.2590		127.256
15°	3.4009	20.8798	22.1118	21.6032	68.0938	69.3258	130.284
30°	3.3598	19.4048	25.3743	60.2183	73.5180	77.4493	138.176
45°	3.2956	17.5289	29.8404	58.2600	80.9488	88.5246	148.8975
60°	3.2136	15.7431	34.8827	55.8921	89.2028	100.7760	155.070

Table 4.4 Natural Frequencies of Twisted Plate Vibration ( $a/b = 1$ ,  $a/h = 5$ )

$$\bar{\omega} = \omega b^2 \sqrt{\rho h / D} \quad , \quad D = \frac{E h^3}{12(1-\nu^2)} \quad , \quad \nu = 0.3$$

Twist Angle	Mode					
	1	2	3	4	5	6
0°	* 3.33916 **(3.3390)	7.3948 (7.3559)	10.8083 (10.883)	18.4930 (17.757)	23.7907 (22.769)	26.0552 (24.125)
15°	3.31713 (3.3170)	7.4816 (7.4504)	10.8053 (10.774)	18.4043 (17.771)	23.6767 (22.694)	24.9474 (24.083)
30°	3.2538 (3.2538)	7.7593 (7.7089)	10.5248 (10.478)	18.4091 (17.795)	23.3734 (22.471)	24.6116 (23.943)
45°	3.1570 (3.1569)	8.1435 (8.0728)	10.1270 (10.062)	18.3843 (17.79)	22.9126 (22.117)	24.0566 (23.651)
60°	3.0370 (3.0366)	8.5855 (8.4814)	9.67198 (8.5911)	18.3089 (17.730)	22.3670 (21.684)	23.3533 (23.160)

\* 2 x 2,9-node mesh

\*\*3 x 3,9-node mesh

Table 4.5 Natural Frequencies of Twisted Plate Vibration ( $b/a = 3$ ,  $a/h = 5$ ,  
3 x 3,9-node mesh )

$$\bar{\omega} = \omega b^2 \sqrt{\rho h/D} \quad , \quad D = \frac{Eh^3}{12(1-\nu^2)} \quad , \quad \nu = 0.3$$

Twist angle	1	2	3	Mode	4	5	6
0°	3.3908	15.551	19.124		21.065	59.924	61.949
15°	3.3161	15.192	19.231		21.572	60.088	60.830
30°	3.3336	14.379	19.549		22.811	60.576	58.472
45°	3.2674	13.449	20.060		24.404	61.360	55.874
60°	3.1833	12.548	20.741		26.139	62.416	53.381

ORIGINAL PAGE IS  
OF POOR QUALITY

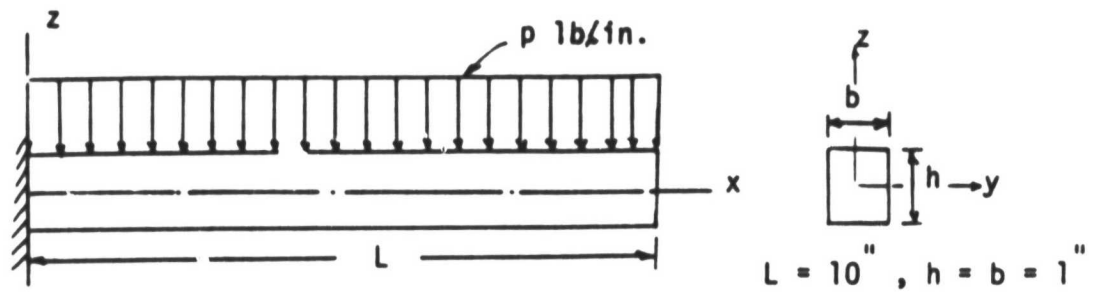


Figure 4.10 Cantilevered beam under uniformly distributed load

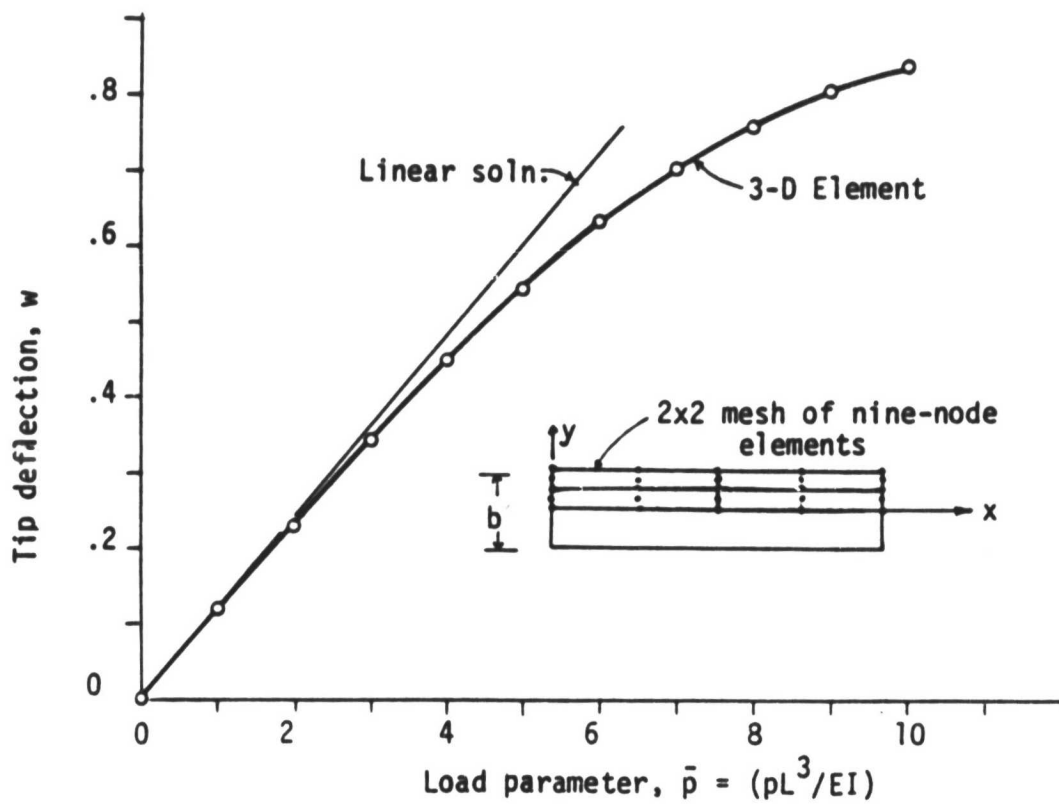


Figure 4.11 Load-deflection curve for the static bending of the cantilevered beam shown in Figure 4.10

ORIGINAL PAGE IS  
OF POOR QUALITY

$$E = 1.2 \times 10^6 \text{ psi}$$

$$\nu = 0.2$$

$$\rho = 10 \text{ lb sec}^2/\text{in}^4$$

The cantilever is analyzed using four nine-node 2-D shell and 3-D degenerated elements (see Fig. 4.11). The load applied is nonconservative, because the load follows the deformed beam and stays normal to it at all times. Figure 4.11 shows the tip deflection versus load obtained in the static analysis. Figure 4.12 contains plots of tip deflection versus time; obtained using the 2-D and 3-D elements and by Bathe et al. [37]. The time step employed is  $1.35 \times 10^{-4}$  sec. The reason for the difference between the solutions predicted by the shell element and 3-D element is that the load in the 3-D element follows the deformed shape and is perpendicular to the deformed beam, whereas in the 2-D shell theory it is always vertical. Consequently, the vertical load component is larger in the 2-D shell element than in the 3-D element, and thus explains the difference in the solutions.

#### 4.4.2 Spherical Cap Under Axisymmetric Pressure Loading

Consider a spherical cap, clamped on the boundary and subjected to axisymmetric pressure loading. The geometric and material properties are

$$R = 22.27 \text{ in}$$

$$h = 0.41 \text{ m}$$

$$E = 10.5 \times 10^6 \text{ psi}$$

$$\nu = 0.3$$

$$\rho g = 0.095 \text{ lb/in}^3$$

$$\theta = 26.67^\circ$$

$$p_0 = 100 \text{ psi}$$

ORIGINAL PAGE IS  
OF POOR QUALITY

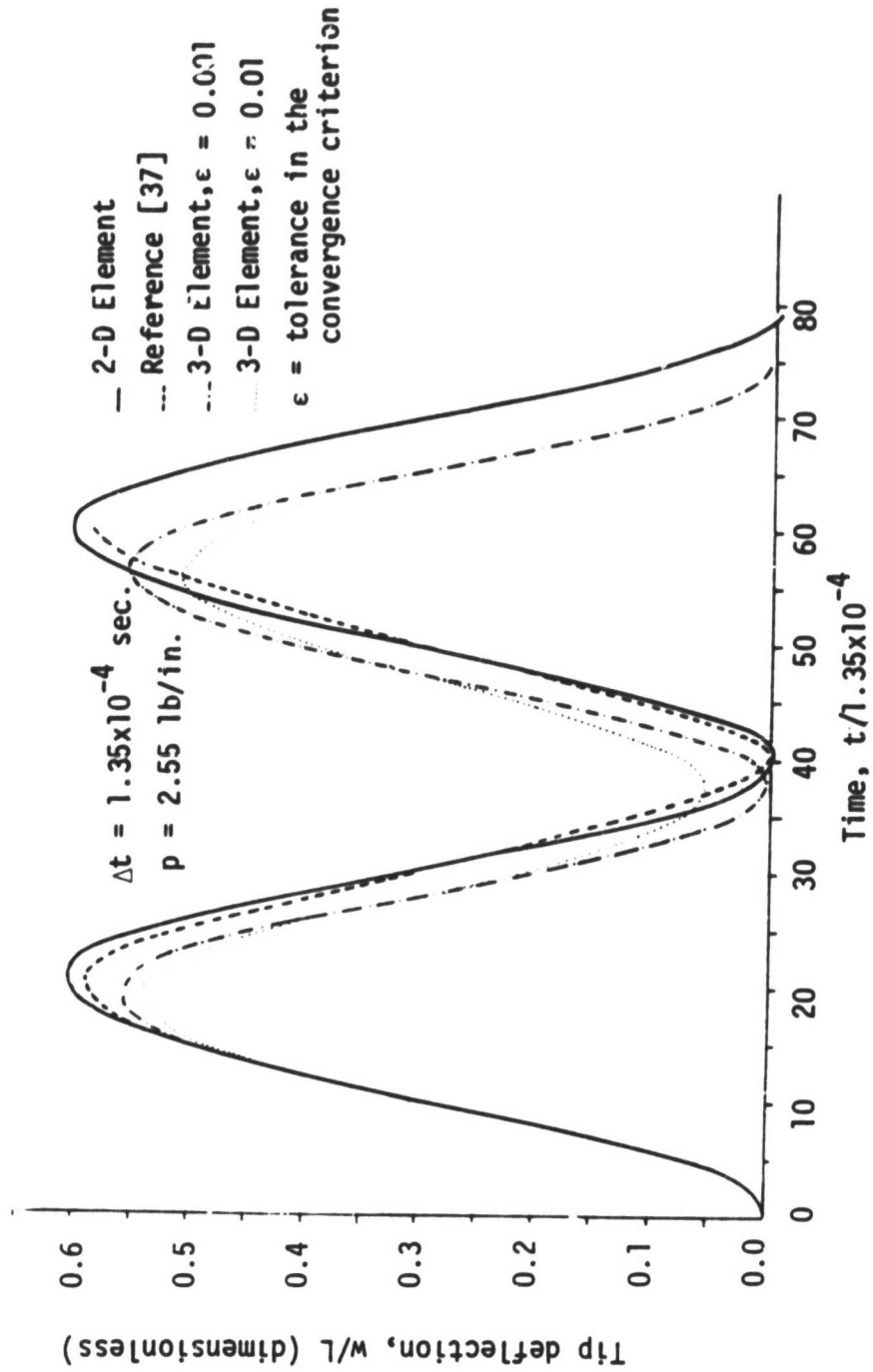


Figure 4.12 Nonlinear deflection at the tip of the cantilevered beam  
(transverse deflection vs. time)



$$\Delta t = 10^{-5} \text{ sec}$$

This problem has been analyzed by Stricklin, et al. [51] using an axisymmetric shell element. In the present study the spherical cap is discretized into five nine-node 2-D and 3-D elements. Fig. 4.13 shows the center deflection versus time. The present solutions are in excellent agreement in most places with that of Stricklin et al. [51]. The difference between the solutions is mostly in the regions of local minima and maxima.

ORIGINAL PAGE IS  
OF POOR QUALITY

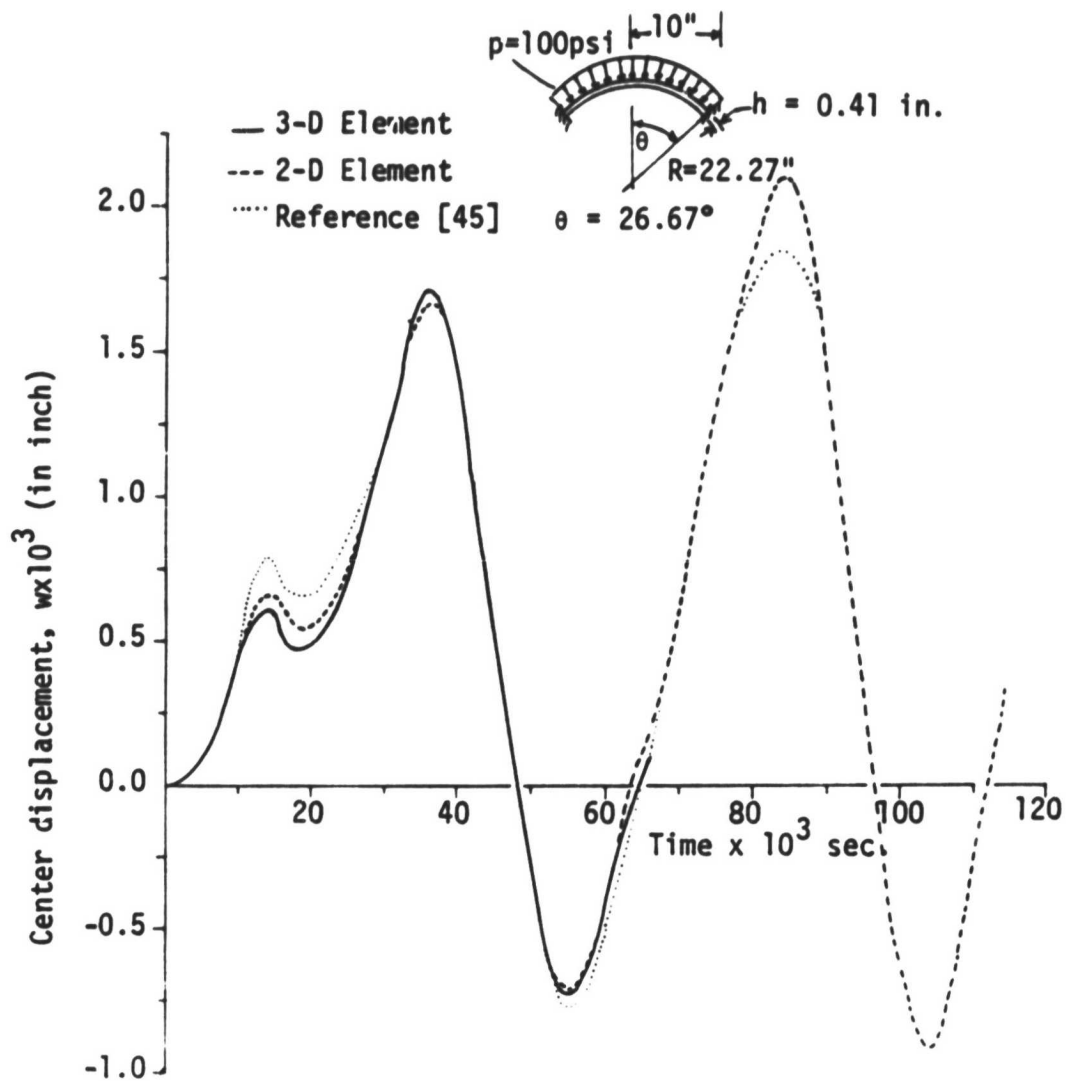


Figure 4.13 Center transverse displacement versus time for a spherical cap under axisymmetric dynamic loading (load = 100 psi.)

## CHAPTER V

## NUMERICAL RESULTS FOR COMPOSITE PLATES AND SHELLS

5.1 Introduction

In this chapter we discuss the numerical results obtained by the 2-D and 3-D elements for the nonlinear analysis of layered anisotropic composite plates and shells. Most of the results presented here are new and therefore cannot be compared with other results to make quantitative judgements concerning their accuracy. Results for both static bending and transient response are discussed.

5.2 Static Analysis5.2.1 Orthotropic Cylinder Subjected to Internal Pressure

Consider a clamped orthotropic ( $E_2 = 2.0 \times 10^6$  psi,  $E_1/E_2 = 3.75$ ,  $G_{12}/E_2 = 0.625$ ,  $\nu = 0.25$ ) cylinder of radius  $R = 20$  in and length 20 in, and subjected to internal pressure  $p_0 = 6.41 \pi$  psi (see Fig. 5.1). The problem was analyzed, for linear deflections only, by Rao [21] using shallow thin shell elements. A mesh of  $2 \times 2$  nine-node elements is used in an attempt to analyze the problem. The linear center deflections obtained by the 2-D and 3-D elements are 0.0003764 in., and 0.0003739 in., respectively. These values compare favorably with 0.000366 in. of Rao [21] and 0.000367 of Timoshenko's analytical solution [52]. The latter two solutions are based on classical shell theory.

In the large-deflection analysis the present results are compared with those of Chang and Sawamiphakdi [30]. A value of 2.5 ksi is used for the load step. Figure 5.2 shows a comparison of the present deflection with that of [30], which used a 3-D degenerated element based on an updated Lagrangian approach. The agreement is very good.

ORIGINAL PAGE IS  
OF POOR QUALITY

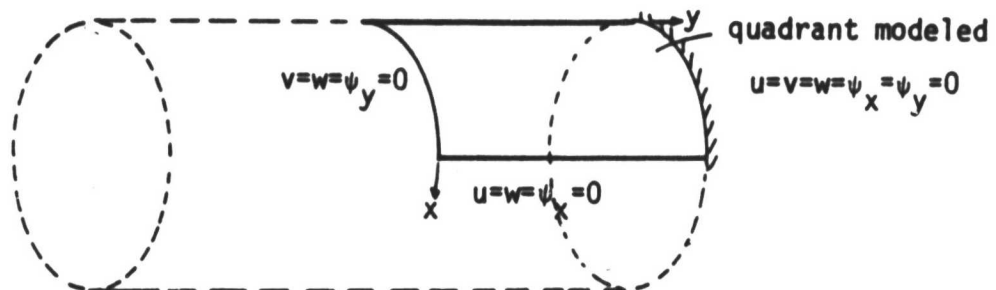
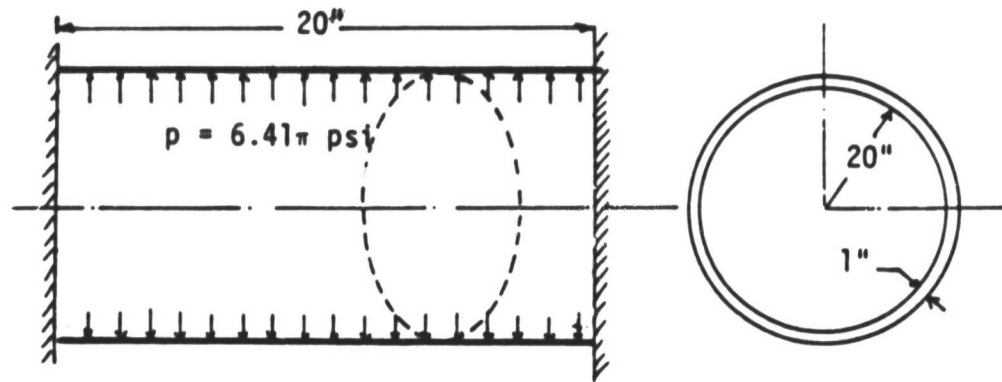


Figure 5.1 Geometry of the cylindrical shell problem  
discussed in Section 5.2.1

ORIGINAL PAGE IS  
OF POOR QUALITY

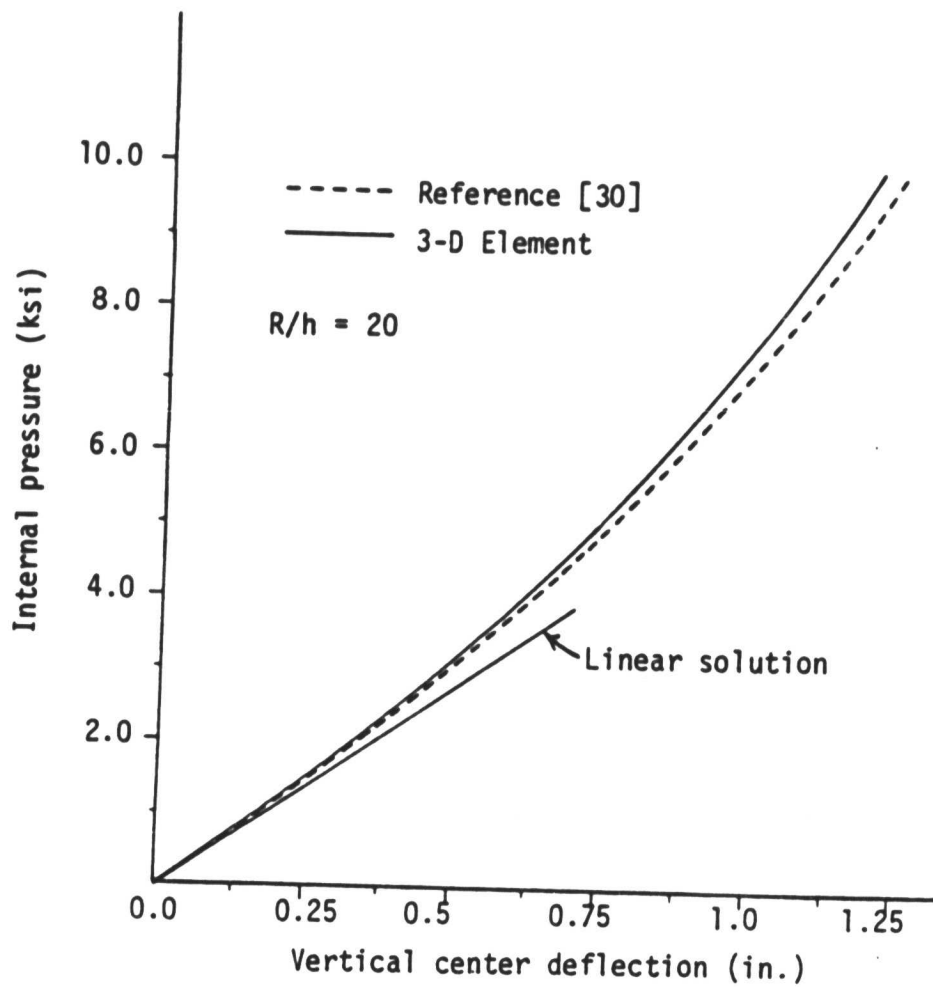


Figure 5.2 Center transverse deflection versus  
internal pressure

### 5.2.2 Nine-Layer Cross-Ply Spherical Shell Subjected to Uniform Loading

Consider a spherical shell cross-ply laminated of nine layers of graphite-epoxy material ( $E_1/E_2 = 40$ ,  $G_{23}/E_2 = 0.6$ ,  $G_{13} = G_{12} = 0.5 E_2$ , and  $\nu_{12} = 0.3$ ), subjected to uniformly distributed loading, and simply supported on all its edges (i.e., transverse deflection and tangential rotations are zero). In Fig. 5.3, a comparison of the load-deflection curves obtained by the present elements with those obtained by Noor and Hartley [29] is presented (for the parameters  $h/a = 0.01$  and  $R/a = 10$ ). The results agree very well with each other, the present 2-0 results being closer to Noor and Hartley's solution. This is expected because their element is based on a shell theory.

### 5.2.3 Two-Layer Cross-Ply and Angle-Ply ( $45^\circ/-45^\circ$ ) Cylindrical Shells Under Uniform Loading

The geometry of the circular cylindrical shell used here is the same as that shown in Fig. 4.1. The shell is assumed to be simply supported on all its edges. The material properties of individual lamina are the same as those used in Problem 2 of this chapter. A mesh of  $2 \times 2$  nine-node elements in a quarter shell is used to model the problem. The results of the analysis are presented in the form of load-deflection curves in Fig. 5.4. From the results, one can conclude that the angle-ply shell is stiffer than the cross-ply shell. This can be due to the bending-stretching coupling.

### 5.2.4 Two-Layer Cross-Ply and Angle-Ply ( $45^\circ/-45^\circ$ ) Spherical Shells Under Uniform Loading

The geometry and boundary conditions used in this problem are the same as those used in Problem 2 of this chapter. The geometric parameters used are:  $R/a = 10$ ,  $a/h = 100$ . The load-deflection curves for the cross-ply and angle-ply shells are shown in Fig. 5.5. From the

ORIGINAL PAGE IS  
OF POOR QUALITY

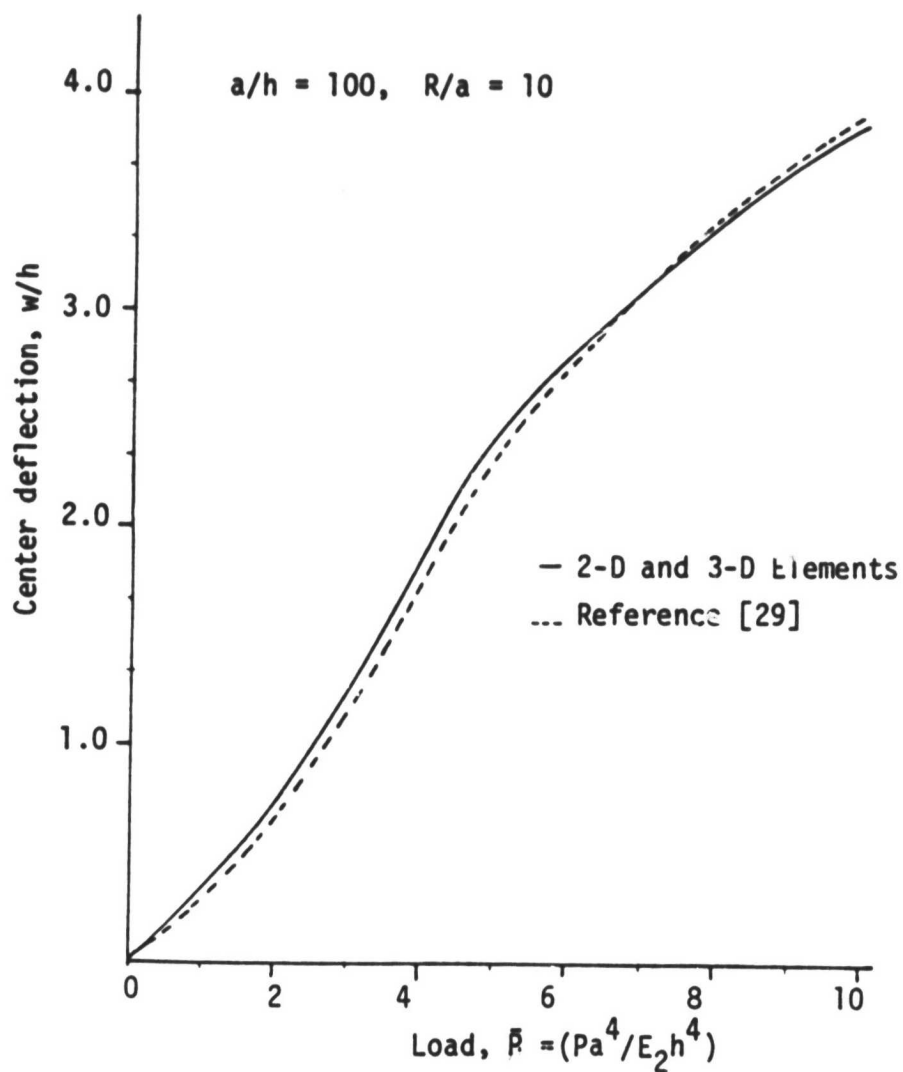


Figure 5.3 Deflection versus load parameter for nine-layer cross-ply ( $0^\circ/90^\circ/0^\circ/\dots$ ) spherical shell discussed in Section 5.2.2.

ORIGINAL PAGE IS  
OF POOR QUALITY

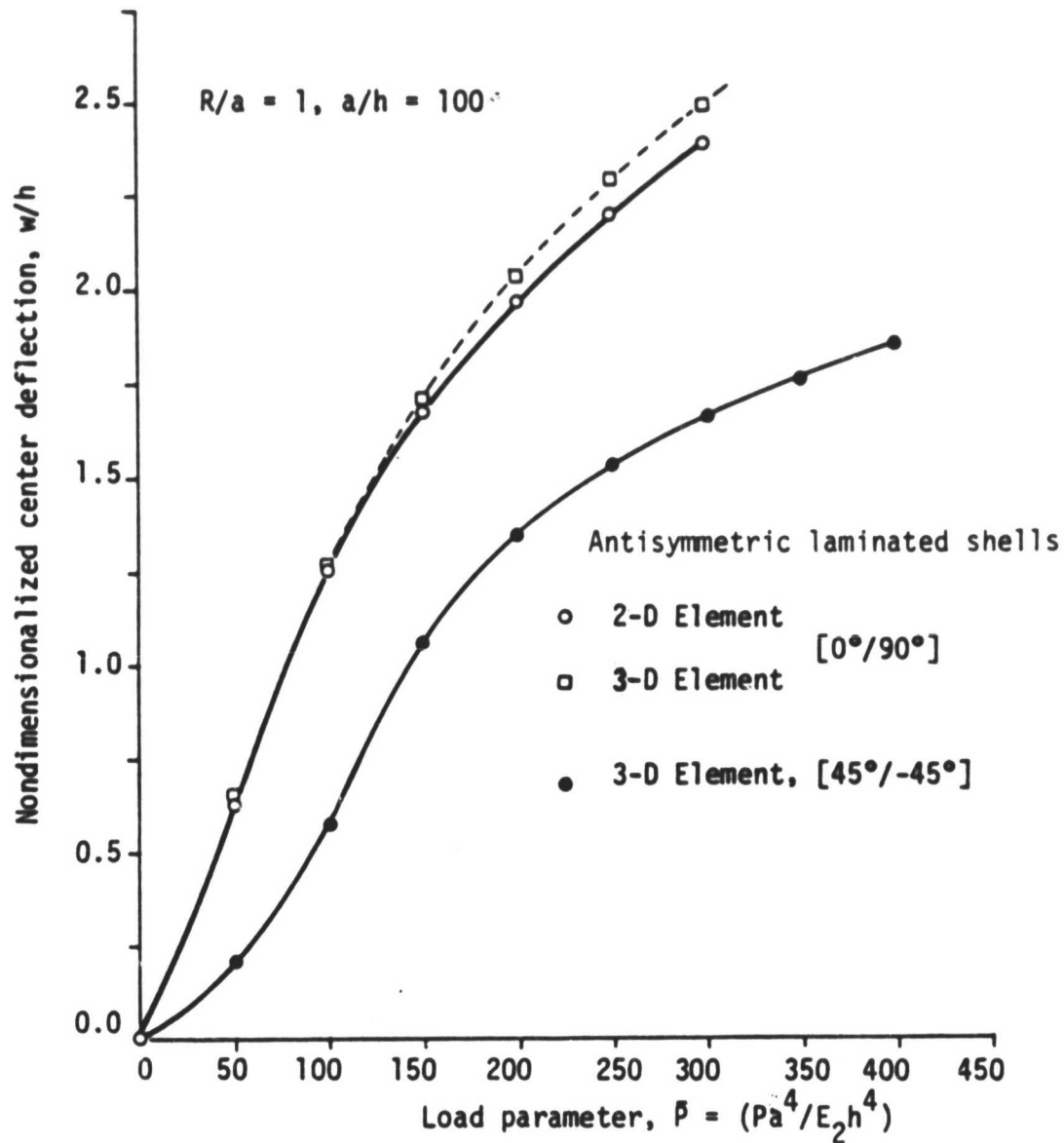


Figure 5.4 Deflection versus the load parameter for two-layer composite cylindrical shell (see Figure 4.1)



ORIGINAL PAGE IS  
OF POOR QUALITY

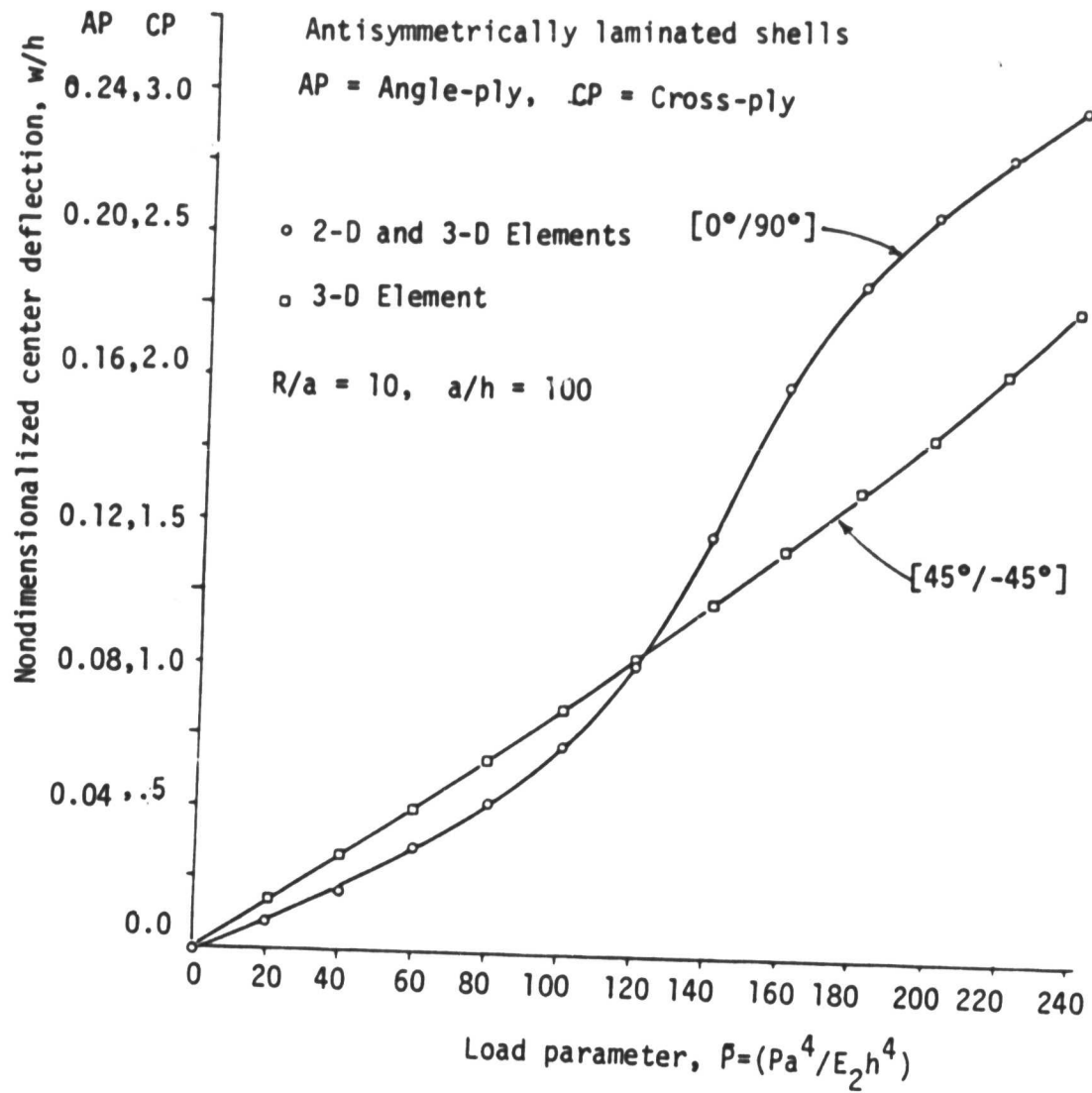


Figure 5.5 Nondimensionalized deflection versus the load for laminated shells discussed in Section 5.2.4.

plot it is apparent that, for the load range considered, the angle-ply shell, being stiffer, does not exhibit much geometric nonlinearity. The load-deflection curve of the cross-ply shell exhibits a varying degree of nonlinearity with the load. For load values between 100 and 150, the shell becomes relatively more flexible. (which can be due to bending-stretching coupling)

### 5.3 Transient Analysis

#### 5.3.1 Two-Layer Cross-Ply Plate Under Uniform Load

The problem is the same as that analyzed by Reddy [53] using a plate element. The geometric and material parameters used are

$$\begin{aligned} a &= b = 244 \text{ in.}, h = 0.635 \text{ in.}, P_0 = 0.5 \times 10^{-2} \text{ psi} \\ E_1 &= 17.578 \times 10^6 \text{ psi}, E_2 = 0.7031 \times 10^6 \text{ psi}, G_{12} = 0.5 \times 10^6 \text{ psi} \\ \rho &= 0.2547 \times 10^{-5} \text{ lb-sec}^2/\text{in}^4, \nu_{12} = 0.25, \delta t = 0.002 \text{ sec.} \end{aligned}$$

Figure 5.6 contains a plot of the center deflection versus time obtained by the 3-D element. The solution is in excellent agreement with that of Reddy [53].

#### 5.3.2 Two-Layer Cross-Ply Cylindrical Shell Under Uniform Load

A cylindrical shell with  $a = b = 5 \text{ in.}$ ,  $R = 10 \text{ in.}$ ,  $h = 0.1 \text{ in.}$  is simply-supported on the four edges. The deep shell is laminated with two layers ( $0^\circ/90^\circ$ ) and loaded by a uniform step load  $\hat{P} = \frac{a^4 P}{E_2 h^4} = 50$ .

Figure 5.7 contains a plot of the center deflection versus time for 2-D and 3-D elements with  $\delta t = 0.1 \times 10^{-4} \text{ sec.}$  The solutions obtained using the two elements are in good agreement. In Fig. 5.8, the solid line indicates the center deflection versus time for load  $\hat{P} = 1000$  and time step  $\delta t = 0.3 \times 10^{-5} \text{ sec.}$  The amplitude is almost twelve times that due to load  $\hat{P} = 50$ , whereas the load increases twenty times. The dotted

ORIGINAL PAGE IS  
OF POOR QUALITY

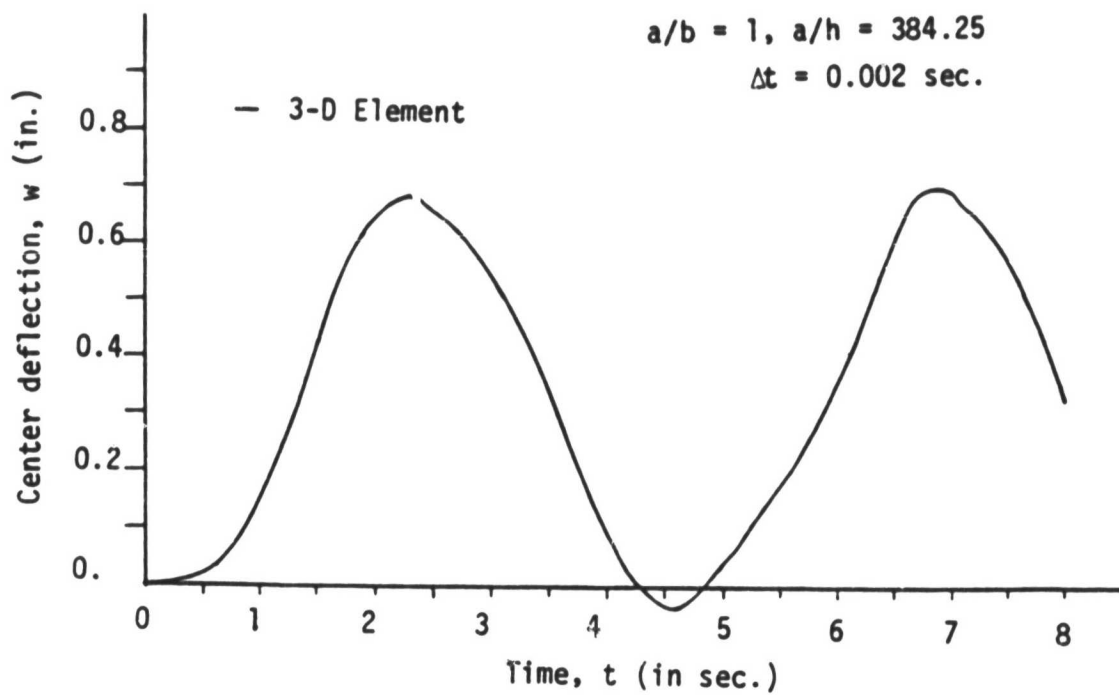


Figure 5.6 Deflection versus time for two-layer plate  $[0^\circ/90^\circ]$  under uniformly distributed step load.

ORIGINAL PAGE IS  
OF POOR QUALITY

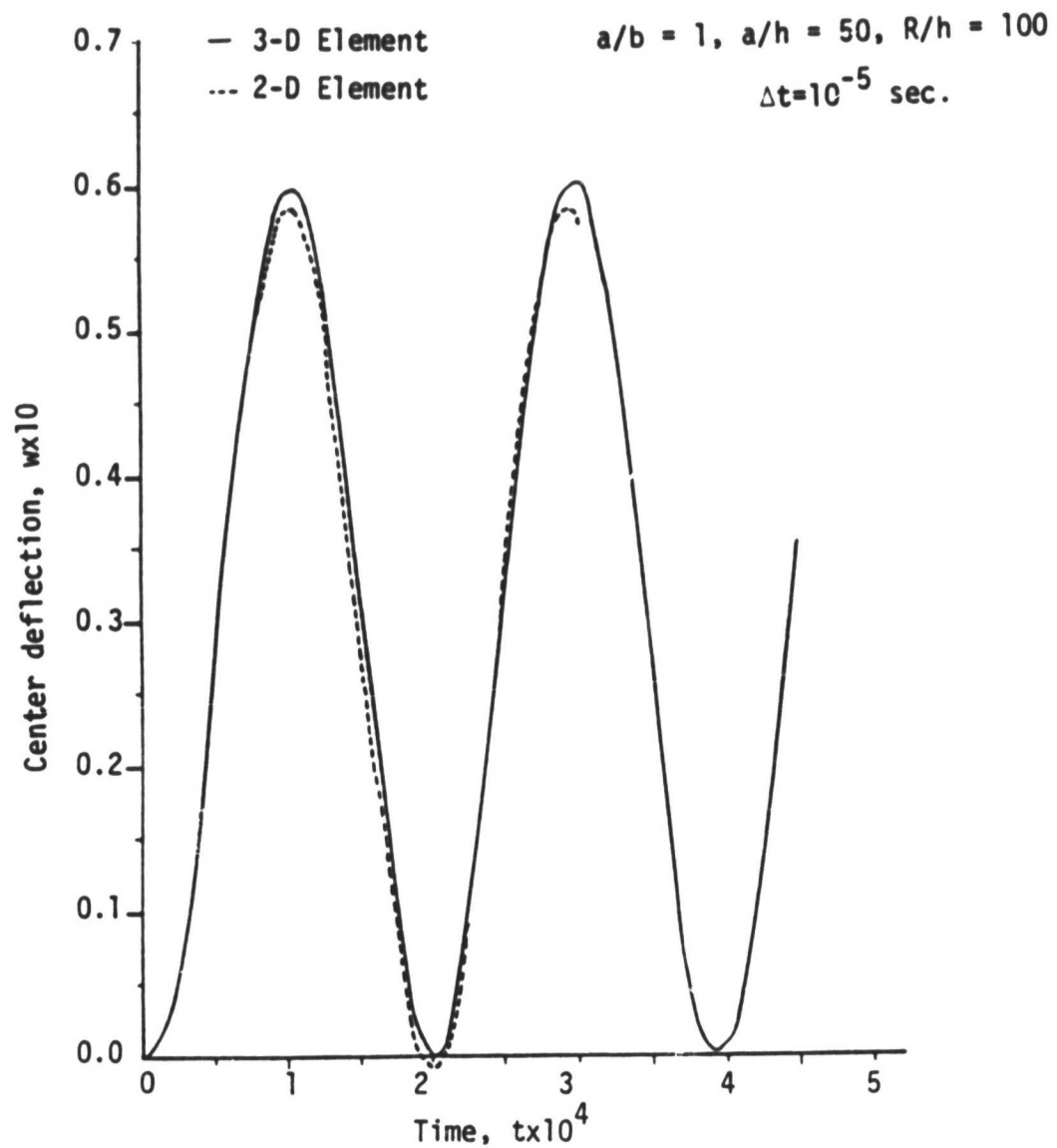


Figure 5.7 Center deflection versus time for two-layer cross-ply cylindrical shell subjected to uniform step load

line in Fig. 5.8 is for  $\Delta t = 0.1 \times 10^{-5}$  sec, which gives slightly smaller deflections.

### 5.3.3 Four-Layer Angle Ply (45°/-45°/45°/-45°) Cylindrical Shell Under Uniform Load

Here we present results for a cylindrical shell which has the same geometry as problem 5.3.2. The four-layer angle ply (45°/-45°/45°/-45°) laminated shell is simply supported on four edges and is subjected to a uniform step load  $\hat{P} = 50$ . Fig. 5.9 contains a plot of the center deflection versus time for 2-D and 3-D elements. The two elements yield solutions that agree very well, except that the 2-D element gives negative values of the deflection at the end of the cycle. The discrepancy is due to the fact that the 2-D element does not account for geometric changes from one time step to the next.

### 5.3.4 Two-Layer Angle-Ply (45°/-45°) Spherical Shell Under Uniform Loading

Consider a spherical shell with  $a = b = 10$  in,  $R = 20$  in and  $h = 0.1$  in, simply supported at four edges and excited by a uniform step load. The shell consists of two layers (45°/-45°). Figure 5.10 shows the center deflection versus time for  $\hat{P} = 50$  and  $\hat{P} = 500$  with time step  $0.2 \times 10^{-5}$  sec. For the small load the curve is relatively smooth compared to that of the larger load. This is due to the fact that the geometric nonlinearity exhibited at  $\hat{P} = 50$  is smaller compared to that at  $\hat{P} = 500$ .

ORIGINAL PAGE IS  
OF POOR QUALITY

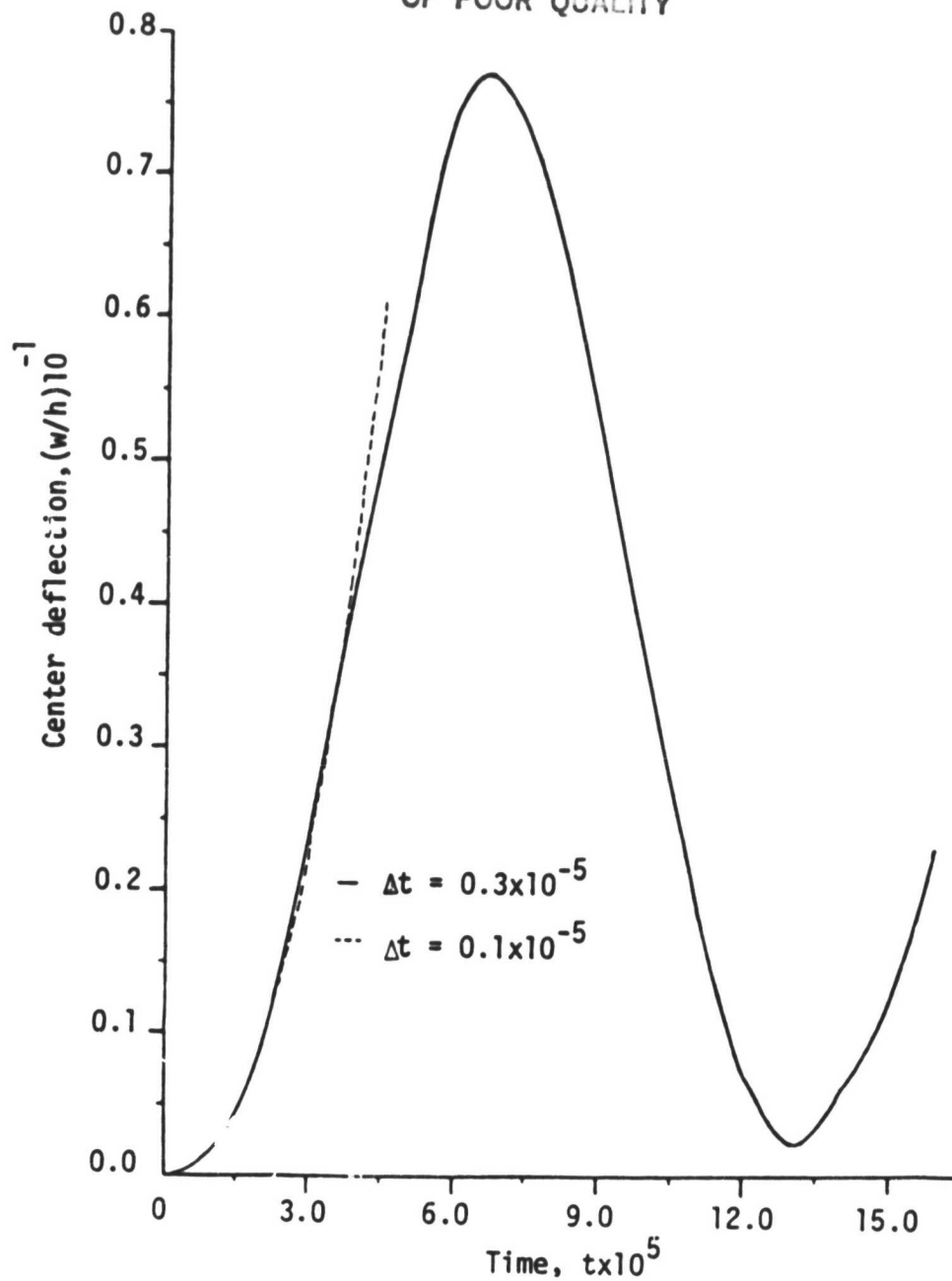


Figure 5.8 Comparison of the center deflection obtained by two different time steps for the problem discussed in Section 5.3.2.

ORIGINAL PAGE IS  
OF POOR QUALITY

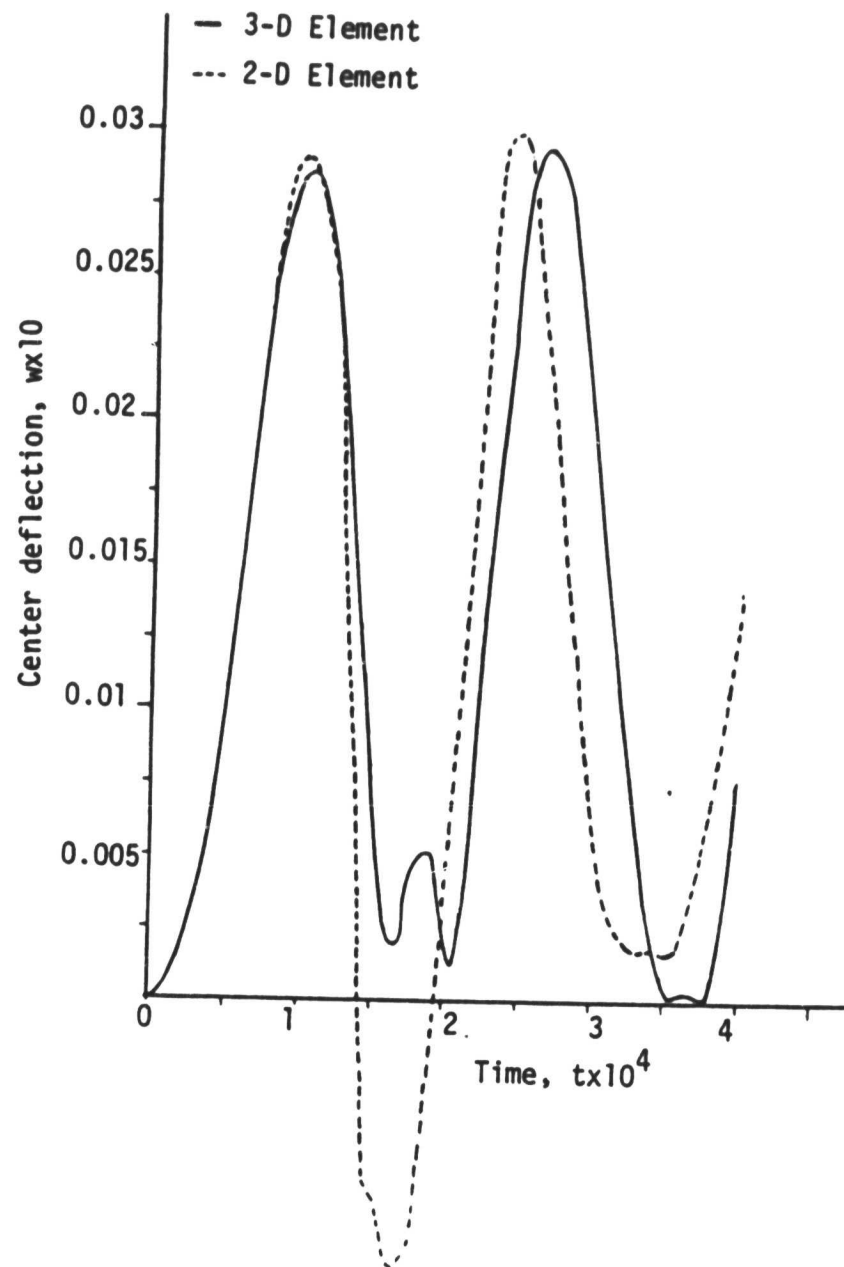


Figure 5.9 Center deflection versus time for four-layer angle-ply  $[45^\circ/-45^\circ/45^\circ/-45^\circ]$  cylindrical shell subjected to uniformly distributed load.

ORIGINAL PAGE IS  
OF POOR QUALITY

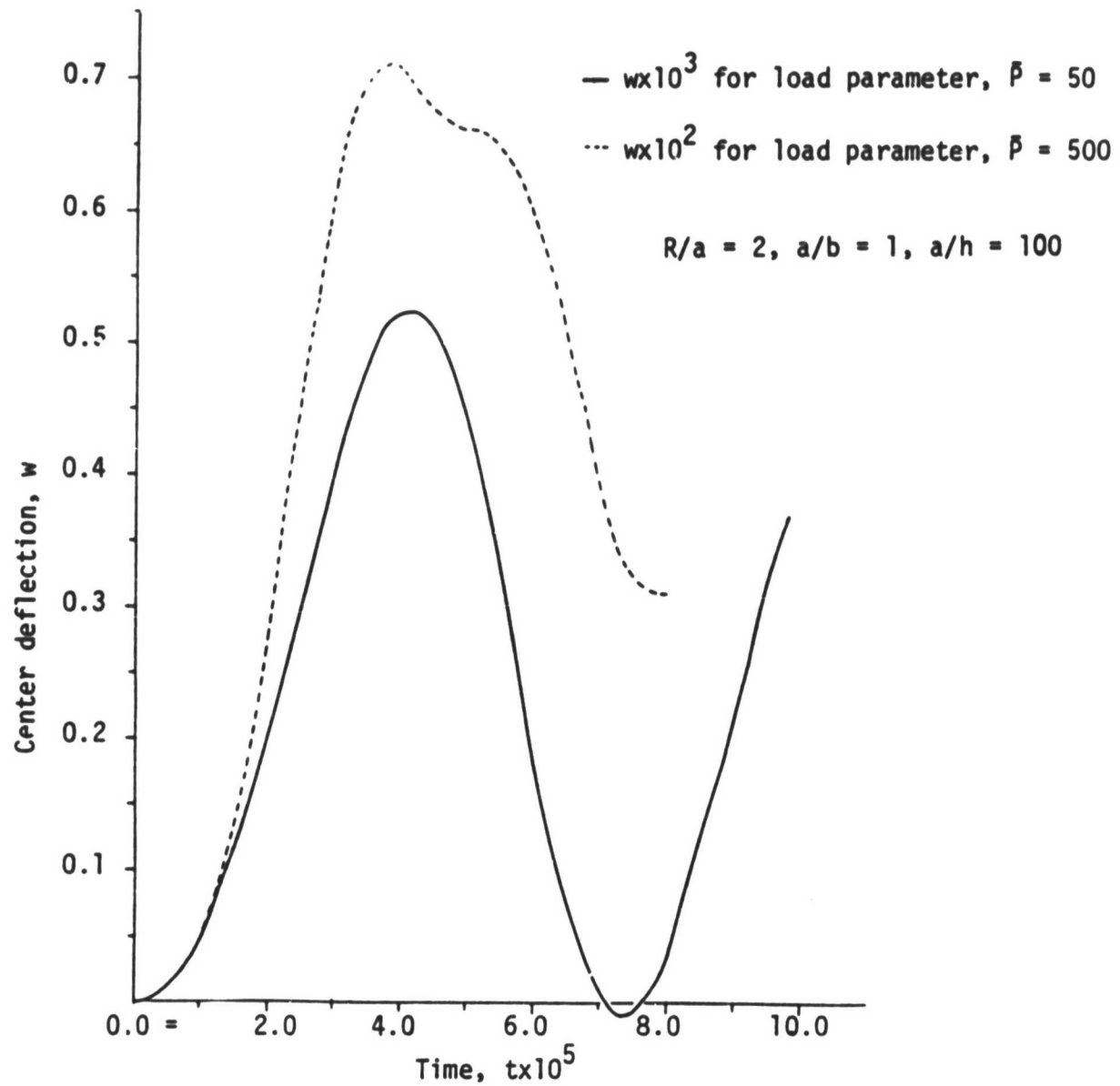


Figure 5.10 Center deflection versus time for two-layer angle-ply  $[45^\circ/-45^\circ]$  spherical shell under uniformly distributed step loading.



## CHAPTER VI

SUMMARY AND CONCLUSIONS6.1 Summary of the Present Study

A special three-dimensional element based on the total Lagrangian description of the motion of a layered anisotropic composite medium is developed, validated, and employed to analyze composite shells. The element has the following options:

- Geometrically linear and nonlinear analyses
- Static and transient analyses
- Natural vibration (linear) analyses
- Plate and shell elements
- Arbitrary loading and boundary conditions
- Arbitrary lamination schemes and lamina properties

The element can be used, with minor changes, in any existing general purpose program.

6.2 Conclusions

The present 3-D degenerated element has computational simplicity over a fully three-dimensional element, such as those developed in [49-50], and the element accounts for full geometric nonlinearities in contrast to 2-D elements based on shell theories. As demonstrated via numerical examples, the deflections obtained by the 2-D shell element deviate from those obtained by the 3-D element for deep shells. Further, the 3-D element can be used to model general shells that are not necessarily doubly-curved. For example, the vibration of twisted plates cannot be studied using the 2-D shell element discussed in Chapter 2. Of course, the 3-D degenerated element is computationally more demanding than the 2-D shell theory element for a given problem.

In summary, the present 3-D element is an efficient element for the analysis of layered composite plates and shells undergoing large displacements and transient motion.

### 6.3 Recommendations for Additional Study

The 3-D element presented herein can be modified to include thermal stress analysis capability and material nonlinearities. While the inclusion of thermal stresses is a simple exercise, the inclusion of nonlinear material effects is a difficult task. An acceptable material model could be a generalization of the Ramberg-Osgood relation to a layered anisotropic medium. Areas that require further study are the inclusion of damping effects, which can be more significant than the shear deformation effects, and material damage effects.

### Acknowledgments

The present study was conducted under a research grant from the Structures Research Section of NASA Lewis Research Center. The authors are very grateful for the support and encouragement by Dr. C. C. Chamis of NASA/Lewis. It is also a pleasure to acknowledge the typing of the manuscript by Mrs. Vanessa McCoy.

## REFERENCES

1. P. M. Naghdi, "A Survey of Recent Progress in the Theory of Elastic Shells," Applied Mechanics Review Vol. 9, 1956, pp. 365.
2. C. W. Bert, "Analysis of Shells," Structural Design and Analysis, Part I, C. C. Chamis (ed.), Vol. 7 of Composite Materials, L. J. Broutman and R. H. Krock (eds.), Academic Press, New York, 1974.
3. S. A. Ambartsumyan, "Calculation of Laminated Anisotropic Shells," Izvestia Akademii Nauk Armenskoi SSR, Ser. Fiz. Mat. Est. Tekh. Nauk., Vol. 6, No. 3, 1953, pp. 15.
4. S. A. Ambartsumyan, Theory of Anisotropic Shells, Moscow, 1961; English Translation, NASA TT F-118, May 1964.
5. S. B. Dong, K. S. Pister and R. L. Taylor, "On the Theory of Laminated Anisotropic Shells and Plates," Journal of Aerospace Sciences, Vol. 29, 1962, pp. 969-975.
6. Y. Stavsky, "Bending and Stretching of Laminated Anisotropic Plates," Journal of the Engineering Mechanics Division, Proc. ASCE, Vol. 87, No. EM6, 1961, pp. 31.
7. S. Cheng and B. P. C. Ho, "Stability of Heterogeneous Aelotropic Cylindrical Shells Under Combined Loading," American Institute of Aeronautics and Astronautics Journal, vol. 1, No. 4, 1963, pp. 892-898.
8. O. E. Widera and S. W. Chung, "A Theory for Non-Homogeneous Anisotropic Cylindrical Shells," Journal of Applied Mathematics and Physics (ZAMP), Vol. 21, 1970, pp. 378-399.
9. S. T. Gulati and F. Essenburg, "Effects of Anisotropy in Axisymmetric Cylindrical Shells," Journal of Applied Mechanics, Vol. 34, Sept. 1967, pp. 659-666.
10. J. A. Zukas and J. R. Vinson, "Laminated Transversely Isotropic Cylindrical Shells," Journal of Applied Mechanics, Vol. 38, 1971, pp. 400-407.
11. J. M. Whitney and C. T. Sun, "A Refined Theory for Laminated Anisotropic, Cylindrical Shells," Journal of Applied Mechanics, Vol. 41, 1974, pp. 471-476.
12. G. E. O. Widera and D. L. Logan, "Refined Theories for Nonhomogeneous Anisotropic Cylindrical Shells: Part I-Derivation," Journal of the Engineering Mechanics Division Proc. ASCE, Vol. 106, No. EM6, 1980, pp. 1053-1074.
13. G. E. O. Widera and D. L. Logan, "Refined Theories for Nonhomogeneous Anisotropic Cylindrical Shells: Part II-Application," Journal of the Engineering Mechanics Division Proc. ASCE, Vol. 106, No. EM6, 1980, pp. 1075-1090.

14. S. B. Dong, "Analysis of Laminated Shells of Revolution," Journal of the Engineering Mechanics Division Proc. ASCE, Vol. 92, EM6, 1966, pp. 135.
15. S. B. Dong and L. G. Selna, "Natural Vibrations of Laminated Orthotropic Shells of Revolution," Journal of Composite Materials, Vol. 4, No. 1, 1970, pp. 2-19.
16. E. A. Wilson and B. Parsons, "The Finite Element Analysis of Filament-Reinforced Axisymmetric Bodies," Fibre Science and Technology, Vol. 2, 1969, pp. 155-156.
17. L. A. Schmit, Jr., and G. R. Monforton, "Finite Element Analysis of Sandwich Plate and Laminated Shells with Laminated Forces," American Institute of Aeronautics and Astronautics Journal, Vol. 8, 1970, pp. 1454-1461.
18. G. L. Thompson and C. W. Bert, "Finite Element Analysis for Free Vibration of General Anisotropic Laminated Thin Shells," Composite Materials in Engineering Design (Proc. 6th St. Louis Symposium, May 11-12, 1972), Norton, B. R. (ed.), American Society for Metals Park, Ohio, 1973, pp. 72-80.
19. S. C. Panda and R. Natarajan, "Finite Element Analysis of Laminated Shells of Revolution," Computers and Structures, Vol. 6, 1976, pp. 61-64.
20. K. N. Shivakumar and A. V. Krishna Murty, "A High Precision Ring Element for Vibrations of Laminated Shells," Journal of Sound and Vibration, Vol. 58, No. 3, 1978, pp. 311-318.
21. K. P. Rao, "A Rectangular Anisotropic Shallow Thin Shell Finite Element," Computer Methods in Applied Mechanics and Engineering, Vol. 15, 1978, pp. 13-83.
22. P. Seide and P. H. H. Chang, "Finite Element Analysis of Laminated Plates and Shells," NASA CR-157106, 1978, 132 pp.
23. A. Venkatesh and K. P. Rao, "A Doubly Curved Quadrilateral Finite Element for the Analysis of Laminated Anisotropic Thin Shell of Revolution," Computers and Structures, Vol. 12, 1980, pp. 825-832.
24. H. S. Hsu, J. N. Reddy and C. W. Bert, "Thermoelasticity of Circular Cylindrical Shells Laminated of Bimodulus Composite Materials," Journal of Thermal Stresses, Vol. 4, No. 2, 1981, pp. 115-127.
25. J. N. Reddy, "Bending of Laminated Anisotropic Shells by a Shear Deformable Finite Element," Fibre Science and Technology, Vol. 17, pp. 9-24, 1982.

26. G. Horrigmoe and P. G. Bergan, "Incremental Variational Principles and Finite Element Models for Nonlinear Problems," Computer Methods in Applied Mechanics and Engineering, Vol. 7, 1976, pp. 201-217.
27. W. Wunderlich, "Incremental Formulations for Geometrically Nonlinear Problems," Formulations and Algorithm in Finite Element Analysis, by K. J. Bathe, J. T. Oden and W. Wunderlich ed., pp. 193-239.
28. A. Stricklin, W. E. Haisler and W. A. Von Riesenmann, "Evaluation of Solution Procedures for Material and/or Geometrically Nonlinear Structural Analysis," AIAA Journal, Vol. 11, 1973, pp. 292-299.
29. A. K. Ncor and S. J. Hartley, "Nonlinear Shell Analysis Via Mixed Isoparametric Elements," Computers and Structures, Vol. 7, 1977, pp. 615-626.
30. T. Y. Chang and K. Sawamiphakdi, "Large Deformation Analysis of Laminated Shells by Finite Element Method," Computers and Structures, Vol. 13, 1981, pp. 331-340.
31. J. L. Sanders, Jr., "An Improved First-Approximation Theory for Thin Shells," NASA Technical Report R-24, June 1959.
32. C. H. Tsao, "Strains - Displacement Relations in Large Displacement Theory of Shells," AIAA Journal, Vol. 2, No. 11, 1964, pp. 2060-2062.
33. J. N. Reddy and W. C. Chao, "A Comparison of Closed-Form and Finite-Element Solutions of Thick Laminated Anisotropic Rectangular Plates," Nuclear Engineering and Design, Vol. 61, 1981, pp. 153-167.
34. J. N. Reddy, "On the Solutions to Forced Motions of Layered Composite Plates," AIAA Journal, Vol. 21, No. 4, 1983, pp. 621-629.
35. O. C. Zienkiewicz, R. L. Taylor and J. M. Too, "Reduced Integration Technique in General Analysis of Plates and Shells," International Journal for Numerical Methods in Engineering, Vol. 3, 1971, pp. 275-290.
36. B. Krakeland, "Nonlinear Analysis of Shells Using Degenerated Isoparametric Elements," Finite Elements in Nonlinear Mechanics, International Conference on Finite Elements in Nonlinear Solid and Structural Mechanics, Geilo, Norway, Aug. 1977, pp. 265-284.
37. K. J. Bathe, E. Ramm and E. L. Wilson, "Finite Element Formulations for Large Deformation Dynamic Analysis," International Journal for Numerical Methods in Engineering, Vol. 9, 1975, pp. 353-386.
38. G. A. Dupuris, H. D. Hibbit, S. F. McNamara and P. V. Marcal, "Nonlinear Material and Geometric Behavior of Shell Structures," Computers and Structures, Vol. 1, 1971, pp. 223-239.

39. G. Horrigmoe and P. G. Bergan, "Nonlinear Analysis of Free-Form Shells by Flat Finite Elements," Computer Methods in Applied Mechanics and Engineering, Vol. 16, 1978, pp. 11-35.
40. S. Ahmad, B. M. Irons and O. C. Zienkiewicz, "Analysis of Thick and Thin Shell Structures by Curved Finite Elements," International Journal for Numerical Methods in Engineering, 2, 1970, pp. 419-451.
41. R. E. Mickell, "On the Stability of Approximation Operators in Problems of Structural Dynamics," Int. J. Solids and Structures, Vol. 7, pp. 301-319, 1971.
42. R. E. Mickell, "Direct Integration Methods in Structural Dynamics," J. Engng. Mech. Div. ASCE, Vol. 99, No. EM2, 1972.
43. G. L. Goudreau, and R. L. Taylor, "Evaluation of Numerical Integration Methods in Elastodynamics," J. Computer Methods in Applied Mechanics and Engineering, Vol. 2, No. 1, pp. 69-97, 1973.
44. T. B. Belytschko and B. J. Hsieh, "Nonlinear Transient Finite Element Analysis with Convected Coordinates," International Journal for Numerical Methods in Engineering, Vol. 7, pp. 255-272, 1973.
45. T. J. R. Hughes, and W. K. Liu, "Implicit-Explicit Finite Elements in Transient Analysis: Stability Theory, and Implementation and Numerical Examples," Vol. 45, No. 2, pp. 371-378, 1978.
46. S. P. Chan, H. L. Cox and W. A. Benfield, "Transient Analysis of Forced Vibrations of Complex Structural Mechanical Systems," Journal of Royal Aeronaut Soc., Vol. 66, pp. 457-460, 1962.
47. L. Fox and E. T. Goodwin, "Some New Methods for the Numerical Integration of Ordinary Differential Equations," Proc. Camb. Phil. Soc. Math. Phys. Sci. Vol. 45, 1949, pp. 373-388.
48. O. C. Zienkiewicz, The Finite Element Method, 3rd ed., McGraw-Hill Book Company.
49. G. S. Dhatt, "Instability of Thin Shells by the Finite Element Method," IASS Symposium for Folded Plates and Prismatic Structures, Vienna, 1970.
50. R. H. Leicester, "Large Elastic Deformations and Snap-Through of Shallow Doubly-Curved Shells," Ph.D. Thesis, Department of Civil Engineering, University of Illinois, Urbana, 1966.
51. J. A. Stricklin, J. E. Martinez, J. R. Tillerson, J. H. Hong, and W. E. Haisler, "Nonlinear Dynamic Analysis of Shells of Revolution by Matrix Displacement Method," AIAA Journal, Vol. 9, No. 4, April 1974, pp. 629-638.
52. S. Timoshenko and S. Woinowsky-Krieger, Theory of Plates and Shells, McGraw-Hill, New York, 1959.

53. J. N. Reddy, "Dynamic (Transient) Analysis of Layered Anisotropic Composite-Material Plates," International Journal for Numerical Methods in Engineering, Vol. 19, No. 2, pp. 237-255, 1983.
54. J. R. Dana and R. M. Barker, "Three-Dimensional Analysis for the Stress Distribution Near Circular Holes in Laminated Composites," Research Report No. VPI-E-74.18, Virginia Polytechnic Institute and State University, Blacksburg, VA, 1974.
55. J. N. Reddy and T. Kuppasamy, "Analysis of Layered Composite Plates by Three-Dimensional Elasticity Theory," Research Report No. VPI-E-82.31, Virginia Polytechnic Institute and State University, Blacksburg, VA, 1982.

APPENDIX I: ELEMENT STIFFNESS AND MASS MATRICES

$$\begin{aligned}
[K^{11}] &= A_{11}[S^{11}] + (A_{16} + c_o B_{16})([S^{12}] + [S^{12}]^T) \\
&\quad + (A_{66} + 2c_o B_{66} + c_o^2 D_{66})[S^{22}] + \frac{1}{R_1^2} A_{55}[S^{00}] \\
[K^{12}] &= (A_{16} - c_o B_{16})[S^{11}] + (A_{66} - c_o^2 D_{66})[S^{12}]^T + A_{12}[S^{12}] \\
&\quad + (A_{26} + c_o B_{26})[S^{22}] + \frac{1}{R_1 R_2} A_{45}[S^{00}] \\
[K^{13}] &= \left(\frac{A_{11}}{R_1} + \frac{A_{12}}{R_2}\right)[S^{10}] + \left[\frac{A_{16}}{R_1} + \frac{A_{26}}{R_2} + c_o\left(\frac{B_{16}}{R_1} + \frac{B_{26}}{R_2}\right)\right][S^{20}] \\
&\quad - \frac{1}{R_1} (A_{45}[S^{02}] + A_{55}[S^{01}]) \\
[K^{14}] &= B_{11}[S^{11}] + B_{16}[S^{12}] + (B_{16} + c_o D_{16})[S^{12}]^T \\
&\quad + (B_{66} + c_o D_{66})[S^{22}] - \frac{A_{55}}{R_1}[S^{00}] \\
[K^{15}] &= B_{12}[S^{12}] + B_{16}[S^{11}] + (B_{26} + c_o D_{26})[S^{22}] \\
&\quad + (B_{66} + c_o D_{66})[S^{12}]^T - \frac{1}{R_1} A_{45}[S^{00}] \\
[K^{22}] &= A_{22}[S^{22}] + (A_{26} - c_o B_{26})([S^{12}] + [S^{12}]^T) \\
&\quad + (A_{66} - 2c_o B_{66} + c_o^2 D_{66})[S^{11}] + \frac{A_{44}}{R_2^2}[S^{00}] \\
[K^{23}] &= \left[\frac{A_{16}}{R_1} + \frac{A_{26}}{R_2} - c_o\left(\frac{B_{16}}{R_1} + \frac{B_{26}}{R_2}\right)\right][S^{10}] \\
&\quad + \left(\frac{A_{12}}{R_1} + \frac{A_{22}}{R_2}\right)[S^{20}] - \frac{1}{R_2} (A_{44}[S^{02}] + A_{45}[S^{01}]) \\
[K^{24}] &= (B_{16} - c_o D_{16})[S^{11}] + (B_{66} - c_o D_{66})[S^{12}] + B_{12}[S^{12}] \\
&\quad + B_{26}[S^{22}] - \frac{1}{R_2} A_{45}[S^{00}] \\
[K^{25}] &= B_{22}[S^{22}] + B_{26}[S^{12}]^T + (B_{26} - c_o D_{26})[S^{12}] \\
&\quad + (B_{66} - c_o D_{66})[S^{11}] - \frac{A_{44}}{R_2}[S^{00}]
\end{aligned}$$



$$[K^{52}] = B_{22}[S^{22}] + B_{26}[S^{12}] + (B_{26} - c_0 D_{26})[S^{12}]^T \\ + (B_{66} - c_0 D_{66})[S^{11}] - \frac{A_{44}}{R_2} [S^{00}]$$

$$[K^{33}] = A_{45}[S^{12}] + A_{55}[S^{11}] + A_{44}[S^{22}] + A_{45}[S^{12}]^T \\ + \left[ \left( \frac{A_{11}}{R_1} + \frac{A_{12}}{R_2} \right) \frac{1}{R_1} + \left( \frac{A_{12}}{R_1} + \frac{A_{22}}{R_2} \right) \frac{1}{R_2} \right] [S^{00}]$$

$$[K^{34}] = A_{55}[S^{10}] + A_{45}[S^{20}] + \left( \frac{B_{11}}{R_1} + \frac{B_{12}}{R_2} \right) [S^{01}] \\ + \left( \frac{B_{16}}{R_1} + \frac{B_{26}}{R_2} \right) [S^{02}]$$

$$[K^{35}] = A_{45}[S^{10}] + A_{44}[S^{20}] + \left( \frac{B_{12}}{R_1} + \frac{B_{22}}{R_2} \right) [S^{02}] \\ + \left( \frac{B_{16}}{R_1} + \frac{B_{26}}{R_2} \right) [S^{01}]$$

$$[K^{44}] = D_{11}[S^{11}] + D_{16}([S^{12}] + [S^{12}]^T) + D_{66}[S^{22}] + A_{55}[S^{00}]$$

$$[K^{45}] = D_{12}[S^{12}] + D_{16}[S^{11}] + D_{26}[S^{22}] + D_{66}[S^{12}]^T \\ + A_{45}[S^{00}]$$

$$[K^{55}] = D_{26}[S^{12}] + D_{66}[S^{11}] + D_{22}[S^{22}] + D_{26}[S^{12}]^T + A_{44}[S^{00}]$$

$$[M^{11}] = [M^{22}] = [M^{33}] = P_1 [S^{00}]$$

$$[M^{44}] = [M^{55}] = P_3 [S^{00}]$$

$$[M^{14}] = [M^{15}] = \bar{P} [S^{00}], \quad \bar{P} = P_3 [1/R_1 + 1/R_2]$$

$$S_{ij}^{\alpha\beta} = \int_{\Omega^e} D_{\alpha} \psi_i D_{\beta} \psi_j dx_1 dx_2, \quad (\alpha, \beta = 0, 1, 2), \quad D_{\alpha} \equiv \frac{\partial}{\partial x_{\alpha}}, \quad D_0 = 1.$$

APPENDIX II: NOMENCLATURE

$A$	- area of element
$A_{ij}$	- stretching stiffness matrix
$\alpha, \beta$	- dimensionless parameters of generalized acceleration
$\alpha_i$	- surface metric
$\epsilon_i$	- strain in the $i$ -th direction
$\epsilon_i^0$	- strain in the $i$ th direction at the reference plane
$B_{ij}$	- bending-stretching stiffness matrix
$C_t$	- configuration at time $t$
$C_{ijkl}$	- elasticity tensor
$D$	- $Eh^3/12(1 - \nu^2)$
$D_{ij}$	- bending stiffness matrix
$\{\Delta\}$	- generalized displacement vector
$c_0$	- $\frac{1}{2} \left( \frac{1}{R_1} - \frac{1}{R_2} \right)$
$E_1$	- Young's modulus
$\hat{E}_T$	- unit vector along the global axes
$\hat{e}$	- unit vector along the local axes
$e_{ij}$	- linear incremental strain
$\xi_1, \xi_2, \xi$	- curvilinear coordinate system
$\{F\}$	- force vector
$\phi_i$	- rotations of the reference surface with respect to $\xi_2$ -axis
$h$	- thickness
$[K]$	- stiffness matrix
$K_i$	- shear correction factor
$L$	- number of layer
$M_i$	- moment resultant
$[M]$	- mass matrix

$\nu_{ij}$	- Poisson's ratio
$N_i$	- stress resultant
$\eta_{ij}$	- nonlinear incremental strain
$P_i$	- inertias
$q_i$	- distributed load
$Q_i$	- shear force resultant
$\theta_1, \theta_2$	- rotations about unit vector $\hat{e}_1, \hat{e}_2$
$\{R\}$	- balance force vector
$R_1, R_2$	- radii of curvature
$\rho$	- density
$S_{ij}$	- 2nd Piola Kirchhoff stress tensor
$[S]$	- stress matrix
$\{\hat{S}_j\}$	- stress vector
$dS$	- length of line element of the shell
$\sigma_i$	- stress vector
$\phi_i$	- interpolation function at node i
$[T]$	- transformation matrix between displacement vector $\{u\}$ and generalized displacement vector $\{\Delta\}$
$T_i$	- traction component
$\Delta t$	- time increment
$\tilde{u}$	- incremental displacement vector
${}^t\tilde{u}$	- displacement vector at time t
$\tilde{u}_n$	- displacement gradient
$\tilde{v}_i$	- vector along the local axes
$V$	- volume
${}^t\tilde{x}$	- coordinate at time t
$\delta W$	- virtual work due to external loads
$\{\Delta\}$	- column of generalized nodal displacements

PROGRAM SHEET 3D

THIS PROGRAM IS DEVELOPED TO ANALYZE LAMINATED ANISOTROPIC  
STRUCTURES (PLATES AND SHEETS) WITH GEOMETRIC NONLINEARITY.  
THE TOTAL LAGRANGIAN DESCRIPTION WITH INCREMENTAL VARIATIONAL  
IS USED. THE THREE-DIMENSIONAL DEGENERATED ELEMENT IS USED  
TO MODEL LAMINATED PLATES AND SHEETS.

DESCRIPTION OF VARIABLES

COORD(I,J)..... GLOBAL COORDINATE OF NODE I IN J-TH DIRECTION.  
WD,VI,VP..... VECTOR OF DISPLACEMENT, VELOCITY AND  
ACCELERATION OF EACH ELEMENT.  
GLO,GI,GP..... VECTOR OF DISPLACEMENT, VELOCITY AND  
ACCELERATION OF THE WHOLE STRUCTURE.  
DIR..... VECTOR INDICATES VARIOUS TIME STEP.  
NTHI..... NUMBER OF THE STEP TO BE PROCESSED.  
NTHX..... MAXIMUM NUMBER OF ITERATION USED IN NONLINEAR  
ANALYSIS.  
THI(I,J)..... ORIENTATION OF I-TH LAYER.  
NCP,IGP..... NO. OF INTEGRATION POINT FOR BINDING PARTS AND  
SHEAR PARTS.  
IPRINT..... 1: PRINT THE ELEMENT STIFFNESS MATRIX.  
0: NOT PRINT ELEMENT STIFFNESS MATRIX.  
NIS..... NO. OF LOAD STEP.  
ITYPE..... FLAG TO INDICATE SHEET TYPE  
0: FLAT PLATE  
1: CYLINDRICAL SHEET  
2: SPHERICAL SHEET  
IPROB..... 0: STATIC PROBLEM.  
1: DYNAMIC PROBLEM.  
THI,TH2..... ANGLE OF SPAN IN RADIAN OF X AND Y DIRECTION.  
RDI,RD2..... RADIUS MEASURED IN PRINCIPAL X AND Y DIRECTION.  
ALFA, BETA AND GAMMA..... PARAMETERS USED IN DYNAMIC  
ANALYSIS.  
IXYZ(I,J)..... GLOBAL COORDINATE IN J-TH DIRECTION OF I NODE.  
VI,V2,V3..... LOCAL COORDINATE VECTORS AFTER EACH TIME STEP.  
VIA,V2B,V3C..... LOCAL COORDINATE VECTORS AT CURRENT TIME.  
VA,VB,VC..... LOCAL COORDINATE VECTORS AT TIME 0.  
V1,VAC..... VELOCITY AND ACCELERATION OF V3 AT TIME (N+1)\*  
V10,VAC0..... VELOCITY AND ACCELERATION OF V3 AT TIME N\*1.  
NNM,NEM..... NO. OF NODE AND ELEMENT IN THIS MESH.  
RHO..... BOOLEAN MATRIX.  
RHO..... DENSITY.

IMPICIT REAL\*8(A=0.0)  
COMMON/MAT/AL(2,3,6,6),CH(9,6,6),CS(9,6,6)  
COMMON/PR SH/COOH(50,3),I1XYZ(9,3),NOD(9,9)

ORIGINAL PAGE IS  
OF POOR QUALITY

```

COMMON/ICV/V1(50,3),V2(50,3),V3(50,3),VA(50,3),VB(50,3),VC(50,3)
1  ,VIA(50,3),V2B(50,3),V3C(50,3)
COMMON/STIFF/STIFF(45,45),EIP(45),W(45),EIQ(45),W0(45),W1(45)
1  ,V2(45),VAC(50,3),VEL(50,3),VACO(50,3),VELO(50,3)
DIMENSION THEIA(16),GE1(145),GSTIFF(145,145),GINSF(145,145),Z(10),
1  ,GM(145),GP(145),GU(145),IBDY(90),VBODY(90),GB(145),GE0(
2  ,145),GE1(145),GE2(145),GIN(3),GP1(145),GC(145)
READ(5,610) DTH(1),DTH(2),DTH(3)
READ(5,620) NDI,NPE,NLM,NMH,NBDY
READ(5,610) THEIA(1),THEIA(2),THEIA(3),THEIA(4)
READ(5,610) I01,I02,RO,RO1,RO2
READ(5,610) I1,I2,GE2,GE3,G23,ANU1?
READ(5,620) I1,NGP,IGP,NEST,NEST,TYPE
READ(5,620) NLINE,NIMAX,IPRINT,PI,S,NKMAX,ILOAD,LAYER
READ(5,610) RH0
READ(5,610) PS,XI,YI,I,PK
DO 2 I=1,NMH
2  READ(5,10)(COORD(I,J),J=1,3)
DO 3 I=1,NMH
3  READ(5,10)(V3(I,J),J=1,3)
CALL MESH1(I01,I02,NEST,NEST,RO,TYPE,XI,YI)
DO 4 I=1,NLM
4  READ(5,20)(NDD(I,J),J=1,NPI)
WRITE(6,500) NBDY
READ(5,22)(IBDY(I),I=1,NBDY)
WRITE(6,23)(IBDY(I),I=1,NBDY)
23 FORMAT(////,2X,BOUNDARY CONDTION',/,2X,20
C 15,/,2X,2015,/,2X,2015)
C
C NA2 ..... FLAG TO SPECIFY ISOTROPIC OR NOT, IT CAN REDUCE
C INTEGRATION TIME IN STIFF SUBROUTINE.
C
C NA2 1
11(1,1,1,1,1) NA2=0
ALFA 0.5
BETA 0.25*(0.5+ALFA)**2
GAHA -2.0/3.0
NIQ NDI*NMH
NN NDI*NP1
PO (-1.0)*(1.2*1**h/(X1**h))**50.0*PR
PO (-1.0)*(1.2*1**h/((2.0*X1)**h))**50.0*PR
PO -2.85
PO 0.5D-2
PO -1.0D2
PO -100.0
157 CONTINUE
C
C CA1, CA2 ARE THE NORMAL AND ROTARY INERTIA COEFFICIENTS.
C
C CA1 RH0*2.0
C CA3 RH0*2.0**3/12.0
DI PO
OP PO
WRITE(6,580) ILOAD
580 FORMAT(//,2X,ILOAD,10A D I N G I Y P I (1: UNIFORM, 2: SINUSOIDAL,

```

ORIGINAL PAGE IS  
OF POOR QUALITY

ORIGINAL PAGE IS  
OF POOR QUALITY

VA 11C:11

1495 RECS

180

A1

NASA  
105-11011

10; CONCENTRATED)'.//,2X,'1 1 0 A D = ',13)					
VRII(6,1)NDI,NPI,NEM,NNH,XI,YI,RDI,RDZ	DGNO1110				
VRII(6,570)NGP,IGP	DGNO1120				
VRII(6,6)E1,12,G12,G13,G23,AND12	DGNO1130				
VRII(6,11)AYER,(THETA(1),1-1,LAYER)	DGNO1140				
VRII(6,12)1,LP\$	DGNO1150				
VRII(6,16)((COORD(I,J),J=1,3),I=1,NNH)	DGNO1160				
VRII(6,21)((NOD(I,J),J=1,NPF),I=1,NEM)	DGNO1170				
C.....	DGNO1180				
G.....	DGNO1190				
FIND OUT THE LOCAL COORDINATES FOR EACH NODE.					
C.....	DGNO1200				
C.....	DGNO1210				
DO 30 I=1,NNH	DGNO1220				
DO 33 K=1,3	DGNO1230				
VAC(I,K)=0.0	DGNO1240				
V1(I,K)=0.0	DGNO1250				
VAC(I,K)=0.0	DGNO1260				
V1(I,K)=0.0	DGNO1270				
33 CONTINUE	DGNO1280				
V1(I,1)=V3(I,1)	DGNO1290				
V1(I,2)=0.0	DGNO1300				
V1(I,3)=V3(I,1)	DGNO1310				
V2(I,1)=V3(I,2)*V3(I,1)	DGNO1320				
V2(I,2)=V3(I,1)**2+V3(I,3)**2	DGNO1330				
V2(I,3)=V3(I,2)*V3(I,3)	DGNO1340				
SUR1=DSQR(V1(I,1)**2+V1(I,2)**2+V1(I,3)**2)	DGNO1350				
SUR2=DSQR(V2(I,1)**2+V2(I,2)**2+V2(I,3)**2)	DGNO1360				
SUR3=DSQR(V3(I,1)**2+V3(I,2)**2+V3(I,3)**2)	DGNO1370				
DO 30 J=1,3	DGNO1380				
V1(I,J)=V1(I,J)/SUR1	DGNO1390				
V2(I,J)=V2(I,J)/SUR2	DGNO1400				
V3(I,J)=V3(I,J)/SUR3	DGNO1410				
30 CONTINUE	DGNO1420				
DO 62 I=1,NNH	DGNO1430				
DO 62 J=1,3	DGNO1440				
VIA(I,J)=V1(I,J)	DGNO1450				
V2B(I,J)=V2(I,J)	DGNO1460				
V3C(I,J)=V3(I,J)	DGNO1470				
VA(I,J)=V1(I,J)	DGNO1480				
VB(I,J)=V2(I,J)	DGNO1490				
VC(I,J)=V3(I,J)	DGNO1500				
62 CONTINUE	DGNO1510				
VRII(6,136)	DGNO1520				
DO 126 I=1,NNH	DGNO1530				
VRII(6,10)(V1(I,1),J=1,3)	DGNO1540				
VRII(6,137)	DGNO1550				
DO 127 I=1,NNH	DGNO1560				
VRII(6,10)(V2(I,1),J=1,3)	DGNO1570				
VRII(6,138)	DGNO1580				
DO 128 I=1,NNF	DGNO1590				
VRII(6,10)(V3(I,1),J=1,3)	DGNO1600				
FORI1(//,2X,'V F C T O R I N 1-D I R E C T I O N',//)	DGNO1610				
FORI1(//,2X,'V F C T O R I N 2-D I R E C T I O N',//)	DGNO1620				
FORI1(//,2X,'V F C T O R I N 3-D I R E C T I O N',//)	DGNO1630				
DO 250 I=1,NFC	DGNO1640				
250 GOTO(1)0.0	DGNO1650				

```

C.      IIR IS A FLAG TO INDICATE THE NUMBER OF TIMES TO FIND
C.      THE TANGENTIAL STIFFNESS AT EACH LOADING STEP
C.      IIR = 1
C.      CALCULATE THE CONSTITUTIVE RELATIONSHIP.
C.      CALL MATPRP(I1,I2,ANU2,G12,G13,G23,I,LAYER,NNM,THEIA,Z,NGP,IGP)
C.      DO 300 NP=1,NIS
C.      WRIT(6,550)PO
C.      INITIALIZATION OF THE MATRICES AND VECTORS.
C.      DO 251 I=1,NIG
C.      GLO(I)=0.0
C.      GL1(I)=0.0
C.      GL2(I)=0.0
C.      DO 251 J=1,NIG
C.      GINSF(I,J)=0.0
C.      GSII(I,J)=0.0
C.      251 CONTINUE
C.      CALCULATION OF THE PARAMETER USED IN DYNAMIC PROBLEMS.
C.      I1=DIH(NP)
C.      I12=I1*11
C.      A0=1.0/BETIA/I12
C.      A1=1.0/BETIA/I1
C.      A2=1.0/2.0/BETIA-1.
C.      A3=A0
C.      A4=-A1
C.      A5=-A2
C.      A6=11*(1.0-A1A)
C.      A7=A1A*I1
C.      I1H=0.0
C.      VR11(6,313)A1A,BETIA,GANA,A0,A1,A2,A3,A4,A5,A6,A7,I1H
C.      323 FORMAT(//,2X,'A11 A',BETIA,'A1 A',GANA,'A0 A',3E13.5,/,2X,'A0 A',
C.      11, A2,/,2X,'BETIA',/,2X,'DENSITY =',E13.5,/)
C.      VR11(6,313)
C.      DO 290 N11=1,N1H1
C.      I1H=I1H+1
C.      IIR=0
C.      I1IAG INDICATES TO UPDATE THE TANGENTIAL STIFFNESS MATRIX
C.      I1IAG = 0 UPDATE THE TANGENTIAL STIFFNESS MATRIX.
C.      I1IAG = 1 DON'T UPDATE THE TANGENTIAL STIFFNESS MATRIX.
C.      NS,N11
C.      IT(11PROB,EQ,0)NSS=NP
C.      I1IAG=0
C.      N1A NSS/10
C.      N1B N1A*10
C.      IT(N1B,N1NSS) I1IAG=1
C.      IT(NSS,EQ,1) I1IAG=0

```

ORIGINAL PAGE IS  
OF POOR QUALITY

```

240 CONTINUE
      ITER=ITER+1
      IF (ITER*G1*NTMAX) GO TO 410
C.....
C.....INITIALIZATION OF THE GLOBAL MATRICES.
C.....
      DO 40 I=1,NEQ
      GO(1)=0.0
      GB(1)=0.0
      GC(1)=G1(1)
      IF (FLAG.NE.0) GO TO 40
      DO 45 J=1,NEQ
      GWSI(I,J)=0.0
      GSI1(I,J)=0.0
45 CONTINUE
40 CONTINUE
C.....
C.....CALCULATE THE GLOBAL MATRIX FOR EACH ELEMENT AND ASSEMBLE THEM.
C.....
      DO 50 N=1,NEM
      I=0
      DO 60 I=1,NPI
      NI=MOD(N,I)
      I1XYZ(1,1)=COORD(NI,1)
      I1XYZ(1,2)=COORD(NI,2)
      I1XYZ(1,3)=COORD(NI,3)
      I1=(NI-1)*NDF
      DO 65 J=1,NDF
      I1=I+J
      I1=I+1
      IF (PROB.IQ.0) GO TO 60
      W0(1)=G0(I)
      W1(1)=G1(I)
      W2(1)=G2(I)
      W3(1)=G3(I)
      CALL STIFF(NI,NPI,NDI,N,1,PO,ITER,LOAD,NP,I1IAG,NCP,IGP,CA1,CA3,
      1      A0,A1,A2,N11,NTMAX,NA2,1,PROB)
      IF (PROB.IQ.1) GO TO 77
      IF (N.NE.1) GO TO 77
      PRINT 79,(I,P(1),I=1,N,N)
      DO 78 I=20,25
      78 WRITE(6,79)(S1(I,1),I=1,20,25)
      79 FORMAT(7(2X,F13.5))
      77 DO 70 I=1,NPI
      NR=(MOD(N,I)-1)*NDF
      DO 70 I=1,NDF
      NR=NR+1
      I=(I-1)*NDF+1
      GO(NR)=GO(NR)+I*P(1)
      IF (LOAD.IQ.0) GO TO 489
      GB(NR)=GB(NR)+I*Q(1)
489 IF (I1IAG.NE.0) GO TO 70
      DO 490 J=1,NPI
      NC=(MOD(N,J)-1)*NDF
      DO 490 J=1,NDF

```



ORIGINAL PAGE IS  
OF POOR QUALITY

VA TECH

1495 RECS

F 80

A1

SHEL 3D NASA

```

M (J-1)*NDI+JJ
NC NC+1
GSTT(NR,NC)=GSTT(NR,NC)+STTT(I,H)
490 CONTINUE
70 CONTINUE
50 CONTINUE
IT(1,LOAD,IQ,0) GB(63)-P0
C
C APPLY THE BOUNDARY CONDITIONS
C
C CALL BOU(NRMAX,GSTT,CD,GB,NEQ,NBDY,IBDY,ITER,IFLAG)
C
C SOLVE THE EQUATION WITH THE NEWTON-RAPHSON METHOD.
C
C IT(1,IFLAG,NE,0)GO TO 480
CALL LINVT(GSTT,NEQ,NRMAX,GINST,O,CW,ITER)
480 DO 80 J=1,NEQW
GP(11)=0.0
DO 80 J=1,NEQW
GP(11)*GINST(11,J)*(GB(J1)+GR(J1))
80 CONTINUE
C
C PUT THE SPECIFIED BOUNDARY TERMS BACK TO THE GP VECTOR.
C
C NBDW NEQ-NEQW
K 0
DO 90 I=1,NEQ
DO 100 J=1,NBDW
I=BDY(NBDY+1-J)
IT(1,IQ,1)GO TO 110
IT(1,GP,1)GO TO 120
100 CONTINUE
120 GP(11)=GP(11)+GP(1-K)
GO TO 90
110 K=1
GP(11)=0.0
90 CONTINUE
C
C CALCULATE THE NORM OF THE DIFFERENCE OF THE CONSECUTIVE SOLUTIONS.
C
C 310 ERR=0.0
DO 130 I=1,NEQ,NDI
130 ERR=ERR+(GP(11)-GC(11))**2
ERR DABS(DSQRT(ERR)/GF(63))
IFLAG=1
IT(MHAX,IQ,1)GO TO 321
C
C FIND OUT THE LOCAL COORDINATE VECTORS AT CURRENT TIME.
C
C 340 N1 NDI-1
N2 NDI-2
DO 255 I=1,NNH
I=NDI*(I-1)+1
DO 170 J=1,3
V3C(I,J)=V3(I,J)+V1(I,J)*GI(1+N2)-V2(I,J)*GI(1+NI)

```

DCN02760

DCN02770

DCN02780

DCN02790

DCN02800

DCN02810

DCN02820

DCN02830

DCN02840

DCN02850

DCN02860

DCN02870

DCN02880

DCN02890

DCN02900

DCN02910

DCN02920

DCN02930

DCN02940

DCN02950

DCN02960

DCN02970

DCN02980

DCN02990

DCN03000

DCN03010

DCN03020

DCN03030

DCN03040

DCN03050

DCN03060

DCN03070

DCN03080

DCN03090

DCN03100

DCN03110

DCN03120

DCN03130

DCN03140

DCN03150

DCN03160

DCN03170

DCN03180

DCN03190

DCN03200

DCN03210

DCN03220

DCN03230

DCN03240

DCN03250

DCN03260

DCN03270

DCN03280

DCN03290

DCN03300



[illegible]

ORIGINAL PAGE IS  
OF POOR QUALITY

[illegible]



ORIGINAL PAGE IS  
OF POOR QUALITY



ORIGINAL PAGE IS  
OF POOR QUALITY

DO 460 K-1,5  
DO 460 I-1,5  
A1(K,1)-A(NW,1,K,1)\*CNSI  
A2(K,1)-A(NW,2,K,1)\*CNSI  
A3(K,1)-A(NW,3,K,1)\*CNSI  
460 CONTINUE  
CALL STRATENDI,NDI,1,NPI)  
DO 210 I=1,5  
DO 210 J=1,NN  
D11(I,J)=0.0  
D12(I,J)=0.0  
D11(I,J)=0.0  
D12(I,J)=0.0  
D11(I,J)=0.0  
D12(I,J)=0.0  
210 CONTINUE  
DO 22 I=1,NPI  
ND=NDI(NOF,I)  
MA=NDI\*(I-1)+1  
CALL ZERO(DH)  
DH(1,1)=DSI(1,1)  
DH(2,1)=DSI(2,1)  
DH(3,1)=0.0  
CALL MXMUT2(GJINV,XV,XU,DH)  
CALL DISTR(DH,DH1,MA,0)  
CALL ZERO(DH)  
DH(1,2)=DSI(1,1)  
DH(2,2)=DSI(2,1)  
DH(3,2)=0.0  
CALL MXMUT2(GJINV,XV,XU,DH)  
CALL DISTR(DH,DH1,MA,1)  
CALL ZERO(DH)  
DH(1,3)=DSI(1,1)  
DH(2,3)=DSI(2,1)  
DH(3,3)=0.0  
CALL MXMUT2(GJINV,XV,XU,DH)  
CALL DISTR(DH,DH1,MA,2)  
CALL ZERO(DH)  
DH(1,1)=DSI(1,1)\*V1(ND,1)\*0.5\*1  
DH(1,2)=DSI(1,1)\*V1(ND,2)\*0.5\*1  
DH(2,1)=DSI(2,1)\*V1(ND,1)\*0.5\*1  
DH(2,2)=DSI(2,1)\*V1(ND,2)\*0.5\*1  
DH(1,3)=DSI(1,1)\*V1(ND,3)\*0.5\*1  
DH(2,3)=DSI(2,1)\*V1(ND,3)\*0.5\*1  
CALL MXMUT2(GJINV,XV,XU,DH)  
CALL DISTR(DH,DH2,MA,3)  
CALL ZERO(DH)  
DH(1,1)=DSI(1,1)\*V2(ND,1)\*0.5\*1  
DH(1,2)=DSI(1,1)\*V2(ND,2)\*0.5\*1  
DH(2,1)=DSI(2,1)\*V2(ND,1)\*0.5\*1  
DH(2,2)=DSI(2,1)\*V2(ND,2)\*0.5\*1  
DH(1,3)=DSI(1,1)\*V2(ND,3)\*0.5\*1  
DH(2,3)=DSI(2,1)\*V2(ND,3)\*0.5\*1  
CALL MXMUT2(GJINV,XV,XU,DH)  
CALL DISTR(DH,DH2,MA,4)  
CALL ZERO(DH)  
DH(3,1)=DSI(1,1)\*V1(ND,1)\*0.5\*1

C-2



DH(3,2) - SI(1)\*V1(ND,2)\*0.5\*1  
 DH(3,3) - SI(1)\*V1(ND,3)\*0.5\*1  
 CALL HXMD12(GJINV, XV, XU, DH)  
 CALL DISTR(DH, DH1, HA, 3)  
 CALL ZERO(DH)  
 DH(3,1) - SI(1)\*V2(ND,1)\*0.5\*1  
 DH(3,2) - SI(1)\*V2(ND,2)\*0.5\*1  
 DH(3,3) - SI(1)\*V2(ND,3)\*0.5\*1  
 CALL HXMD12(GJINV, XV, XU, DH)  
 CALL DISTR(DH, DH1, HA, 4)  
 CALL ZERO(DH)

22 CONTINUE

DO 63 J=1,6  
 DO 63 J=1,9  
 SD(1,J) = 0.0  
 ID(1,J) = 0.0

63 CONTINUE

SD(1,1) = 1.0\*GU(1)  
 SD(1,4) = GU(4)  
 SD(1,7) = GU(7)  
 SD(2,2) = GU(2)  
 SD(2,5) = GU(5)+1.  
 SD(2,8) = GU(8)  
 SD(3,1) = GU(2)  
 SD(3,2) = GU(3)+1.  
 SD(3,4) = GU(5)+1.  
 SD(3,5) = GU(4)  
 SD(3,7) = GU(8)  
 SD(3,8) = GU(7)  
 SD(4,1) = GU(3)  
 SD(4,3) = GU(1)+1.  
 SD(4,4) = GU(6)  
 SD(4,6) = GU(4)  
 SD(4,7) = GU(9)+1.  
 SD(4,9) = GU(7)  
 SD(5,2) = GU(3)  
 SD(5,3) = GU(2)  
 SD(5,5) = GU(6)  
 SD(5,6) = GU(5)+1.  
 SD(5,8) = GU(9)+1.  
 SD(5,9) = GU(8)  
 ID(1,1) = GS(1)  
 ID(1,4) = GS(4)  
 ID(1,7) = GS(7)  
 ID(2,2) = GS(2)  
 ID(2,5) = GS(5)  
 ID(2,8) = GS(8)  
 ID(3,1) = GS(2)  
 ID(3,2) = GS(1)  
 ID(3,4) = GS(5)  
 ID(3,5) = GS(4)  
 ID(3,7) = GS(8)  
 ID(3,8) = GS(7)  
 ID(4,1) = GS(3)  
 ID(4,3) = GS(1)

ORIGINAL PAGE IS  
 OF POOR QUALITY

DCNO/160  
 DCNO/170  
 DCNO/180  
 DCNO/190  
 DCNO/200  
 DCNO/210  
 DCNO/220  
 DCNO/230  
 DCNO/240  
 DCNO/250  
 DCNO/260  
 DCNO/270  
 DCNO/280  
 DCNO/290  
 DCNO/300  
 DCNO/310  
 DCNO/320  
 DCNO/330  
 DCNO/340  
 DCNO/350  
 DCNO/360  
 DCNO/370  
 DCNO/380  
 DCNO/390  
 DCNO/400  
 DCNO/410  
 DCNO/420  
 DCNO/430  
 DCNO/440  
 DCNO/450  
 DCNO/460  
 DCNO/470  
 DCNO/480  
 DCNO/490  
 DCNO/500  
 DCNO/510  
 DCNO/520  
 DCNO/530  
 DCNO/540  
 DCNO/550  
 DCNO/560  
 DCNO/570  
 DCNO/580  
 DCNO/590  
 DCNO/600  
 DCNO/610  
 DCNO/620  
 DCNO/630  
 DCNO/640  
 DCNO/650  
 DCNO/660  
 DCNO/670  
 DCNO/680  
 DCNO/690  
 DCNO/700

10(4,4) GS(6)  
 10(4,6) GS(4)  
 10(4,7) GS(9)  
 10(4,9) GS(7)  
 10(5,2) GS(3)  
 10(5,3) GS(2)  
 10(5,5) GS(6)  
 10(5,6) GS(5)  
 10(5,8) GS(9)  
 10(5,9) GS(8)  
 00 60 1 1,3  
 11 3\*(1-1)  
 00 60 1 1,3  
 00 60 1 1,NN  
 00 60 K 1,3  
 11 11\*K  
 00 60 11(1,1) D1(11+J,1)GJNV(J,K)\*D11(1,1)  
 00 D12(11+J,1) D12(11+J,1)GJNV(J,K)\*D12(1,1)  
 00 SD1,SD2,SD3...RELATION BETWEEN STRAIN AND INCREMENTAL DISPLACEMENT  
 00 70 1 1,5  
 00 70 J 1,NN  
 SD1(1,1) 0.0  
 SD2(1,1) 0.0  
 SD3(1,1) 0.0  
 00 70 K 1,9  
 SD1(1,1) SD1(1,1)+SD(1,K)\*D11(K,1)  
 SD2(1,1) SD2(1,1)+SD(1,K)\*D12(K,1)  
 SD2(1,1) SD2(1,1)+D(1,K)\*D11(K,1)  
 SD3(1,1) SD3(1,1)+D(1,K)\*D12(K,1)  
 70 CONTINUE  
 11(11AG,NN) 00 10 96  
 CALL DS111(A1,SD1,SD1,DS11,6,NN,6,NN,6,NN)  
 11(NA2,1Q,1)CALL DS111(A2,SD1,SD2,DS11,6,NN,6,NN,6,NN,6,NN)  
 11(NA2,1Q,1)CALL DS111(A2,SD2,SD1,DS11,6,NN,6,NN,6,NN,6,NN)  
 CALL DS111(A3,SD2,SD2,DS11,6,NN,6,NN,6,NN,6,NN)  
 96 CONTINUE  
 72 11(11AG,NN) 00 10 85  
 00 495 1 1,9  
 00 495 J 1,NN  
 11(11,1,1) 0.0  
 CALL DS113(D11,S1,A1,1,1,1,NN)  
 11(NA2,1Q,1)CALL DS113(D11,S2,A2,1,1,1,NN)  
 11(NA2,1Q,1)CALL DS113(D12,S1,A2,1,1,1,NN)  
 CALL DS113(D12,S2,A3,1,1,1,NN)  
 CALL DS113(D11,1,1,1,1,1,1,NN)  
 00 505 1 1,9  
 00 505 J 1,NN  
 11(11,1,1) 0.0  
 11(NA2,1Q,1)CALL DS113(D11,S1,A2,1,1,1,NN)  
 CALL DS113(D11,S2,A3,1,1,1,NN)  
 CALL DS113(D12,S1,A3,1,1,1,NN)  
 CALL DS113(D12,1,1,1,1,1,1,NN)  
 85 CALL D11(SD1,S1,A1,1,1,NN)

ORIGINAL PAGE IS  
OF POOR QUALITY

ORIGINAL PAGE IS  
OF POOR QUALITY

```

SHEET 30  NASA  A1  1 80  1495 RECS  VA TECH  DGN08260
11 (NA2, LQ, 1) CALL D111(SD1, S2, A2, L1P, NN) DGN08270
11 (NA2, LQ, 1) CALL D111(SD2, S1, A2, L1P, NN) DGN08280
CALL D111(SD2, S2, A3, L1P, NN) DGN08290
20 CONTINUE DGN08300
420 CONTINUE DGN08310
11 (L1AG, NL, 0) GO TO 521 DGN08320
11 (NL, NL, 1) GO TO 313 DGN08330
313 DO 310 J=1, NN DGN08340
DO 310 J=1, NN DGN08350
310 DS11(1, J) = DS11(1, J) + AD*H(1, J) * CS11(1, J) DGN08360
521 11 (L1OP, EQ, 0) GO TO 610 DGN08370
DO 213 NI=1, NGP DGN08380
DO 213 NI=1, NGP DGN08390
XI GAUSS(NI, NGP) DGN08400
11A GAUSS(NJ, NGP) DGN08410
CALL SHAPE(DI, L1A, XI, NPI, NOI, L, 000) DGN08420
CNS1 DI*VI(NI, NGP)*VI(NJ, NGP) DGN08430
86 DO 305 I=1, NPI DGN08440
NI=NOI DGN08450
PI PO*V3(NI, 1) DGN08460
P2 PO*V3(NI, 2) DGN08470
I3 PO*V3(NI, 3) DGN08480
I (I-1)*NDI+1 DGN08490
11Q(1) 11Q(1)*CNS1*SI(1)*P1*2.0 DGN08500
11Q(1+1) 11Q(1+1)*CNS1*SI(1)*P2*2.0 DGN08510
11Q(1+2) 11Q(1+2)*CNS1*SI(1)*P3*2.0 DGN08520
205 CONTINUE DGN08530
213 CONTINUE DGN08540
610 CONTINUE DGN08550
RETURN DGN08560
END DGN08570
SUBROUTINE STRESS(NGP, NOI, L, NN, Z, NPI, LAYER) DGN08580
IMPLICIT REAL*8(A-H, O-Z) DGN08590
COMMON/HAL/A(2, 3, 6, 6), CH(9, 6, 6) DGN08600
COMMON XV(3, 3) DGN08610
COMMON/ST111/DS111(45, 45), L1P(45), V(45), V1(45), V2(45) DGN08620
, V2(45), VAC(50, 3), V1(50, 3), VAC(50, 3), V1(50, 3) DGN08630
COMMON/MSH1/COB(50, 3), L1XZ(9, 3), NOB(9, 9) DGN08640
COMMON/SHIP/SH(9), GJNV(3, 3), DS1(2, 9) DGN08650
COMMON/ICV/V1(50, 3), V2(50, 3), V3(50, 3), VA(50, 3), VB(50, 3), VC(50, 3) DGN08660
, VIA(50, 3), V2B(50, 3), V3C(50, 3) DGN08670
DINENSION GAUSS(4, 4), Z(10), S1(5), S2(5), T1(5), T2(5) DGN08680
COMMON/STK/GU(9), GV(9), ST(6), S2(6), S3(6), XU(3, 3), XV(3, 3), G1(9), DGN08690
GS(9), G2(3, 3) DGN08700
DATA GAUSS/4*0.000, -5.773502/DO, -5.773502/DO, -5.773502/DO, -5.773502/DO, DGN08710
20.000, -7.745966/DO, 0.000, -8.611363/DO, DGN08720
3-3399810000, -3399810000, -8611363100/ DGN08730
MG11(6, 10) DGN08740
DO 20 NI=1, 1 DGN08750
DO 20 NJ=1, 1 DGN08760
XI GAUSS(NI, NGP) DGN08770
11A GAUSS(NJ, NGP) DGN08780
CALL SHAPE(DI, L1A, XI, NPI, NOI, L) DGN08790
X=0.0 DGN08800
Y=0.0 DGN08810
ZZ=0.0 DGN08820

```

VA 11CII

1495 RECS

I 80

AI

SHU 13D NASA

```

DO 2,0 1-1,NPI
X=X+1XYZ(1,1)*SI(1)
Y=Y+1XYZ(1,2)*SI(1)
ZZ=ZZ+1XYZ(1,3)*SI(1)
220 CONTINUE
WRITE(6,230)X,Y,ZZ
230 FORMAT(2X,'*** X- GOOD ***',3X,'*** Y- GOOD ***',3X,'*** Z- GOOD ***',/,'2X,3(13.5,2X))
CALL STRAIN(NDI,NDI,1,NPI)
DO 20 1-1,LAYER
DO 30 11 1,5
SI(11)=0.0
SB(11)=0.0
DO 35 11-1,5
11(11)=SI(11)*Z(11)*S2(11)+Z(11)*S2(11)*S3(11)
DO 37 M1 1,5
DO 37 M2 1,5
SI(M1)=SI(M1)+CM(1,M1,M2)*11(M2)
SB(M1)=SB(M1)+CM(1,M1,M2)*11(M2)
WRITE(6,15)(SI(11),11=1,5)
WRITE(6,15)(SB(11),11=1,5)
20 CONTINUE
15 FORMAT(2X,6(13.5,1X))
10 FORMAT(/,'*****')
1 *****/
RETURN
END
SUBROUTINE SHAP1(DI,1,11A,XI,NPI,NDI,11)
IMPLICIT REAL*8(A-H,O-Z)
THIS SUBROUTINE EVALUATES THE SHAP1 FUNCTIONS AND THEIR DERIVATIVE
THE GAUSSIAN POINTS (TSOP/KANTRIC QUADRILATERAL ELEMENT WITH NINE
NODS).
COMMON/MSH1/COORD(50,3),1XYZ(9,3),NOD(9,9)
COMMON/ICV/V1(50,3),V2(50,3),V3(50,3),VA(50,3),VB(50,3),VC(50,3)
1 VIA(50,3),V2B(50,3),V3C(50,3)
COMMON XV(3,3)
COMMON/SHF/SH(9),G3NV(3,3),DSI(2,9)
DIMENSION XNOD(9,2),NP(9),G1(3,3),MKA(3)
DATA XNOD /-1.000,2*1.000,-1.000,0.000,1.000,0.000,-1.000,0.000,
2*-1.000,2*1.000,-1.000,0.000,1.000,2*0.000/
DATA NP/1,2,3,0,0,1,6,8,9/
1K=(A,B) A*B
11 (NP1-B) 50,5,65
DO 40 1-1,NPI
NP1=NP(1)
XP=XNOD(NP1,1)
YP=XNOD(NP1,2)
X10=1.0001*XP
Y10=1.0001*YP
X11=1.0-X1*XP
Y11=1.0-Y1*YP
11A1=1.0-11A*11A
11(1,1,1) G0 10 10
SI(N1)=0.25*INC(X10,Y10)*INC(X11,Y11)*INC(X10,Y10)*INC(X11,Y11)
DSI(1,N1)=0.25*INC(X10,Y10)*INC(X11,Y11)*INC(X10,Y10)*INC(X11,Y11)

```

ORIGINAL PAGE IS  
OF POOR QUALITY

DC:N18810  
DC:N18820  
DC:N18830  
DC:N18840  
DC:N18850  
DC:N18860  
DC:N18870  
DC:N18880  
DC:N18890  
DC:N18900  
DC:N18910  
DC:N18920  
DC:N18930  
DC:N18940  
DC:N18950  
DC:N18960  
DC:N18970  
DC:N18980  
DC:N18990  
DC:N19000  
DC:N19010  
DC:N19020  
DC:N19030  
DC:N19040  
DC:N19050  
DC:N19060  
DC:N19070  
DC:N19080  
DC:N19090  
DC:N19100  
DC:N19110  
DC:N19120  
DC:N19130  
DC:N19140  
DC:N19150  
DC:N19160  
DC:N19170  
DC:N19180  
DC:N19190  
DC:N19200  
DC:N19210  
DC:N19220  
DC:N19230  
DC:N19240  
DC:N19250  
DC:N19260  
DC:N19270  
DC:N19280  
DC:N19290  
DC:N19300  
DC:N19310  
DC:N19320  
DC:N19330  
DC:N19340  
DC:N19350

ORIGINAL PAGE IS  
OF POOR QUALITY

VA 11CH

1495 RECS

1 80

A1

SHU 10 NASA

```

DSI(2,N1) = 0.25*INC(X10,YP)*(2.0*E1A*YP+X1*XP)
GO 10 40
10 IF(.GT.6) GO 10 20
SI(N1) 0.5*INC(X11,E1A0)
DSI(1,N1) = -INC(X1,E1A0)
DSI(2,N1) = 0.5*INC(YP,X11)
GO 10 40
20 SI(N1) = 0.5*INC(E1A1,X10)
DSI(1,N1) = 0.5*INC(XP,E1A1)
DSI(2,N1) = -INC(E1A,X10)
40 CONTINUE
GO 10 70
50 CONTINUE
DO 60 I = 1, NPI
XP XNODI(1,1)
YP XNODI(1,2)
X10 1.0+X1*XP
E1A0 1.0+E1A*YP
SI(1) 0.25*INC(X10,E1A0)
DSI(1,1) 0.25*INC(XP,E1A0)
DSI(2,1) 0.25*INC(YP,X10)
60 CONTINUE
GO 10 70
65 DO 69 J = 1, NPJ
NI = NP(1)
XP XNODI(N1,1)
YP XNODI(N1,2)
X10 1.0+X1*XP
E1A0 1.0+E1A*YP
X11 1.0-X1*X1
E1A1 1.0-E1A*E1A
X12 XP*X1
E1A2 YP*E1A
IF(.GT.4) GO 10 66
SI(N1) 0.25*INC(X10,E1A0)*X12*E1A2
DSI(1,N1) 0.25*XP*INC(E1A2,E1A0)*(1.0+2.0*X12)
DSI(2,N1) 0.25*YP*INC(X12,X10)*(1.0+2.0*E1A2)
GO 10 69
66 IF(.GT.6) GO 10 67
SI(N1) 0.5*INC(X11,E1A0)*E1A2
DSI(1,N1) = -X1*INC(E1A2,E1A0)
DSI(2,N1) = 0.5*INC(X11,YP)*(1.0+2.0*E1A2)
GO 10 69
67 IF(.GT.8) GO 10 68
SI(N1) 0.5*INC(E1A1,X10)*X12
DSI(2,N1) = -E1A*INC(X12,X10)
DSI(1,N1) = 0.5*INC(E1A1,XP)*(1.0+2.0*X12)
GO 10 69
68 SI(N1) = INC(X11,E1A1)
DSI(1,N1) = -2.0*X1*E1A1
DSI(2,N1) = -2.0*E1A*X11
69 CONTINUE
70 DO 80 I = 1,3
DO 80 J = 1,3
C1(1,1) = 0.0

```

DCM193360  
 DCM19370  
 DCM19380  
 DCM19390  
 DCM19400  
 DCM19410  
 DCM19420  
 DCM19430  
 DCM19440  
 DCM19450  
 DCM19460  
 DCM19470  
 DCM19480  
 DCM19490  
 DCM19500  
 DCM19510  
 DCM19520  
 DCM19530  
 DCM19540  
 DCM19550  
 DCM19560  
 DCM19570  
 DCM19580  
 DCM19590  
 DCM19600  
 DCM19610  
 DCM19620  
 DCM19630  
 DCM19640  
 DCM19650  
 DCM19660  
 DCM19670  
 DCM19680  
 DCM19690  
 DCM19700  
 DCM19710  
 DCM19720  
 DCM19730  
 DCM19740  
 DCM19750  
 DCM19760  
 DCM19770  
 DCM19780  
 DCM19790  
 DCM19800  
 DCM19810  
 DCM19820  
 DCM19830  
 DCM19840  
 DCM19850  
 DCM19860  
 DCM19870  
 DCM19880  
 DCM19890  
 DCM19900

ORIGINAL PAGE IS  
OF POOR QUALITY

VA TECH

1495 RECS

F 80

SHUTTLE NASA

```

DO 80 K = 1,NPI
  IF (I,Q,3) GO TO 90
  GJ(1,3) = GJ(1,3) + DS1(I,K)*I(YZ(K,J))
  GO TO 80
90 NI=MOD(NOT,K)
  GJ(1,3) = GJ(1,3)+SI(K)*VC(NI,3)*0.5*H
80 CONTINUE
  XV(1,3) = GJ(1,2)*GJ(2,3)-GJ(2,2)*GJ(1,3)
  XV(2,3) = GJ(2,1)*GJ(1,3)-GJ(1,1)*GJ(2,3)
  XV(3,3) = GJ(1,1)*GJ(2,2)-GJ(2,1)*GJ(1,2)
  XV(1,1) = XV(3,3)
  XV(2,1) = 0.0
  XV(3,1) = -XV(1,3)
  XV(1,2) = -XV(2,3)*XV(1,3)
  XV(2,2) = -XV(1,3)*XV(2,3)*XV(1,3)
  XV(3,2) = -XV(2,3)*XV(3,3)
  SUM1 DSORT(XV(1,1)*XV(2,1)*XV(3,1)*XV(1,2))
  SUM2 DSORT(XV(1,2)*XV(2,2)*XV(3,2)*XV(1,3))
  SUM3 DSORT(XV(1,3)*XV(2,3)*XV(3,3)*XV(1,1))
  DO 30 J = 1,3
    XV(J,1) = XV(J,1)/SUM1
    XV(J,2) = XV(J,2)/SUM2
    XV(J,3) = XV(J,3)/SUM3
30 CONTINUE
  DE = GJ(1,1)*GJ(2,2)*GJ(3,3)+GJ(1,2)*GJ(2,3)+GJ(2,1)*GJ(3,2)+GJ(3,1)*GJ(2,2)*GJ(3,3)
  1 GJ(3,2)*GJ(1,3)-GJ(1,3)*GJ(2,2)*GJ(3,1)-GJ(2,3)*GJ(3,2)*GJ(1,1)
  2 GJ(1,1)*GJ(2,2)*GJ(3,3)+GJ(1,2)*GJ(2,3)+GJ(2,1)*GJ(3,2)+GJ(3,1)*GJ(2,2)*GJ(3,3)
  CALL TURN(GJ,3,3,GJINV,0,VARIA,11R)
  RETURN
END
SUBROUTINE DS13(D2,B,A,A2,NN)
  IMPLICIT REAL*8(A-H,O-Z)
  DIMENSION D2(9,45),A(6,6),A1(6),B1(9,9),
  1 A2(9,45),B(6)
  DO 10 I = 1,5
    A1(I) = 0.0
  DO 10 J = 1,5
    A1(J) = 0.0
  DO 5 I = 1,9
    B1(I,1) = 0.0
  DO 20 I = 1,3
    1 3*(1-1)
    3 3*(1-1)
    B1(I+1,11+1) = A1(I)
    B1(I+1,11+2) = A1(3)
    B1(I+1,11+3) = A1(4)
    B1(I+2,11+1) = A1(3)
    B1(I+2,11+2) = A1(2)
    B1(I+2,11+3) = A1(5)
    B1(I+3,11+1) = A1(4)
    B1(I+3,11+2) = A1(5)
    B1(I+3,11+3) = 0.0
20 CONTINUE
  DO 30 I = 1,3

```

DCM19910  
 DCM19920  
 DCM19930  
 DCM19940  
 DCM19950  
 DCM19960  
 DCM19970  
 DCM19980  
 DCM19990  
 DCM10000  
 DCM10010  
 DCM10020  
 DCM10030  
 DCM10040  
 DCM10050  
 DCM10060  
 DCM10070  
 DCM10080  
 DCM10090  
 DCM10100  
 DCM10110  
 DCM10120  
 DCM10130  
 DCM10140  
 DCM10150  
 DCM10160  
 DCM10170  
 DCM10180  
 DCM10190  
 DCM10200  
 DCM10210  
 DCM10220  
 DCM10230  
 DCM10240  
 DCM10250  
 DCM10260  
 DCM10270  
 DCM10280  
 DCM10290  
 DCM10300  
 DCM10310  
 DCM10320  
 DCM10330  
 DCM10340  
 DCM10350  
 DCM10360  
 DCM10370  
 DCM10380  
 DCM10390  
 DCM10400  
 DCM10410  
 DCM10420  
 DCM10430  
 DCM10440  
 DCM10450

ORIGINAL PAGE IS  
OF POOR QUALITY

VA TECH

1495 RECS

1 80

A1

SHIP 3D

NASA

```

12 3*(11-1)
DO 30 I3 1,3
12 12+1
DO 30 J1 1,NH
K2 3*(11-1)
DO 30 K1 1,3
K2 K2+1
A2(12,11) A2(12,J1)+B1(12,K2)*D2(K2,J1)
30 CONTINUE
RETURN
END
SUBROUTINE B00(NRMAX,A,D,DD,NIQ,NIQV,NBDY,IBDY,ITER,IFLAG)
IMPLICIT REAL*8(A,D,DD)
DIMENSION A(NRMAX,NRMAX),D(NRMAX),D(NRMAX),IBDY(NBDY),DD(NRMAX)
300 DO 2 1,NBDY
  ITHX IBDY(1)
  DO 1 J 1,NBDY
    I1 (IBDY(J),1,1,INAX) GO TO 1
  ITHX IBDY(1)
  I1PT J
  1 CONTINUE
  IBDY(I1PT)-IBDY(1)
  IBDY(1) ITHX
  2 CONTINUE
  NIQV NIQ
  DO 14 I 1,NBDY
    8 I1 IBDY(1)
    I1 (IB,IG,NIQV)GO TO 13
    NIQV NIQV-1
    DO 12 I1 1,NIQV
      DO 9 J1 1,NIQV
        D(I1) D(I1+1)
      DD(I1) DD(I1+1)
      I1(I1AG,NIQ) GO TO 9
      A(I1,J1) A(I1+1,J1)
    9 CONTINUE
    I1(I1AG,NIQ)GO TO 12
    DO 10 J1 1,NIQV
      10 A(J1,11) A(J1,11+1)
    12 CONTINUE
    13 NIQV NIQV-1
    14 CONTINUE
    RETURN
  END
SUBROUTINE H1SH1(THA1,THA2,ML,MP,R,TYPE,XI,YI)
C ..... THIS SUBROUTINE IS TO FIND THE GLOBAL COORDINATE OF A DOUBLY
C ..... CURVED SHEET WITH EQUAL RADII
C
  IMPLICIT REAL*8(A,D,DD)
  COMMON/H1SH1/COORD(50,3),I1XY(9,3),MOD(9,9)
  COMMON/ICV/V1(50,3),V2(50,3),V3(50,3),VA(50,3),VB(50,3),VC(50,3)
  1 VIA(50,3),V2B(50,3),V3C(50,3)
  DIMENSION X1(15),Y1(15)
  I1TYPE 1,.... CYLINDRICAL SHEET

```

DGN10460  
 DGN10470  
 DGN10480  
 DGN10490  
 DGN10500  
 DGN10510  
 DGN10520  
 DGN10530  
 DGN10540  
 DGN10550  
 DGN10560  
 DGN10570  
 DGN10580  
 DGN10590  
 DGN10600  
 DGN10610  
 DGN10620  
 DGN10630  
 DGN10640  
 DGN10650  
 DGN10660  
 DGN10670  
 DGN10680  
 DGN10690  
 DGN10700  
 DGN10710  
 DGN10720  
 DGN10730  
 DGN10740  
 DGN10750  
 DGN10760  
 DGN10770  
 DGN10780  
 DGN10790  
 DGN10800  
 DGN10810  
 DGN10820  
 DGN10830  
 DGN10840  
 DGN10850  
 DGN10860  
 DGN10870  
 DGN10880  
 DGN10890  
 DGN10900  
 DGN10910  
 DGN10920  
 DGN10930  
 DGN10940  
 DGN10950  
 DGN10960  
 DGN10970  
 DGN10980  
 DGN10990  
 DGN11000

ORIGINAL PAGE IS  
OF POOR QUALITY

VA TECH

1495 RECS

F 80

AI

SHEET 3D NASA

TYPE 2... SPHERICAL SHEET

C  
C  
C

DCN11010  
DCN11020  
DCN11030  
DCN11040  
DCN11050  
DCN11060  
DCN11070  
DCN11080  
DCN11090  
DCN11100  
DCN11110  
DCN11120  
DCN11130  
DCN11140  
DCN11150  
DCN11160  
DCN11170  
DCN11180  
DCN11190  
DCN11200  
DCN11210  
DCN11220  
DCN11230  
DCN11240  
DCN11250  
DCN11260  
DCN11270  
DCN11280  
DCN11290  
DCN11300  
DCN11310  
DCN11320  
DCN11330  
DCN11340  
DCN11350  
DCN11360  
DCN11370  
DCN11380  
DCN11390  
DCN11400  
DCN11410  
DCN11420  
DCN11430  
DCN11440  
DCN11450  
DCN11460  
DCN11470  
DCN11480  
DCN11490  
DCN11500  
DCN11510  
DCN11520  
DCN11530  
DCN11540  
DCN11550

```

N1 M1+1
N2 M2+1
IF (TYPE, I, Q, 0) GO TO 100
100 10A1/M1
11 (TYPE, M, 1) GO TO 10
Y1 Y1/M2
GO TO 11
10 10A2/M2
11 10B-0.0
DO 1 1, N1
X1H(1) R*DSIN(10B)
10B 10B+101
1 CONTINUE
10B 0.0
DO 2 1, N2
11 (TYPE, M, 1) GO TO 13
Y1H(1) 10B
10B 10B+Y1
GO TO 2
13 Y1H(1) R*DSIN(10B)
10B 10B+102
2 CONTINUE
11 1
DO 3 1, N2
DO 4 1, N1
OC1 DSIN(X1H(1)*2+Y1H(1)*2)
11 (TYPE, I, Q, 1) OC1 X1H(1)
PHI DAKSIN(OC1/R)
11 (OC1, I, Q, 0) 10B 0.0
11 (OC1, I, Q, 0) GO TO 5
11 (TYPE, I, Q, 1) 10B 3.1159625/2.0
11 (TYPE, I, Q, 1) GO TO 5
10B DAKCOS(Y1H(1)/OC1)
5 COORD(1, 1) R*DSIN(PHI)*DSIN(10B)
COORD(1, 3) R*DCOS(PHI)
V3(1, 1) DSIN(PHI)*LSIN(10B)
V3(1, 3) DCOS(PHI)
11 (TYPE, M, 1) GO TO 15
V3(1, 2) 0.0
COORD(1, 2) Y1H(1)
GO TO 16
15 V3(1, 2) DSIN(PHI)*DCOS(10B)
COORD(1, 2) R*DSIN(PHI)*DCOS(10B)
16 11 11+1
4 CONTINUE
3 CONTINUE
RETURN
X1 X1/M1
Y1 Y1/M2
Y1 Y1/M2
B 0.0

```

100



ORIGINAL PAGE IS  
OF POOR QUALITY



```

A3(2)=0.0
A3(3)=1.
Q(1,1)=C(1,1)*(CN**4)+2.0*(C(1,2)+2.0*C(3,3))*SN*SN*CN*CN*C(2,2)
I=(SN**4)
Q(1,2)=C(1,1)*C(2,2)-4.0*C(3,3)*SN*SN*CN*CN+C(1,2)*(SN**4+CN**4)
Q(2,2)=C(1,1)*(SN**4)+2.0*(C(1,2)+2.0*C(3,3))*SN*SN*CN*CN*C(2,2)
I=(CN**4)
Q(1,3)=C(1,1)-C(1,2)-2.0*C(3,3)*SN*(CN**3)+C(1,2)-C(2,2)+2.0*
IC(3,3)*(SN**3)*CN
Q(2,3)=C(1,1)-C(1,2)-2.0*C(3,3)*(SN**3)*CN+C(1,2)-C(2,2)+2.0*
IC(3,3)*SN*(CN**3)
Q(3,3)=C(1,1)+C(2,2)-2.0*C(1,2)-2.0*C(3,3)*SN*SN*CN*CN*C(3,3)*
I=(SN**4+CN**4)
Q(2,1)=Q(1,2)
Q(3,1)=Q(1,3)
Q(3,2)=Q(2,3)
CM(1A,4,4)=(G23*CN*CN+G13*SN*SN)*AK
CM(1A,4,5)=(G23-G13)*CN*SN)*AK
CM(1A,5,5)=(G13*CN*CN+G23*SN*SN)*AK
I1(NCP,IQ,IGP)Q(4,4)=(G23*CN*CN+G13*SN*SN)*AK
I1(NCP,IQ,IGP)Q(4,5)=(G23-G13)*CN*SN)*AK
I1(NCP,IQ,IGP)Q(5,5)=(G13*CN*CN+G23*SN*SN)*AK
I1(NCP,NI,IGP)Q(4,4)=(G23*CN*CN+G13*SN*SN)*AK
I1(NCP,NI,IGP)Q(4,5)=(G23-G13)*CN*SN)*AK
I1(NCP,NI,IGP)Q(5,5)=(G13*CN*CN+G23*SN*SN)*AK
DO 91 1 1,3
DO 91 1 1,3
CM(1A,1,3) Q(1,1)
DO 90 1 1,5
DO 90 1 1,5
A(1,1,1) A(1,1,1)+Q(1,1)*(Z(1A+1)-Z(1A))
A(1,2,1) A(1,2,1)+Q(1,1)*(Z(1A+1)*2-Z(1A)**2)/2.0
A(1,3,1) A(1,3,1)+Q(1,1)*(Z(1A+1)**3-Z(1A)**3)/3.0
A(2,1,1) A(2,1,1)+Q(1,1)*(Z(1A+1)-Z(1A))
A(2,2,1) A(2,2,1)+Q(1,1)*(Z(1A+1)*2-Z(1A)**2)/2.0
A(2,3,1) A(2,3,1)+Q(1,1)*(Z(1A+1)**3-Z(1A)**3)/3.0
DO CONTINUE
DO CONTINUE
RETURN
END
SUBROUTINE MAXH2 (GJNV,XV,XU,DI)
IMPLICIT REAL*8(A-H,O-Z)
DIMENSION GJNV(3,3),XV(3,3),XU(3,3),DI(3,3),DK(3,3)
CALL MIPY(DI,XV,DK)
CALL MIPY(GJNV,DK,DI)
CALL MIPY(XU,DI,DK)
DO 1 1 1,3
DO 1 1 1,3
DI(1,3) DK(1,1)
RETURN
END
SUBROUTINE MIPY(A,B,C)
IMPLICIT REAL*8(A-H,O-Z)
DIMENSION A(3,3),B(3,3),C(3,3)

```

ORIGINAL PAGE IS  
OF POOR QUALITY

VA TECH

1495 RECS

1 80

SUBT 30 NASA A1

DCN13210  
DCN13220  
DCN13230  
DCN13240  
DCN13250  
DCN13260  
DCN13270  
DCN13280  
DCN13290  
DCN13300  
DCN13310  
DCN13320  
DCN13330  
DCN13340  
DCN13350  
DCN13360  
DCN13370  
DCN13380  
DCN13390  
DCN13400  
DCN13410  
DCN13420  
DCN13430  
DCN13440  
DCN13450  
DCN13460  
DCN13470  
DCN13480  
DCN13490  
DCN13500  
DCN13510  
DCN13520  
DCN13530  
DCN13540  
DCN13550  
DCN13560  
DCN13570  
DCN13580  
DCN13590  
DCN13600  
DCN13610  
DCN13620  
DCN13630  
DCN13640  
DCN13650  
DCN13660  
DCN13670  
DCN13680  
DCN13690  
DCN13700  
DCN13710  
DCN13720  
DCN13730  
DCN13740  
DCN13750

```

DO 1 J=1,3
DO 1 J=1,3
C(1,J)=0.0
DO 1 K=1,3
1 C(1,J)=C(1,J)+A(1,K)*B(K,J)
RETURN
END
SUBROUTINE ZIR0(A)
IMPLICIT REAL*8(A-H,O-Z)
DIMENSION A(3,3)
DO 1 J=1,3
DO 1 J=1,3
1 A(1,J)=0.0
RETURN
END
SUBROUTINE DISK(A,B,I,J)
IMPLICIT REAL*8(A-H,O-Z)
DIMENSION A(3,3),B(9,45)
B(1,15)=B(1,15)+A(1,1)
B(2,15)=B(2,15)+A(2,1)
B(3,15)=B(3,15)+A(3,1)
B(4,15)=B(4,15)+A(1,2)
B(5,15)=B(5,15)+A(2,2)
B(6,15)=B(6,15)+A(3,2)
B(7,15)=B(7,15)+A(1,3)
B(8,15)=B(8,15)+A(2,3)
B(9,15)=B(9,15)+A(3,3)
RETURN
END
SUBROUTINE DISK2(A,B)
IMPLICIT REAL*8(A-H,O-Z)
DIMENSION A(3,3),B(9)
A(1,1)=B(1)
A(2,1)=B(2)
A(3,1)=B(3)
A(1,2)=B(4)
A(2,2)=B(5)
A(3,2)=B(6)
A(1,3)=B(7)
A(2,3)=B(8)
A(3,3)=B(9)
RETURN
END
SUBROUTINE DISK2(A,B)
IMPLICIT REAL*8(A-H,O-Z)
DIMENSION A(3,3),B(9)
B(1)=A(1,1)
B(2)=A(2,1)
B(3)=A(3,1)
B(4)=A(1,2)
B(5)=A(2,2)
B(6)=A(3,2)
B(7)=A(1,3)
B(8)=A(2,3)
B(9)=A(3,3)

```





1 GS(4)+GU(7)\*GS(9)+GU(9)\*GS(7)  
 S2(5) S2(5)+GS(8)+GU(3)\*GS(2)+GU(2)\*GS(3)+GU(6)\*GS(5)+GU(5)\*  
 1 GS(6)+GU(9)\*GS(8)+GU(8)\*GS(9)  
 S3(1) 0.5\*(GS(1)\*2+GS(4)\*2+GS(7)\*2)  
 S3(2) 0.5\*(GS(2)\*2+GS(5)\*2+GS(8)\*2)  
 S3(3) GS(1)\*GS(2)+GS(4)\*GS(5)+GS(7)\*GS(8)  
 S3(4) GS(1)\*GS(3)+GS(4)\*GS(6)+GS(7)\*GS(9)  
 S3(5) GS(2)\*GS(3)+GS(5)\*GS(6)+GS(8)\*GS(9)  
 RETURN  
 END

DGN14860  
 DGN14870  
 DGN14880  
 DGN14890  
 DGN14900  
 DGN14910  
 DGN14920  
 DGN14930  
 DGN14940  
 DGN14950

ORIGINAL PAGE IS  
 OF POOR QUALITY

# INITIAL REPORT

MAG 3 208  
GLUE INITIALITY NUMERICAL ANALYSIS ON LAYERED COMPOSITE PLATES  
AND STRUCTURES  
NASA CR 168182

Advanced Research Projects Agency  
Washington, DC 20525  
Attn: Library

Advanced Technology Center, Inc.  
114 Aerospace Corporation  
P. O. Box 6144  
Dallas, TX 75222  
Attn: D. H. Petersen  
W. J. Benton

Air Force Flight Dynamics Laboratory  
Wright Patterson Air Force Base, OH 45433  
Attn: E. E. Bally  
G. P. Sendeky (IBC)  
R. S. Sandhu

Air Force Materials Laboratory  
Wright Patterson Air Force Base, OH 45433  
Attn: H. S. Schwarz (LM)  
I. J. Reinhardt (MBC)  
G. P. Peterson (IC)  
E. J. Morrissey (LAI)  
S. W. Tsai (NBM)  
M. J. Pagano  
J. M. Whitney (NMM)

Air Force Office of Scientific Research  
Washington, DC 20333  
Attn: J. F. Mast (SRP)

Air Force Office of Scientific Research  
1400 Wilson Blvd  
Arlington, VA 22209

AFOSR/MA  
Balling Air, DC 20332  
Attn: A. K. Amos

Air Force Rocket Propulsion Laboratory  
Edwards, CA 93523  
Attn: Library

Babcock & Wilcox Company  
Advanced Composites Department  
P. O. Box 419  
Alliance, Ohio 44601  
Attn: P. M. Leopold

Bell Helicopter Company  
P. O. Box 482  
Ft. Worth, TX 76101  
Attn: M. Zinberg

The Boeing Company  
P. O. Box 3999  
Seattle, WA 98124  
Attn: J. T. Hoggatt, MS. 88-33  
T. R. Porter

The Boeing Company  
Vertol Division  
Morton, PA 19070  
Attn: E. C. Durchlaub

Battelle Memorial Institute  
Columbus Laboratories  
505 King Avenue  
Columbus, OH 43201  
Attn: L. E. Hulbert

Bendix Advanced Technology Center  
9140 Old Annapolis Rd/MD. 108  
Columbia, MD 21045  
Attn: O. Hayden Griffin

Brunswick Corporation  
Defense Products Division  
P. O. Box 4594  
43000 Industrial Avenue  
Lincoln, NE 68504  
Attn: R. Morse

Commander  
Naval Air Systems Command  
U. S. Navy Department  
Washington DC 20360  
Attn: M. Stander, AIR-430320

Commander  
Naval Ordnance Systems Command  
U. S. Navy Department  
Washington DC 20360  
Attn: B. Brimmer, 088-033  
M. Kinne, 088-033A

Cornell University  
Dept. Theoretical & Applied Mech.  
Thurston Hall  
Ithaca, NY 14853  
Attn: S. L. Phoenix

Defense Metals Information Center  
Battelle Memorial Institute  
Columbus Laboratories  
505 King Avenue  
Columbus, OH 43201

Department of the Army  
U. S. Army Aviation Materials Laboratory  
Ft. Eustis, VA 23604  
Attn: I. E. Figge, Sr.  
Library

Department of the Army  
U. S. Army Aviation Systems Command  
P. O. Box 209  
St. Louis, MO 63166  
Attn: R. Vollmer, AMSAV-A-UE

Department of the Army  
Plastics Technical Evaluation Center  
Picatinny Arsenal  
Dover, NJ 07801  
Attn: M. E. Pably, Jr.

Department of the Army  
Watervliet Arsenal  
Watervliet, NY 12189  
Attn: C. D'Andrea

Department of the Army  
Watervliet Arsenal  
Watervliet, NY 12189  
Attn: A. Thomas

Department of the Army  
Redstone Arsenal  
Huntsville, AL 35899  
Attn: R. J. Thompson, AMSA-855

Department of the Navy  
Naval Ordnance Laboratory  
White Oak  
Silver Spring, MD 20910  
Attn: R. Simon

Department of the Navy  
U. S. Naval Ship R&D Laboratory  
Annapolis, MD 21402  
Attn: C. Harsner, Code 2724

Director  
Deep Submergence Systems Project  
6900 Wisconsin Avenue  
Washington DC 20015  
Attn: H. Bernstein, DSSP-221

Director  
Naval Research Laboratory  
Washington DC 20390  
Attn: Code 8430  
I. Moloach, Code 8433

Drexel University  
32nd and Chestnut Streets  
Philadelphia, PA 19104  
Attn: P. C. Chou

E. I. DuPont de Nemours & Co.  
DuPont Experimental Station  
Wilmington, DE 19880  
Attn: D. L. G. Sturgeson

Fiber Science, Inc.  
245 East 157 Street  
Gardena, CA 90248  
Attn: E. Dunahoo

General Dynamics  
P. O. Box 748  
Ft. Worth, TX 76100  
Attn: D. J. Wilkins  
Library

ORIGINAL PAGE IS  
OF POOR QUALITY



General Dynamics/Convair  
P.O. Box 1128  
San Diego, CA 92112  
Attn: J. L. Christian  
R. Adair

General Electric Co.  
Evendale, OH 45215  
Attn: C. Stotler  
R. Ravenhall

General Motors Corporation  
Detroit Diesel Allison Division  
Indianapolis, IN 46244  
Attn: M. Herman

Georgia Institute of Technology  
School of Aerospace Engineering  
Atlanta, GA 30332  
Attn: L. W. Rehfield

Grumman Aerospace Corporation  
Bethpage, Long Island, NY 11714  
Attn: S. Dastin  
J. B. Whiteside

Hamilton Standard Division  
United Aircraft Corporation  
Windsor Locks, CT 06096  
Attn: W. A. Percival

Hercules, Inc.  
Allagheny Ballistics Laboratory  
P.O. Box 210  
Cumberland, MD 21053  
Attn: A. A. Vitaro

Hughes Aircraft Company  
Culver City, CA 90230  
Attn: A. Knoll

Illinois Institute of Technology  
10 West 32 Street  
Chicago, IL 60616  
Attn: L. J. Broutman

I. M. Daniel  
Dr. Joseph Wolf, Engineering Mechanics  
General Motors Research Labs.  
256 Research Drive  
Warren, MI 48090

Jet Propulsion Laboratory  
4800 Oak Grove Drive  
Pasadena, CA 91103  
Attn: Library

Lawrence Livermore Laboratory  
P.O. Box 808, L-421  
Livermore, CA 94550  
Attn: T. T. Chiao  
E. M. Wu

Lehigh University  
Institute of Fracture &  
Solid Mechanics  
Bethlehem, PA 18015  
Attn: G. C. Sih

Lockheed-Georgia Co.  
Advanced Composites Information Center  
Dept. 72-14, Zone 402  
Marietta, GA 30060  
Attn: T. N. Hsu

Lockheed Missiles and Space Co.  
P.O. Box 504  
Sunnyvale, CA 94087  
Attn: R. W. Fenn

Lockheed-California  
Burbank, CA 91503  
Attn: J. T. Ryder  
K. M. Lauriat  
J. C. Elvill

McDonnell Douglas Aircraft Corporation  
P.O. Box 516  
Lambert Field, MS 63166  
Attn: J. C. Watson

McDonnell Douglas Aircraft Corporation  
3855 Lakewood Blvd.  
Long Beach, CA 90810  
Attn: L. B. Gressczuk

Material Sciences Corporation  
1777 Walton Road  
Blue Bell, PA 19422  
Attn: B. W. Rosen

Massachusetts Institute of Technology  
Cambridge, MA 02139  
Attn: F. J. McGarry  
J. F. Mandell  
J. W. Mar

NASA-Ames Research Center  
Moffett Field, CA 94035  
Attn: Dr. J. Parker  
Library

NASA-Flight Research Center  
P.O. Box 273  
Edwards, CA 93523  
Attn: Library

NASA-George C. Marshall Space Flight Center  
Huntsville, AL 35812  
Attn: C. E. Cataldo, SGE-ASTM-WK  
Library

NASA-Goddard Space Flight Center  
Greenbelt, MD 20771  
Attn: Library

NASA-Langley Research Center  
Hampton, VA 23365  
Attn: J. H. Starnes  
J. G. Davis, Jr.  
M. C. Card

NASA-Lewis Research Center  
21000 Brookpark Road, Cleveland, OH 44135  
Attn: Contracting Officer, MS 501-11

Tech. Report Control, MS 5-5  
Tech. Utilization, MS 3-16  
AFSC Liaison, MS 501-3  
SAMTD Contract Files, MS 49-6  
L. Berke, MS 49-6  
M. T. Saunders, MS 49-1  
R. F. Lark, MS 49-6  
J. A. Ziemlanski, MS 49-6  
R. M. Johns, MS 49-6  
C. C. Chamis, MS 49-6 (4 copies)  
R. L. Thompson, MS 49-6  
T. T. Serafini, MS 49-1  
Library, MS 60-3 (2 copies)  
NASA-Lyndon B. Johnson Space Center  
Houston, TX 77001  
Attn: S. Glorioso, SMD-ESS2  
Library

NASA Scientific and Tech. Information Facility  
P.O. Box 8757  
Belt/Wash International Airport, MD 21240  
Attn: Acquisitions Branch (IC -proc.)

National Aeronautics & Space Administration  
Office of Advanced Research & Technology  
Washington DC 20546  
Attn: L. Harris, Code RTM-6  
M. Greenfield, Code RTM-6  
C. Bersch, Code RTM-6

National Aeronautics & Space Administration  
Office of Technology Utilization  
Washington DC 20546

National Bureau of Standards  
Eng. Mech. Section  
Washington DC 20231  
Attn: R. Mitchell

National Science Foundation  
Engineering Division  
1800 G. Street, NW  
Washington DC 20540  
Attn: Library

Northrop Corporation Aircraft Group  
3901 West Broadway  
Northridge, CA 90250  
Attn: R. M. Verette  
G. C. Grimes

Pratt & Whitney Aircraft  
East Hartford, CT 06108  
Attn: J. M. Woodward

Raytheon Co., Missile System Division  
Mechanical Systems Laboratory  
Bedford, MA  
Attn: P. R. Digiovanni

Rensselaer Polytechnic Institute  
Troy, NY 12181  
Attn: R. Looney

Rockwell International  
Los Angeles Division  
International Airport  
Los Angeles, CA 90009  
Attn: L. M. Lockman  
D. V. Konishi

Sikorsky Aircraft Division  
United Aircraft Corporation  
Stratford, CT 06602  
Attn: Library

Southern Methodist University  
Dallas, TX 75275  
Attn: R. M. Jones

Space & Missile Systems Organization  
Air Force Unit Post Office  
Los Angeles, CA 90045  
Attn: Technical Data Center

ORIGINAL PAGE IS  
OF POOR QUALITY

ORIGINAL PAGE IS  
OF POOR QUALITY

Structural Composites Industries, Inc.  
6344 N. Irwindale Avenue  
Azusa, CA 91702  
Attn: R. Gordon

V.P. I. and S. U.  
Dept. of Eng. Mech.  
Blacksburg, VA 24061  
Attn: R. H. Heller  
H. J. Brinson  
C. T. Herakovich  
K. L. Reifsnider

Texas A&M  
Mechanics & Materials Research Center  
College Station, TX 77843  
Attn: R. A. Schapery

Y. Weitsman  
TRW, Inc.  
23555 Euclid Avenue  
Cleveland, OH 44117  
Attn: I. J. Toth

Celanese Research Company  
86 Morris Ave.  
Summit, NJ 07901  
Attn: H. S. Kliger

Union Carbide Corporation  
P. O. Box 6116  
Cleveland, OH 44101  
Attn: J. C. Bowman

Commander  
Natick Laboratories  
U. S. Army  
Natick, MA 01762  
Attn: Library

United Technologies Research Center  
East Hartford, CT 06108  
Attn: R. C. Novak  
Dr. A. Dennis

University of Dayton Research Institute  
Dayton, OH 45409  
Attn: R. W. Kim

University of Delaware  
Mechanical & Aerospace Engineering  
Newark, DE 19711  
Attn: B. R. Pipes

University of Illinois  
Department of Theoretical & Applied Mechanics  
Urbana, IL 61801  
Attn: S. S. Wang

University of Oklahoma  
School of Aerospace Mechanical & Nuclear Engineering  
Norman, OK 73069  
Attn: C. W. Bert

University of Wyoming  
College of Engineering  
University Station Box 3295  
Laramie, WY 82071  
Attn: D. F. Adams

U. S. Army Materials & Mechanics Research Center  
Watertown Arsenal  
Watertown, MA 02172  
Attn: E. M. Lence  
D. W. Oplinger